UNIVERSITÀ DEGLI STUDI DI TRIESTE

XXXI CICLO DEL DOTTORATO DI RICERCA IN

INGEGNERIA ED ARCHITETTURA

THE CLIMATE DATA EFFECT ON BUILDING ENERGY SIMULATION

SSD: ING-IND/10 FISICA TECNICA INDUSTRIALE

DOTTORANDO
GIORGIO LUPATO

COORDINATORE
PROF. DIEGO MICHELI

SUPERVISORE
PROF. MARCO MANZAN

Anno Accademico 2017/2018

Acknowledgements

I would like to thank Prof. Marco Manzan for the support of my Ph.D study and for encouraging me to learn the numerical code approach.

I would like to thank Prof. Enrico Nobile, Mr. Walter Moze, Prof. Ezio Zandegiacomo De Zorzi, Prof. Stefano Cirilli, Mr. Riccardo Rossi, Mr. Amedeo Pezzi from the University of Trieste for their valuable support.

I would like to thank Mr. Juan Rodríguez Santiago from the Fraunhofer institute for being important in my scientific and professional growth.

I would like to thank Mr. Giovanni Murano from the Comitato termotecnico Italiano for his willingness and help.

I would like to thank Mr. Francesco Spinelli from ENEA for his precious advices.

I would like to thank Mr. Daniele Alberico and all the SGM Architecture for the generous commitment taken and for funding my Ph.D scholarship.

I would like to thank my family for supporting me at any time and in every way.

I would like to thank Joanna for her help and patience.

The author wish to thank the CTI (Comitato Termotecnico Italiano) for the valuable information.

The author wish to thank the ATER (Azienda Territoriale per l'Edilizia Residenziale di Trieste) for the valuable information.

The author wish to thank Design Builder Italia for their support.

Contents

Chapter 1

Introduction

1.1 Building sector energy consumption

According to the International Energy Agency [1], from 1971 to 2015, the world energy consumption and CO2 emissions had rapidly grown. In addition, the trend forecast shows a steadily increase, also due to the emerging economic nations' energy demand and the world population growth [2]. The scenario is a matter of concern also considering the fossil source supply difficulties and exhaustion [3, 2].

The building heating and cooling has been one of the most rapidly-increasing fields in the uses of the world energy resources [4]. The building sector energy consumption has an important role, it covers nearly 33% of the total energy [5] and more than 40% of the world primary energy [6]. As for the energy sources, it consumes over one half of electricity and one-third of the global natural gas demand [7]. The developed countries' building consumption involves a great part of the final energy demand: in Italy, for example, 35% is mainly related to building heating and cooling processes [8]. In the U.S., the total primary energy use covers 41%, with 50% dedicated to space heating and cooling. [9, 10]

The building energy field has a significant investment potential as well: in the IPCC fourth assessment report (AR4, 2007), it is indicated as the the sector with the highest economic mitigation potential of any other energy sector [11]. Thanks to cutting-edge technologies, the energy use of new buildings and existing buildings can be reduced by 50% and 30% or more, respectively [4, 12].

The economic potential, the climate change and the fossil source supply difficulties and exhaustion have driven some countries to introduce regulations that encourage the energy efficiency, the emission reductions and the use of renewable sources. In 1997, the Kyoto Protocol [13] was the first agreement between nations to mandate country-by-country reductions in greenhouse-gas emissions [14]. The Directive 2002/91/EC [15] "aims to promote the improvement of the energy performance of buildings" [16] and the Directive 2009/28/EC [17] "establishes a common framework for the promotion of energy from renewable sources" [18]. In addition, the EN 15251:2007 "specifies the indoor environmental parameters which have an impact on the energy performance of buildings" [19].

According to Crawley [11], building energy simulation can be used by politicians to address location-specific responses to potential scenarios.

1.2 Building energy simulation

In order to obtain the energy savings introduced in section 1.1, the accurate prediction of the long-term building energy behaviour is required. However, building responses are complicated, nonlinear, and dynamic [5]: to address the analysis, simulation programs have been in use and development for more than 40 years [11, 20]. The building energy simulation embodies numerous calculation procedures which envisage the use of simulation softwares for evaluating energy efficiency, renewable energy, and building sustainability [21].
These tools are efficient methods to predict the building future performance [5, 22, 23] and can be used for building design or retrofit, overheating prediction, heating and cooling system design, new system installation impact and more [11]. The simulation codes are also needed because a simplified analysis (e.g. based on degree day analysis) may lead to large deviations, if compared to more sophisticated methods that take into account solar radiation, thermal mass or air humidity [9, 24, 11].

1.3 Climate impact

According to IEA Annex 53 [25], six main terms were identified as building energy performance influencing factors [6]:

- climate
- building envelope
- building equipment
- operation and maintenance
- occupant behaviour
- indoor environmental conditions

Among the required inputs in simulation tools, the meteorological data are one of the highest source of uncertainty [7]. The simulation codes need several data that are, among others, the hygrometric air conditions, solar and wind data. These weather parameters affect both the building energy behaviour [6, 8] and HVAC sizing outcomes [5]. Therefore, deepening the analysis of the interactions between building energy performance and climate is foundamental [3].

1.4 Global warming

Until recently, world societies did not realize the potential effects of the global warming on the atmosphere and world climate [4]. Today, the world scientific community has recognized the impact of anthropogenic behaviour on global warming [26]. The effects are alarming and they imply, among others, warmer summers, colder winters, and more frequent extreme weather events [27].

The Intergovernmental Panel on Climate Change (IPCC) has analysed greenhouse gas emissions derived from human activities, focusing on the potential effects on climate. General Circulation Models were developed to address the issue with numerical codes. The GCMs are defined as "numerical models representing physical processes in the atmosphere, ocean, cryosphere and land surface, for simulating the response of the global climate system to increasing greenhouse gas concentrations" [28]. The four primary GCMs are [11]:

- HadCM3 (United Kingdom)
- CSIRO2 (Australia)
- CGCM2 (Canada)
- PCM (USA)

In literature, several authors focused their studies on global warming effects on building energy performances, showing that climate change has significant impacts on building energy consumption [5, 29, 30, 9, 31, 32]. The climate change impact on buildings has become crucial for both mitigation and adaptation purposes [33, 34, 35]. Despite the impact in the short term being low, significant variations are highlithed for long term scenarios and should be taken into account for long-life projects [36].

Crawley [11] studied the impact of the main climate change scenarios for 25 locations and applied them to prototypical small office buildings. The author highlighted that, depending on the climate type, a general heating decrease and cooling increase is detectable. The overall energy consumption trend is strongly influenced by the climate typology [37, 31]: an energy reduction is estimated for cold climates [3, 38], whereas an increase may occur for warmer areas [11, 38]. However, the savings also depend on the building typology and its use [3].

1.5 Weather station

Accurate and reliable weather data are fundamental for the building energy simulation practitioners [5]. The climate boundary conditions, introduced in section 1.3 and described in Chapter 3, are usually stored in text files whose data are read by building simulation softwares. According to Lund [39], it is important that the climate information maintain the cross-correlation between the variables. Therefore, the weather conditions need to be measured and recorded: weather stations are used to fulfill this task. Automatic weather stations are defined as "meteorological stations at which observations are made and transmitted automatically" [40].

However, automatic and manual weather stations use sensors that share the same functionalities [41].
An average process is recommended to reduce the uncertainty of the reported data [41]. Except for the wind and wave measurements, most of the variables are reported as 1 to 10 min averages, obtained with a linearisation of the sensor output. The averaged values may be considered as "instantaneous" for most of the applications in which they are assessed; however, these values do not have to be mistaken for the raw sensor data.
In Table 1.1 the sensors' types are summarized.

Variable	**Unit**
Atmospheric pressure	[Pa]
Temperature	[°C]
Humidity	*
Wind speed	[m/s]
Wind direction	[°]
Precipitation	[mm]
Sunshine	[hours]
Radiation	[Wh/m^2]
Cloud height	[m]
Visibility	[m]

Table 1.1: Sensors typologies. *: the unit may change depending on the reference variable

Temperature: Many measurement techniques exist: those usually adopted in weather stations are resistance thermometers or thermistors [41]. These measurements usually require linearisation. The instrument has to be shielded from solar radiation and artificially ventilated, avoiding aerosol and drizzles content in the ventilation air flow rate [41].

Humidity: A hygrometer is defined as an instrument that can measure the humidity or psychrometric state of air [42]. It can measure different air properties such as wet-bulb temperature, relative humidity, humidity ratio, dew-point temperature. Relative humidity sensors are widely used due to their relatively low cost. Critical aspects may occur when dealing with pollutants in the air or with air temperatures below 0°C. The dew-point measure is the most promising technique although it presents high sensibility to power failures, if adopting lithium chloride sensors [41]. Since the dew-point is a temperature, radiation shields and ventilation are required.

Radiation: The global solar radiation is the most common solar measurements recorded by weather stations [43]. It is usually recorded on horizontal plane. It is the total irradiation evaluated in a specific point and it is the sum of three components: direct, diffuse and reflected radiations [44]. The diffuse solar radiation is defined as the solar shortwave energy scattered downwards by various elements present in the atmosphere [45]. The three components can be measured with different instruments. As regard the global solar radiation on horizontal plane, the pyranometers

are widely used. They are characterized by an hemispherical field of view [46] and can measure diffuse horizontal radiation, if installed with a shadow element (e.g. a shadow band). Finally, the direct horizontal radiation (assuming the absence of reflected radiation) is obtained by subtraction. Therefore, two or more pyranometers are often installed in a single weather station.

The direct normal radiation, DNI, is defined as the direct irradiance received on a plane normal to the sun [47]. It is measured with the pyrheliometer that present a narrow field of view [46]. Due to the solar apparent path, the instrument needs to be installed on a solar tracker to measure the DNI during the day.

As for radiation measure instruments, the critical aspects are the cables' electromagnetic interference and the presence of contaminants, such as dust, in the front aperture.

Wind: Two wind characteristics are recorded: wind speed and direction.
As regards wind speed, anemometers are widely used. Anemometers are composed of three or four hemispherical cups, radially displaced from a vertical support: the wind leads the cups to rotate [42]. The main issue is related to mechanical parts' freezing, during cold periods; however the risk can be avoided with electric resistances [41]. Wind averages are collected between 2 and 10 minutes, while wind gusts are usually based on 3-second measurements. As for the wind direction, wind-vane devices with digital encoders are used [41].

Chapter 2

Solar split model impact

2.1 Problem definition

Dynamic building energy simulations, usually carried at least on hourly basis, require detailed environmental data such as temperature, humidity, wind velocity and direction usually available from a number of climatic stations. However, direct normal radiation and diffuse horizontal radiation are also required in order to compute solar load. Unfortunately, continuous records of DNI are scarce due to the cost of the equipment: the monitoring stations equipped with solar trackers are very rare. An intermediate solution is to record diffuse and global irradiance, but there are numerous locations around the world where global insolation has only been monitored. Therefore, a great number of climatic data report only this value.

Starting from the work of Liu and Jordan [48], many efforts were made to develop separation models to estimate the diffuse horizontal irradiation component and, by subtraction, the direct horizontal component. Thereafter, the direct normal radiation is obtained dividing direct horizontal radiation by the cosine of the zenith angle, properly averaged on the interval monitored. In literature, more than 150 models have been developed with numerous comparison papers. Nevertheless, defining a universal model able to provide the best possible result at any specific location is complex, because algorithms are usually expressed in terms of first to fourth degree polynomial functions, empirically derived from site-specific measurements. This technique usually tends to suffer for excessive model localization and/or overfitting which implies that one model can lead to accurate results for a location, while performing poorly for a different one.

2.2 Analysis scope

This analysis describes the performance of different split algorithms using a dataset containing global and diffuse irradiance measurements recorded in Trieste. The availability of a large number of climatic data, which spans a period of ten years, allows for a deep comparison among split methods. Therefore, the former part of this chapter is focused on the statistical analysis of the models while the latter explores the effect of the different split methods on building energy simulations.

2.3 Dataset

The data used is composed by a 10 year records from Trieste (45.65°, 13.76°), collected by the Meteorology and Oceanography Laboratory of the University of Trieste and containing global and diffuse horizontal irradiation measurements with 10-minutes interval detection. The total number of available data is 525888 and includes also these exogenous measurements: dry bulb temperature, relative humidity, wind speed and wind direction. Solar position has been considered in the middle of the measurement interval, shifting the time detection back of 5 minutes for all the dataset, since the row data were originally recorded as averaged solar measurement in Wh/m^2 and reported at the end of the interval. The global horizontal irradiation has been used as the input data for the application of split methods, while the diffuse, and hence the direct horizontal data, have been used as the reference value.

2.3.1 Weather Station

The weather station is located on the top of the roof of the Nautical State Institute of Secondary Education ("Istituto Statale di Istruzione Superiore Nautico"), in piazza Hortis, Trieste. The weather station is not shaded by any surrounding building. The solar radiation is recorded by two pyranometers: one was dedicated to the global radiation and the other to diffuse radiation measurement. The second is equipped with a shadow band, therefore, the direct radiation on the horizontal plane could be obtained by subtraction with the equation 2.1.

$$DIR_h = GLO_h - DIF_h \tag{2.1}$$

Where:

GLO_h	is the global solar radiation on horizontal plane
DIR_h	is the direct solar radiation on horizontal plane
DIF_h	is the diffuse solar radiation on horizontal plane

The two pyranometers used to measure the global solar radiation and the diffuse solar radiation are the same model, the Kipp & Zonen CM 11. One of them is provided with a shadow ring CM 121 that was manually adjusted during all the recording period. The pyranometers are classified as "secondary standard" in accordance with the World Meteorological Organization (WMO).
The sensitivity is $\pm 0.5\%$ and it was calibrated by comparison with an outdoors calibrated reference pyranometer: the pyranometers were mounted horizontally, side by side. The source was a tungsten-halogen lamp with 1000 W power, 3300°color temperature and normal incidence angle.
According to our information, it was not possible to estimate an overall uncertainty on the measurements.
The weather station also included a combined sensor for dry-bulb air temperature and relative humidity, a sensor for wind direction, an anemometer and a rain sensor. The sensor list is showed in Table 2.1.

Type	Make	Model	Variable	Unit	Sensitivity
Data Logger	Nesa Srl	AND-TMF500			WMO Annex n.8
Pyranometer	Kipp & Zonen	CM 11	Global radiation	W/m^2	± 0.5% W/m^2)
Pyranometer	Kipp & Zonen	CM 11 + CM 121	Diffuse radiation	W/m^2	± 0.5% W/m^2)
Temperature Sensor	Nesa Srl	ANS-UTA-N	Dry-bulb air temperature	°C	WMO Annex n.8
Relative Humidity Sensor	Nesa Srl	ANS-UTA-N	Relatve Humidity	%	WMO Annex n.8
Wind Speed Sensor	Nesa Srl	ANS-VV-N	Wind Speed	m/s	WMO Annex n.8
Wind Direction Sensor	Nesa Srl	ANS-DV-N	Wind Direction	°	WMO Annex n.8

Table 2.1: The weather station sensors' list

2.4 Model Selection

Since the first split model proposed by Liu and Jordan in 1960 [48], many models were developed in literature. According to Lannini [49], three different types of models can be considered: polynomial models, exponential models and logistic models. All of these categories use predictors, intended as a measurement or an evaluated variable, which is required for applying the model. In all the proposed models of this analysis the clearness index k_t, defined in equation 2.2, is used as predictor. The diffuse fraction k_d, defined in equations 2.3, is the model outcome.

$$k_t = GLO_h / E_{oh} \tag{2.2}$$

$$k_d = DIF_h / GLO_h \tag{2.3}$$

Where:

GLO_h	is the global solar radiation on horizontal plane
E_{oh}	is the extraterrestrial solar radiation on horizontal plane
DIF_h	is the diffuse solar radiation on horizontal plane

The extraterrestrial solar radiation was calculated with Spencer Fourier series expansion. Other predictors can be used as well. As highlighted in Paulescu 2015, they can be grouped in kt class predictors and exogenous predictors as dry bulb temperature, dew point temperature or relative humidity. Table 2.2 presents the chosen models: it is not a comprehensive list of the models that can be found literature, that are more than 140 [50].

Id	Model	# predictors
1	Orgill and Hollans	1
2	Reindl1	1
3	Reindl2	2
4	Hawlader	1
5	De Miguel	1
6	Karatasou	1
7	Erbs	1
8	Chandrasekaran	1
9	Oliveira	1
10	Soares	1
11	Lam Li	1
12	Furlan 1	1
13	Lee	1
14	Maxwell	2
15	Macagnan	2
16	Boland 2001	1
17	Louche	2
18	Spencer	1
19	Jacovides	1
20	Boland 2008	1
21	Reindl3	4(2)
22	Perez	4(1)
23	Ulgen Hepbash	1
24	Ruiz-Arias	2
25	Chikh	1
26	Engerer2+Bird	5
27	Paulescu and Blaga 1	1
28	Paulescu and Blaga 3	1
29	Paulescu and Blaga 4	4(2)
30	Paulescu and Blaga 5	2
31	Elminir	1
32	Al Riahi	1
33	Torres	1

Table 2.2: Models analysed with total number of required predictors and number of exogenous predictors in brackets

2.5 Quality control

The a posteriori quality control of the measured data was followed as described in Gueymard [50] and summarized in Table 2.3. Applying this quality check, the number of valid points were reduced from the original 525888 to 239594, taking into account night hours too. The PSA algorithm (Blanco-Muriel [51]) was used to calculate the position of the sun. Finally, the maximum allowable value of clearness index kt has been forced to 1, but this condition had to be enforced 3 times only.

Id	Limit	Npe
a	$Z < 85°$	284736
b	$GLO_h > 0$ and $DIF_h > 0$ and $DIR_h \geq 0$	267586
c	$DIF_h < 0.95 \cdot E0 \cdot \cos^{1.2} Z + 50$	95
d	$GLO_h < 1.5 \cdot E0 \cdot \cos^{1.2} Z + 100$	71
e	$DIF_h/GLO_h < 1.05$ and $Z < 75°$	934
f	$DIF_h/GLO_h < 1.10$ and $Z > 75°$	1120

Table 2.3: Quality checks applied and number of eliminated points (Npe) for each rule

An additional correction has been adopted by limiting minimum and maximum values of the estimated diffuse fraction to 0 and 1 respectively, in order to prevent unphysical results. This last quality check avoids negative diffuse irradiation or diffuse irradiation greater than the global irradiation. It is worth noting that the diffuse radiation lower limit of 0 represents an unreal value too, since even with the clearest sky condition, the diffuse fraction should be present too.

2.6 Statistical Indicators

In order to evaluate the performance of the models, three statistical errors were used: mean bias deviation, mean absolute deviation and root mean square deviation, defined as it follows.

$$MDB = \frac{\sum_1^n (DIFe_i - DIFm_i)}{n} \tag{2.4}$$

$$MAD = \frac{\sum_1^n |DIFe_i - DIFm_i|}{n} \tag{2.5}$$

$$RMSD = \sqrt{\frac{\sum_1^n (DIFe_i - DIFm_i)^2}{n}} \tag{2.6}$$

Where subscript “e” indicates the estimated value, subscript “m” the measured values and n is the number of valid points after quality check. To develop a model comparison in depth, different location datasets should be considered. However, our purpose is to investigate the error that occurs because of the split model selection in defining climatic datasets for building energy simulations. The statistical analysis could help the designer in making a conscious choice between the proposed models. In this analysis, four models have been selected for a subsequent energy simulation analysis.

2.7 Results: Statistical Indicators

Tables 2.4 to 2.6 present, for each statistical indicator, the results obtained for the top five performing models

Model	MBD [W/m^2]
Oliveira	0.2
Maxwell	2.6
Ulgen Hepbasli	3.6
Torres	4.1
Perez	4.5

Table 2.4: Models with lowest mean bias deviation

Model	MAD [W/m^2]
Perez	26
Louche	27.7
Spencer	27.8
Soares	28.3
Ruiz-Arias	28.6

Table 2.5: Models with lowest mean absolute deviation

Model	RMSD [W/m^2]
Perez	45.6
Oliveira	46.6
Erbs	46.6
Torres	46.8
De Miguel	47.3

Table 2.6: Models with lowest root mean square deviation

From the analysis of the results, the Perez model shows remarkable results and performs slightly better than the others. Taking into account the full results, whose Tables 2.4, 2.5 and 2.6 are just a summary, the Perez, Oliveira and Torres models were chosen for carrying on building energy simulations. It is interesting to consider that the Oliveira and Torres models were obtained by linear regression applied to datasets collected in San Paulo (Brazil) and Pamplona (Spain), respectively. Probably, these models perform well also with the present dataset of Trieste because those locations have similar solar irradiation. Figure 2.1 presents the performance of each model applying the statistical indicator for each year of the dataset, therefore for each model a distribution over ten values is obtained. To compare the performance of the complete set of models the results are reported as box plots. The box extends from the first to the third quartile, the upper and lower whisker represent the minimum and maximum values of the set while the line drawn into the box represents the median of the distribution. Therefore, an idea of the distribution over the years can be obtained at a glance.

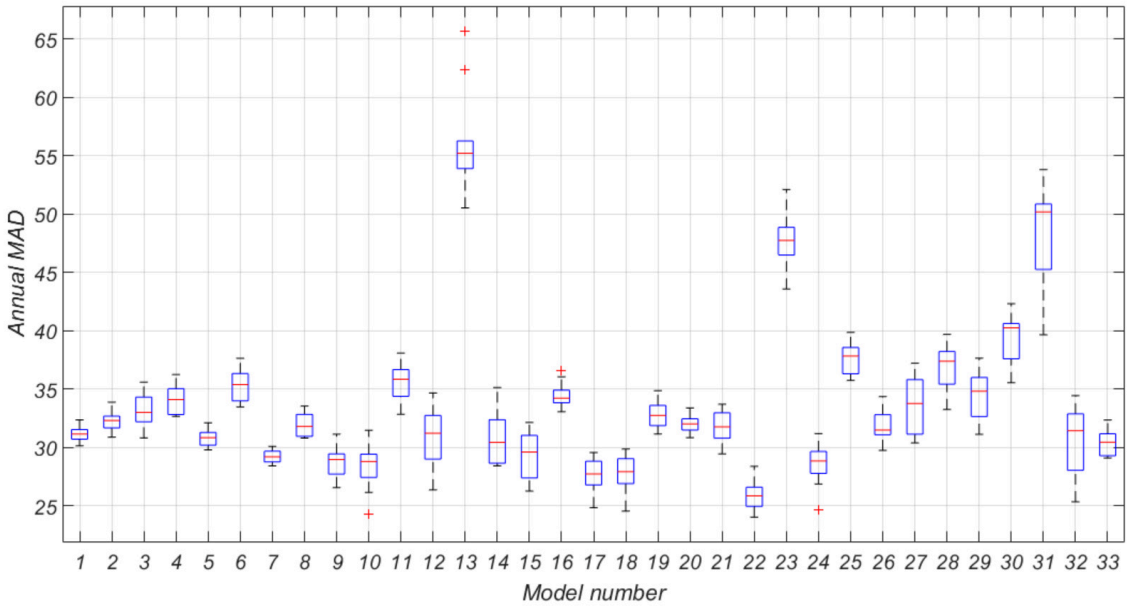

Figure 2.1: Distribution of MAD computed for every year of the dataset and each model

The inspection of Figure 2.1 shows which model performs better compared to the others, not only in an absolute manner, but also considering the results' dispersion: one model can perform well for one year but can give unsatisfactory results for other situations, with large dispersed values. Due to this consideration, we focused also on the Al Riahi model. As can be seen in Figure 2.1, the Torres model (model n. 33) and the Al Riahi model (model n. 32) have a comparable overall MAD on the entire dataset (red line within the box). However, it can also be noticed that the amplitude of Al Riahi box is remarkably greater than Torres box. Al Riahi model has therefore been added to the selected models: the goal is to observe how the performance discrepancy between different years influences the building energy simulation. In detail, the Al Riahi model has its lowest MAD for year 2003 (MAD 25.4) and its highest for the 2004 (MAD 34.5). This can be explained through the inspection of Figure 2.2: the year 2003 is catheterized by high mean global and direct irradiation, with a low diffuse fraction; on the contrary, the year 2004 shows low global and direct solar radiation paired with high diffuse fraction. The last condition is different from Trieste solar irradiation and from the original Al Riahi dataset, monitored in Baghdad. For the same reasons also the Torres model, collected in Pamplona, Spain, has its lowest MAD in 2003 while the highest is recorded in 2004.

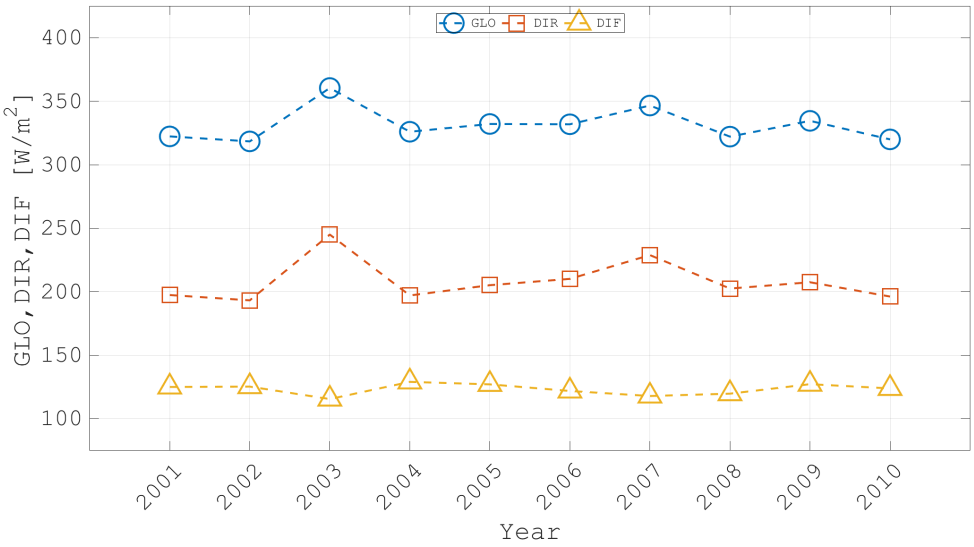

Figure 2.2: The mean yearly values of irradiance: Global, Direct and Diffuse on the horizontal plane

2.8 Model choice

Following the observation explained in the previous paragraph, we selected four split models: Oliveira, Perez, Al Riahi and Torres models. According to Lannini [49], except the Perez model that is classified as exponential model, the three others are polynomial models. Figure 2.4 presents the dispersion of diffuse fraction over the clearness index for the Perez model, while Figure 2.3 compares the same dataset with the Oliveira, Al Rhiai and Torres models.

2.8.1 The Oliveira model

The Oliveira model can be illustrated with a conditional equation, reported in equation 2.8.1. k_d varies with a fourth degree polynomial curve when k_t is lower than 0.75 and higher than 0.17, otherwise it is set to a constant value.

$$k_d = \begin{cases} k_t = 0 : & 0 \\ 0 < k_t \leq 0.17 : & 1 \\ 0.17 < k_t \leq 0.75 : & 0.97 + 0.8 \cdot k_t - 3 \cdot k_t^2 - 3.11 \cdot k_t^3 + 5.2 \cdot k_t^4 \\ k_t > 0.75 : & 0.18 \end{cases} \tag{2.7}$$

2.8.2 The Torres model

Similarly to the Oliveira model, the Torres model can be illustrated with a conditional equation 2.8.1. k_d varies with a fourth degree polynomial curve within a slightly different clearness index range: when k_t is lower than 0.755 and higher than 0.225. If k_t is less than 0.225, it uses a low slope linear curve, while k_d is constant when k_t is higher than 0.755.

$$k_d = \begin{cases} k_t = 0: & 0 \\ 0 < k_t \leq 0.225: & 0.9943 - 0.1165 \cdot k_t \\ 0.225 < k_t \leq 0.755: & 1.4101 - 2.9918 \cdot k_t + 6.4599 \cdot k_t^2 - 10.329 \cdot k_t^3 + 5.514 \cdot k_t^4 \\ k_t > 0.755: & 0.18 \end{cases} \tag{2.8}$$

2.8.3 The Al Riahi model

As showed in figure 2.3, the Oliveira, the Torres and the Al Riahi models share the same conditional form: unlike the two above mentioned, a linear equation is used when k_t is between 0.25 and 0.7, otherwise it is constant.

$$k_d = \begin{cases} k_t = 0: & 0 \\ 0 < k_t \leq 0.25: & 0.932 \\ 0.25 < k_t \leq 0.7: & 1.293 - 1.631 \cdot k_t \\ k_t > 0.7: & 0.151 \end{cases} \tag{2.9}$$

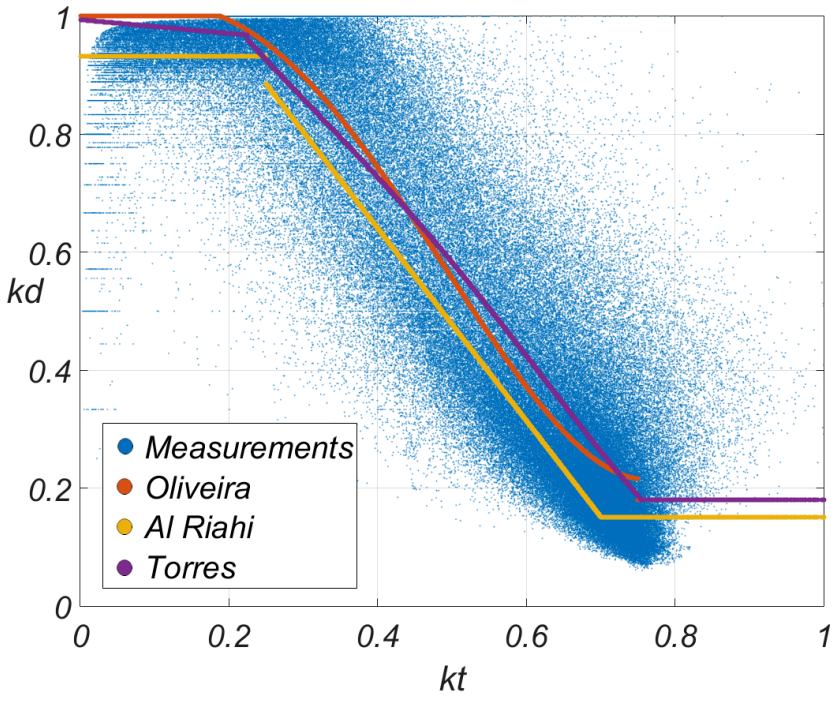

Figure 2.3: Oliveira, Al Riahi and Torres models

2.8.4 The Perez model

The Perez model was developed by Perez and al. [52] in 1992, also known as "DIRINT" model. It is based on the previous work of Maxwell [53] that introduced the "DISC" model in 1987: the Perez model can be presented as an improvement of the DISC model. It uses coefficients to adjust four sky-condition parameters accessible through bins (a sort of sky-condition based coefficients table indexing):

the coefficients are presented in multidimensional "look-up" tables. This approach, despite introducing a large number of coefficients, proves to be less computational demanding. The external conditions are parametrized as a multidimensional space: each dimension is referred to a sky parameter. Both the DIRINT and the DISC models use a Δk_t parameter called "stability index" that is based on the time series values: it is obtained from the recorded "last" and "next" k_t values for each iteration. This approach was also used by other authors [54][55][56].

In addition, the DIRINT model uses the atmospheric precipitable water, since it influences absorption and aerosol growth[52]. The atmospheric precipitable water can be directly obtained from the dew point temperature. The Perez model can be used both with the atmospheric precipitable water and without, if unavailable.
In this project the dataset included air dry-bulb temperature and relative humidity, therefore the dew point temperature was obtained. The Perez model was calculated with the atmospheric precipitable water, called "4-D" mode.
The DISC and the DIRINT models are shown below.

The DISC model

$$K_{nc} = 0.866 - 0.122 \cdot AM + 0.0121 \cdot AM^2 + 0.000653 \cdot AM^3 + 0.000014 \cdot AM^4 \quad (2.10)$$

$$\begin{cases} & a = 0.512 - 1.56 \cdot K_t + 2.286 \cdot k_t^2 - 2.222 \cdot k_t^3 \\ k_t \leq 0.6: & b = 0.370 + 0.962 \cdot k_t \\ & c = -0.280 + 0.932 \cdot k_t - 2.048 \cdot k_t^2 \\ & \\ & a = -5.743 + 21.77 \cdot k_t - 27.49 \cdot k_t^2 + 11.56 \cdot k_t^3 \\ k_t > 0.6: & b = 41.4 - 118.5 \cdot k_t + 66.05 \cdot k_t^2 + 31.90 \cdot k_t^3 \\ & c = -47.01 + 184.2 \cdot k_t - 222.0 \cdot k_t^2 + 73.81 \cdot k_t^3 \end{cases} \quad (2.11)$$

$$K_n = K_{nc} - \Delta K_n \quad (2.12)$$

$$\Delta K_n = a + b \cdot e^{C \cdot AM} \quad (2.13)$$

$$DNI = E_0 \cdot K_n \quad (2.14)$$

where:

AM:	Air mass	[-]
k_t	Clearness Index	[-]
E_0	Extraterrestiral Irradiance	W/m^2
DNI	Direct Normal Irradiance	W/m^2
K_n	Direct Normal Transmittance	W/m^2
K_nc	Clear-Sky Direct Normal Transmittance	W/m^2

The DIRINT model

$$k_t' = \frac{k_t}{1.031 \cdot e^{\frac{-1.4}{0.9 + \frac{9.4}{AM}}} + 0.1} \quad (2.15)$$

$$\Delta k_t' = 0.5 \cdot (|k_t' - k_{T,i+1}'| + |k_t' - k_{T,i-1}'|) \quad (2.16)$$

$$W = e^{0.07 \cdot T_d - 0.075} \tag{2.17}$$

k'_t bins table

Condition	Bin
$0 \leq k_t < 0.24$	1
$0.24 \leq k_t < 0.4$	2
$0.4 \leq k_t < 0.56$	3
$0.56 \leq k_t < 0.7$	4
$0.7 \leq k_t < 0.8$	5
$0.8 \leq k_t < 1$	6

Zenith bins table

Condition	Bin
$0 \leq Z < 25$	1
$25 \leq Z < 40$	2
$40 \leq Z < 55$	3
$55 \leq Z < 70$	4
$70 \leq Z < 80$	5
$80 \leq Z$	6

W bins table

Condition	Bin
$0 \leq W < 1$	1
$1 \leq W < 2$	2
$2 \leq W < 3$	3
$3 \leq W$	4
Not available W	5

$\Delta k'_t$ bins table

Condition	Bin
$0 \leq \Delta k'_t < 0.015$	1
$0.015 \leq \Delta k'_t < 0.035$	2
$0.035 \leq \Delta k'_t < 0.07$	3
$0.07 \leq \Delta k'_t < 0.15$	4
$0.15 \leq \Delta k'_t < 0.3$	5
$0.3 \leq \Delta k'_t \leq 1$	6
Not available $\Delta k'_t$	7

$$I_{DIRINT} = I_{DISC} \cdot LookUpCoeffs \tag{2.18}$$

where:

k'_t	Kasten Clearness Index[57]
$\Delta k'_t$	Dynamic Stability Index
W	Atmospheric precipitable water
T_d	Dew point temperature
I_{DIRINT}	Direct normal Irradiance, Dirint model
I_{DISC}	Direct normal Irradiance, Disc model
Z	Zenith angle

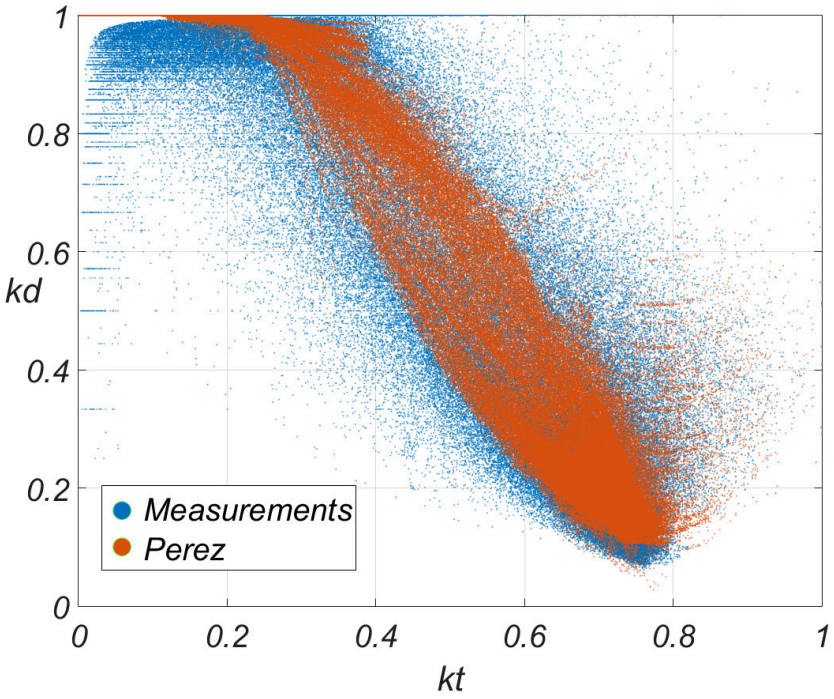

Figure 2.4: Perez model

2.9 Building envelope

The selected models have been used to generate climatic data in order to check the effect on building simulations. According to Pernigotto [58], a simple test building was simulated. It consists of a prism shape building with a square base, oriented to the main cardinal directions. Its internal floor area is 100 m^2 with 3 m internal height. All the opaque constructions are composed by two-layer structure with external isolation and 30 cm of concrete internal structure. Thermal bridges are neglected and no internal partitions were modelled. The material characteristics are reported in Table 2.7. The insulation thickness, reported in Table 2.8, was set in order to obtain the reference thermal transmittance, according to the Italian regulations for climatic zone E. Windows' characteristics were set to Uw = 1.8 W/m^2K and g = 0.35.

Layer:	λ[W/mK]	C_p[kJ/kgK]	ρ[kg/m^3]
Concrete	0.13	1.88	399
Insulation	0.04	1.47	40

Table 2.7: Layer material thermal proprieties

Construction:	U [W/m^{2}K]	s [cm]
External wall	0.3	9.41
External roof	0.25	12.2
Ground floor	0.3	9.25

Table 2.8: Thermal transmittance and insulation layer thickness

According to UNI/TS 11300-1 national technical standard [59], the opaque surfaces solar absorbance was set to 0.3, except for the internal floor and the external roof where a value of 0.6 was set. These values are relatively low and are recommended in the technical standard considering the Italian Mediterranean climate, where cooling system energy demand is relevant. Ground temperature at building surface and at ground deep temperature was considered as constant, respectively of 18 °C and 14 °C. In summary, the test building is composed of a well insulated envelope with external windows on the east, south and west facade, each one of 9,707 m^2 (29,12 m^2 of total area). This last choice was made to analyze a building with a wide window size that, as highlighted from Pernigotto [58], is critical for possible high cooling loads. Internal gains are constant equal to 4 W/m^2 with radiant and convective fraction of 0.5. Ventilation air change was set at 0.3 vol/h.

System	Begin	End	Setpoint [°C]
Heating	1/10	31/03	20
Cooling	1/04	30/09	26

Table 2.9: Beginning, end and setpoint temperature related to heating and cooling systems

Heating and cooling systems were simulated as an ideal system, 100% convective and with an unitary coefficient of performance. Heating and cooling systems are available according to Table 2.9.

2.10 Weather files

EnergyPlus simulation files require input variables, monitored or derived from pre-process, such as the DNI. Except for the Perez model that calculates DNI directly, in the other cases it was estimated through equation 2.19.

$$DNI = \frac{DIR_h}{\cos Z} \tag{2.19}$$

Due to the uncertainty of the measuring instrument at high zenith angles, equation 2.19 can return extremely high values (that were previously eliminated from the quality control, equation 2.4). This can lead to unphysical values, even higher than extraterrestrial solar radiation, which can themselves cause simulation errors if used in building simulation codes. The issue was solved, as was recommended by Spinelli F. (personal communication, 2016, ENEA - Italian National agency for new technologies, Energy and sustainable economic development), with the substitution

of out of range values, identified by applying the check reported in equation 2.20, with the DNI values obtained using the Bird clear-sky model [60]. The model, according to Sengupta [61], can be indicated as a promising model.

$$DNI < 1100 + 0.03 \cdot Elev \tag{2.20}$$

The application of Eqn. 2.20 resulted in 95 points replacement in the dataset, 499 in Oliveira, 533 for Al Riahi and 499 for Torres models. For all the variables previously described, the dataset was reduced from 10 minutes detection to hourly weather files by averaging.
The simulations, that are described in section 2.11, were carried out with 6 timestep per hours. Therefore, EnergyPlus performs an interpolation called "Last Hour Interpolation" to obtain solar values with a lower frequency that matches the calculation process [62]. The approach is repeated for every outdoor weather variable. The method is summarized in equations 2.21, 2.22 and 2.23.

$$\text{Value} = \text{Value}_{\text{LastHour}} \cdot \text{Weight}_{\text{LastHour}} - \text{Value}_{\text{ThisHour}} \cdot \text{Weight}_{\text{ThisHour}} \tag{2.21}$$

$$\text{Weight}_{\text{ThisHour}} = \frac{\text{CurrentTimeStep}}{\text{NumberofTimeStepinHour}} \tag{2.22}$$

$$\text{Weight}_{\text{LastHour}} = 1 - \text{Weight}_{\text{ThisHour}} \tag{2.23}$$

In Table 2.10, showed in EnergyPlus documentation [62], an example of weighing factors for 6 timestep is reported.

Timestep	**Time mm:ss**	**Weight Last Hour**	**Weight This Hour**
1	00:01 to 10:00	0.8333	0.1666
2	10:01 to 20:00	0.6666	0.3333
3	20:01 to 30:00	0.5	0.5
4	30:01 to 40:00	0.3333	0.6666
5	40:01 to 50:00	0.1666	0.8333
6	50:01 to 60:00	0	1.0

Table 2.10: Interpolation weight factors for 6 timesteps

2.11 Simulation results

Ten year measurements and four selected models were used to obtain 40 simulations related to the split models. The results were compared to a reference simulation with weather files obtained using the original dataset. In the following paragraphs the energy required for heating and cooling are analysed. As previously explained, we focused mainly on two different years, 2003 and 2004. The errors reported Tables 2.11 and 2.12 are defined in equation 2.24, where subscripts "se" and "sm" represent the simulation result with estimated and measured weather files, respectively.

$$Error = \frac{Energy_{se} - Energy_{sm}}{Energy_{sm}} \tag{2.24}$$

Year	Sim [kWh]	Oliveira [%]	Perez [%]	Al Riahi [%]	Torres [%]
2001	2678	+1,9	+0,5	+1,9	+1,6
2002	2539	+1,7	+0,2	+1,5	+1,4
2003	3852	+1,8	+0,4	+1,4	+1,4
2004	2585	+2,4	+0,5	+2,2	+1,9
2005	2377	+2,9	+1,3	+2,6	+2,6
2006	2718	+3,2	+0,8	+3,5	+2,7
2007	3001	+3,6	+1,4	+3,3	+3,1
2008	2910	+2,7	+1,8	+2,4	+2,5
2009	3190	+3,9	+2,5	+3,8	+3,6
2010	2580	+3,6	+2,2	+3,3	+3,3

Table 2.11: Cooling energy errors for the various models

Year	Sim [kWh]	Oliveira [%]	Perez [%]	Al Riahi [%]	Torres [%]
2001	2516	-0,3	+3,0	-2,9	+0,1
2002	2381	-1,5	+2,0	-3,9	-1,1
2003	2234	-1,3	+2,8	-4,4	-0,6
2004	2706	-1,8	+1,4	-4,4	-1,3
2005	2839	-2,4	+1,4	-5,1	-2,0
2006	2403	-1,5	+2,6	-4,2	-0,9
2007	2040	-2,7	+2,1	-5,8	-2,3
2008	2429	-2,9	+1,0	-5,5	-2,4
2009	2544	-3,6	+0,6	-6,0	-3,3
2010	3249	-3,0	-0,4	-5,0	-2,8

Table 2.12: Heating energy errors for the various models

As can be seen from Table 2.11, the Perez model performs remarkably better than the others for cooling energy, with errors ranging from 0.2% to 2.5%. Regarding heating energy, the Perez model achieves higher errors than cooling energy, but comparable with the Oliveria and Torres models. Furthermore, the distribution of the statistical error with box plots, presented in Figures 2.1, is confirmed by the numerical simulation: a model can perform very differently if applied to different periods on the same location. Considering Table 2.11, Torres and Al Riahi models present the same error for year 2003 but the former preforms well also for the other years of the dataset, while the latter shows consistently higher errors for numerous years. Finally Figure 2.5 graphically presents the trend of the errors reported in Tables 2.11 and 2.12, showing the best performance of Perez model in cooling simulations and a slightly better performance of Torres and Oliveira models for heating.

2.12 Final remarks

Considering the whole 10-year dataset, the Perez model performs significantly better than the others, both for MAD and RMSD statistic parameters. It shows also

consistency if applied to different years of the same location. Regarding polynomial models, they can perform with satisfying accuracy if the current dataset has similar climatic characteristics to the one originally used for obtaining the model. Those who behave better in this case are Oliveira and Torres.

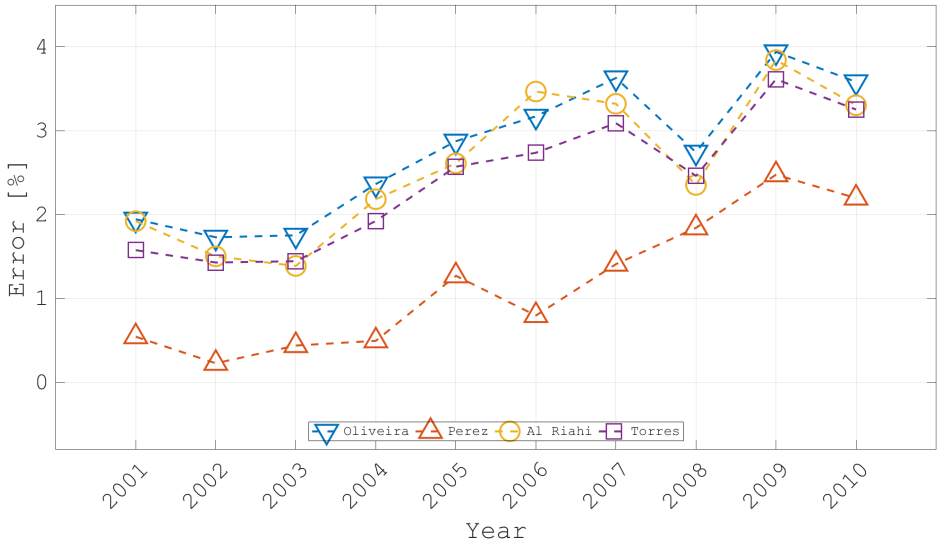

Figure 2.5: Cooling energy, percentage error between models and measured data

Furthermore, Al Riahi model were chosen: it has an overall MAD comparable to the Torres model but shows a greater range of variability between different years, mostly for heating period. This choice was taken deliberately to test this performance inconstancy with building energy simulations.

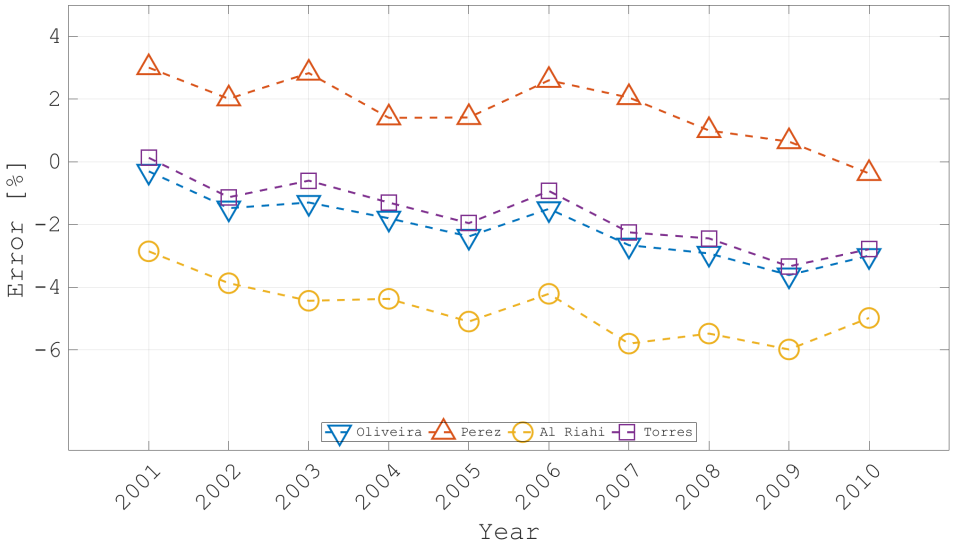

Figure 2.6: Heating energy, percentage error between models and measured data

Simulation results, applied on a test building with a well insulated envelope, has shown that Perez model performs extremely well for what concerns cooling energy. On the other hand, it underestimates the DNI during the coldest months: this

causes an overestimation of the heating energy, constantly higher than the other tested models. The Perez model shows the best overall performance, however, for a detailed simulation analysis, its DNI underestimation during winter time cannot be neglected, especially for insulated buildings. Regarding the influence of split models in simulation applied to insulated buildings, in this case study, the choice can affect the simulation error from 0.2% up to 4%. This result is remarkable and has to be considered when dealing with building detailed energy analysis. Nevertheless, the result is closely linked to the building characteristics: in this case a test building with high WWR was chosen to emphasize the solar radiation effect.

Chapter 3

Weather files typologies

3.1 Introduction

The modern simulations used to assess building energy [58, 63] and solar systems performances [64] need accurate meteorological data to be accomplished[65]. The most uncertain data to be implemented for these simulations are the climatic data [7]. According to Keeble [66], as regards building energy simulation weather files, three typologies can be identified:

- multi-year weather data AMY
- representative days
- typical or reference years TRY, TMY or DRY (8760 hours)

A description of the typologies is presented below.

3.1.1 AMY: actual meteorological years

Actual meteorological years, also known as AMY, are weather single-year series of a specific location [67]. Typical years gained great popularity compared to multi-year weather data also due to the lower computational work needed, that was a constraint for the limited computational power available in the past. Today, multi-core processors are widespread: parallel simulations and single-simulation time decrease allow multi-year simulations to be chosen when analysing building energy behaviour.
Regarding multi-year simulations, several authors studied and compared multi-year and TRY simulations outcomes [5, 6, 68]. Cui [5] performed an analysis related to the Chinese territory. The author wrote a deep introduction, first highlighting reference years' critical aspects which can be summarized as:

- typical year is derived from actual months that are selected using weighting factors that enhance some climate aspects over others. The factors' choice is related to a specific building or system typology that is somehow "an average building"
- typical years are expected to represent long-term climate conditions. While several authors confirmed this aspect [69, 70, 71], others found significant variations [68].

- reference years represent typical conditions, which is why they are not suitable to study extreme conditions building response

Cui illustrated the multi-year simulations benefits as well:

- studying a longer period leads to a more comprehensive and thorough analysis
- building designers and policy makers can employ result-based regulations

Also Barnaby and Crawley [36, 72] highlighted that the usage of single-year simulations cannot show the long-term variations and the peak energy consumption. The author also specified that uncertainty analysis can be unreliable. In addition, when dealing with a multi-year approach, the wrong or missing data represent an issue [68] that needs to be treated with interpolation methods [73].

3.1.2 TMY and TRY: Typical or reference years

According to Skeiker [74], TMY, TRY or DRY consists of 8670 hourly values made of single-month climate data selected from different years within a reasonably long [75] dataset. There are several versions with major or minor differences in the statistical methods used to generate them. They include: TRY, TMY, WYEC, CWEC, IWEC, DRY. Even though these datasets sometime contain synthetic solar data, they share a common feature: the selected months that compose the reference year are obtained from actual recordings [65, 74].
Although a multi-year approach shows undeniable benefits [5], at the state of the art, reference years are generally preferred [76, 77, 72]. Several authors studied the variability between single-year and multi-year energy consumption [78, 79, 80, 81]: for the U.S. and Hong Kong climates the maximum difference is around 10%. Therefore, single-year simulations can be used to obtain typical building energy performances [68] and are reasonably accurate [36]. For these reasons, the project takes into account reference weather data. Moreover, the choice of the weather file typology demands a pre-analysis: the case-study needs to be considered and, according to its characteristics, the appropriate weather file type has to be selected (Crawley D. B., personal communication, 8/11/2018).

3.1.3 SMY: synthetically generated meteorological year

Using dynamic simulation softwares, missing or invalid weather data (e.g. non-physical) need to be handled with care: for each simulation timestep, every climate variable has to be defined. As previously illustrated in section 3.1, missing or invalid data may be filled or replaced with interpolation methods [73].
Solar irradiation measurements are collected with instruments that require more maintenance and are relatively expensive. As a result, many weather stations do not record solar data, which is why the dataset is incomplete and the radiation has to be integrated through numerical models. As clarified in chapter 2, solar models take benefit of empirical-derived coefficients that are based on cloud conditions, for example, in the TMY3 data set, less than 40 out of 1020 stations include solar records [36]. According to Meteonorm sources [82], the most accurate data are provided by well-maintained weather stations.

In the last years, satellite-based values have taken root: they are presented as valuable sources [82]. Accordingly, Perez [83] showed that, for locations which are more than 25 km far from the closest weather station, satellite values appear to be the most accurate for hourly global irradiance [36].
Hourly weather data are not always provided [5], especially in developing countries that may not have meteorological stations at all [84]: a SMY is a practical option [85]. Weather data at higher detecting frequency (daily or monthly) are used to obtain hourly values [5], which enables the acquisition of data related to actual recordings. Knight [86] developed a methodology to provide synthetic data from limited recordings: the method was integrated into the TRNSYS simulation tool [87] with Type 54 and it is based on the algorithm developed by numerous authors [88, 89, 90, 91, 92, 93, 94, 95]. According to TRNSYS documentation [96], monthly average values enable the Type 54 component to generate hourly weather data as typical years. This methodology is widely used: Celink [97] and Argiriou [77] studied the method accuracy and applied it to PV systems and building simulations, respectively. As reported by Lhendup [84], this approach has been widely adopted for research purposes [98, 99, 100, 101, 102].

3.2 Required data

Barnaby [36] analysed the most important weather variables, the ones affecting energy simulations are listed in Table 3.1.

Weather variable	**Usage**
Dry-bulb air temperature	• Exterior surface convection • Infiltration/Ventilation sensible heat transfer • Equipment
Humidity	• Infiltration/Ventilation latent heat transfer • Equipment
Solar irradiance	• Fenestration heat gain • Exterior surface heat balance • Solar thermal photovoltaic system
Wind velocity and direction	• Exterior surface convection • Infiltration • Natural ventilation
Sky temperature	• Exterior surfaces heat balance
Ground temperature	• Heat transfer
Ground surface albedo	• Reflected irradiance

Table 3.1: Main weather variables affecting energy simulation

As highlighted from Barnaby [36], the items described in Table 3.1 present critical issues. Dry-bulb air temperature and a second psychometric variable, which could be relative humidity, wet-bulb air temperature or dew-point temperature, are commonly collected. Care must be taken when using a weather file obtained from open space locations outside cities (e.g. from airports) to simulate urban context building: the heat island effect could significantly affects simulation outcomes [36].

As regard solar irradiation, direct measurements are rarely taken and they mostly collect global horizontal radiation only. However, building energy simulation requires the solar radiation to be split into its components: the diffuse horizontal radiation and the direct normal radiation. As explained in chapter 2, the measurement instruments able to collect direct normal radiation data are extremely rare because of their cost. Therefore, if the global solar radiation is the only one available, numerical methods are used to calculate its components. The same view can be considered for sky temperature, it is usually calculated with appropriate models. Wind observations include wind velocity and directions. The wind data are used to calculate infiltrations, natural ventilations and external convection heat transfers: nonetheless, compared to primary variables, its effect on simulations' results is lower for some building typologies and climates [103, 104]. In addition, since wind parameters are strongly affected by territory topography and surrounding buildings, they cannot be modeled with simple methods. The estimation of wind velocity and direction often requires on-site measurements, scale model wind tunnel studies or CFD modeling [36] that are all time-consuming operations. Ground temperatures affect below-grade heat transfer, however, the measurements are scarce and they are usually referred to "undisturbed" soil temperature that does not consider the heat storage capacity of the ground over time [105]. Finally, ground surface albedo is important for solar radiation on snow-covered territories and its effect was studied by Skartveit [56].

3.3 Methodologies

According to UNI EN ISO 15927-4 [75], a reference year is an artificial year that is suitable to determine the average annual energy for heating and cooling. It is a representative database that is usually known as typical meteorological year (TMY) in the U.S.A. and test reference year (TRY) in Europe [74].
In literature, several methodologies were proposed; one of the first was released in 1976 by National Climate Data Center [106]: these weather files are called TRY-US. Unlike more modern methods, and similar to the EWY [67], the outcome does not consist of a collection of months, but rather of an entire year that actually occurred, that is not an artificial year. In this case, the selected year is identified gradually removing the years that contain months with outliers mean temperatures. Since they are obtained from totally different approaches, the TRYs described below and TRY-US are not comparable.
In 1978, Hall presented a different methodology [107]. It was based on Filkenstein–Schafer statistic [108] and it selected single months from different years of the dataset [74]. The outcome was an artificial year that collected the most representative months of the dataset [68]. According to Lund [39], the approach allowed to maintain the cross-correlation between the variables.
Other methods present a roughly equivalent procedure, but they differ in terms of:

- Weighting factors, used to select reference year' months [5, 68]
- Number of parameters to consider [5]
- The statistic used. Many of the methods use the Finkelstein-Schafer, while others [109] used the Kolmogorov–Smirnov [68]

Therefore, these methodologies are intended to identify hourly data, from a much wider dataset, that are representative of a specific location' climate.
The following table, Table 3.2, summarizes the main methodologies, sorted by date.

Name	Authors	Year	Reference
TRY-US	National Climatic Data Center	1976	[106]
Belgian method	Dogniaux and Sneyers	1977	[110]
TMY	Hall, Prairie, Anderson and Boes	1978	[107]
	Crow	1984	[111]
Pissimanis T	Pissimanis, Karras, Notaridou and Gavra	1988	[112]
Pissimanis R	Pissimanis, Karras, Notaridou and Gavra	1988	[112]
	Festa and Ratto	1993	[109]
TMY2	Marion and Urban	1995	[113]
Danish method	Lund	1995	[39]
	Argiriou	1999	[77]
	Gazela and Mathioulakis	2001	[114]
	ISO 15927-4 methodology	2005	[75]
	Miquel and Bilbao	2005	[115]
TMY3	Wilox and Marion	2008	[116]
Best Rank 1	Pernigotto, Prada, Gasparella and Hensen	2014	[117]
Best Rank 2	Pernigotto, Prada, Gasparella and Hensen	2014	[117]

Table 3.2: Methodologies summary table

Chapter 4

Wheather file impact: simulation

4.1 Problem definition

As highlighted in chapter 1, computer-aided simulation is a powerful tool used by designers and researchers to study building energy aspects. Simulations are carried out with boundary conditions defined into a weather file that considerably affects energy outcomes. Despite weather data impact on building simulation results being widely analysed in literature, the topic is still meaningful especially because of climate change, which affects external building conditions. In Italy, two weather files are widely used: the oldest, the IGDG dataset, is already available to the users through the EnergyPlus database. More recently, a new dataset has been provided by CTI, and has been generated using recent weather data measurements.

4.2 Literary review

Weather data are widespread and largely used in building simulations. In literature, the weather file impact was analysed in single simulations, multiple-years simulations and in building optimization. Typical weather data, for a one-year period, consists of hourly meteorological parameters obtained from long-term data. They can be generated using different calculation methodologies that aim to create some form of a most average year: it is a common approach [118] and it is generally preferred to AMY, that is recorded data spanning multiple years [104, 76, 119]. The climate parameters are connected with each other [120, 121, 122] the methodologies to obtain reference years are expected to maintain cross-correlation between the climate data [39]. The typical meteorological year and the test reference year are the most popular methods in literature [104]. The test reference year is a weather file typology obtained from weather recordings statistically identified to compose a climatic representative year. The Finkelstein-Schafer statistic, described in EN ISO 15927-4 technical standard [75], is an approach frequently found in literature to generate TRY [107, 104]. Several methods were nonetheless developed both for TRY [7, 104] and for TMY [74]. Sorrentino [7] studied three statistical methods to calculate TRYs applied to a dataset collected in Palermo: he compared their impact on PV systems and building energy simulations. The results highlight a better performance for the Hall, Prairie, Anderson and Boes method. Crawley [72] presented results for an office building simulated with multiple-year weather data and different single-year weather data-set types for eight U.S. locations. He com-

pared the influence of the various weather data sets on simulated annual energy use, costs and annual peak loads. Tianzhen Hong [6] analysed the weather impact on peak electric demand and energy use via building simulations using 30-year actual weather data for three types of office buildings at two design efficiency levels across all 17 climate zones. The simulated results from the AMY are compared to those from TMY3 to determine and analyse the differences. Also Cui [5] focused on actual weather data, comparing simulation results assessed with a 55-year dataset in 10 cities in China. The author underlined that weather varied significantly from year to year and typical year cannot reproduce the fluctuation: in particular, peak loads are more affected than energy consumption. Pernigotto [68] studied the representativeness of EN ISO 15927-4 method, applied to northern Italy climate. The author compared energy consumptions derived from the reference year and multi-year simulations and analysed energy variability. TRY are generated using past weather data measurements. However, the efficiency of a refurbishing measure is assessed in the future, which is why numerous authors focused on applying future climate scenarios to building simulations, comparing energy demand and refurbishment effectiveness. Hosseini [123] generated future weather condition files using a prediction model for roof design optimization. Huws [124] analysed the impact of retrofit measures on future carbon emissions using current and future climatic data. Ciulla [125] adopted a similar approach to investigate the refurbishment effects on a social housing stock in Italy, highlighting the cost optimality of moderate measures. Eames [126] investigated climate spatial distribution derived from UKCP09 weather generator, in the UK territory. The author studied both current and future climate change spatial variation scenarios, focusing on the differences of the UKCP09 adjacent areas. Rubio-Bellido [127] investigated climate data for future scenarios and the effect on energy demand in office buildings in Chile. Unlike the previous cases, the author implemented the monthly model defined in EN ISO 13790:2008 [128]. Considering the Italian climatic panorama, research was conducted on the effect of weather files and thus on building energy simulations. Chiesa [129] performed a parametric study on the effect of different TMY. The author analysed three Italian cities with dynamic simulations and 21 Italian locations calculating CDD, HDD, annual global horizontal radiation and wind speed. As underlined by the author, further applications to a larger variety of climate zones and building types is expected to consolidate such outcomes. Murano [130] carried out a similar research, focusing on an NZEB single-family house and extended it to seven different locations which were representative of the Italian climate. The author highlighted the cooling and heating differences, calculating also the percentage differences. Pierangioli [131] developed a refurbishment energy saving analysis based on six different buildings from the IEE TABULA [132] project method. Different building types were used: small multi-family houses, medium multi-family houses and apartment blocks. He carried out dynamic simulations using a representative weather file and two different future data sets obtained with morphing techniques related to the periods 2036-2065 and 2066-2095. He applied this methodology to two different locations in central Italy: Florence and San Vincenzo. The author focused on different design solutions selected with an energy-economic analysis.

4.3 Analysis scope

The aim of this analysis is to study the impact of the choice of weather files on building energy simulations, comparing the results obtained using two datasets recorded in different periods. The results refer to the Italian multifamily-house stock and illustrate both energy consumption and energy savings, derived from refurbishment activities. The major objective of this work is to highlight the differences a practitioner can obtain in choosing an already available, but outdated dataset instead of a newer one. It is worth noting that the different results can be due to the period of data collection for weather file generation and possibly different locations, if the same site is not available in both datasets. To enhance the significance of the results the analysis covers the entire Italian territory analysing 52 locations. Furthermore, for each location the energy analysis is carried out on 7 buildings typologies considering also the effect of refurbishing activities. In author's knowledge, such analyses have never been realised considering the whole Italian territory and existing Italian building stock.

4.4 Methodology

As highlighted in the introduction, the locations in the territory and the building archetypes have a key role in the analysis. To operate with different weather data, locations and building fabrics, a procedure had to be implemented in order to run multiple simulations, to modify the building characteristics taking into account the location across the Italian territory and to collect the results. Furthermore, since the weather stations in the two datasets are not in the same position, a matching method is also needed. The simulations workflow is summarized in Figure 4.1: the red letters show the different steps of the implemented procedure. First, the models were obtained from TABULA data (a) and modelled with DesignBuilder [133] (b). The IDF file (EnergyPlus text model file) was exported (c) and edited with EPPY [134], a python scripting language precisely aimed at IDF editing (d) generating new IDF files referring to a specific simulation (e). The EPPY script in step (d) takes care of the matching between CTI and IGDG weather files (f), starting from the location of the CTI weather file (g). The matching method is described in section 4.7. The process required data related to the building location as an input: building location information and heating schedules, according to different climatic zones, were procedurally modified. Therefore, 52 models were obtained for every TABULA building, for both uninsulated and insulated buildings, for a total of 728 models (e). Finally, within the same script, the simulations were carried out (f) and the related results were read from EnergyPlus output files and converted into dataframes for data analysis (h). The dotted box represents the iterative workflow (i), applied to all the not-rejected matchings obtained between the CTI and IGDG weather files. Section 4.5 describes the generation of building geometries and characteristics, Tables from 4.1 to 4.7 collect the main assumptions regarding building definitions. Section 4.6 presents the characteristics of the weather datasets used. The key problem in the comparison methodology between different datasets is the algorithm for selecting the pairs of location to be used in case weather stations do not coincide, to solve the problem the matching algorithm is presented in section 4.7 with the selected pairs listed in Tables 4.8 and 4.9. The results are then analysed

in section 4.8.

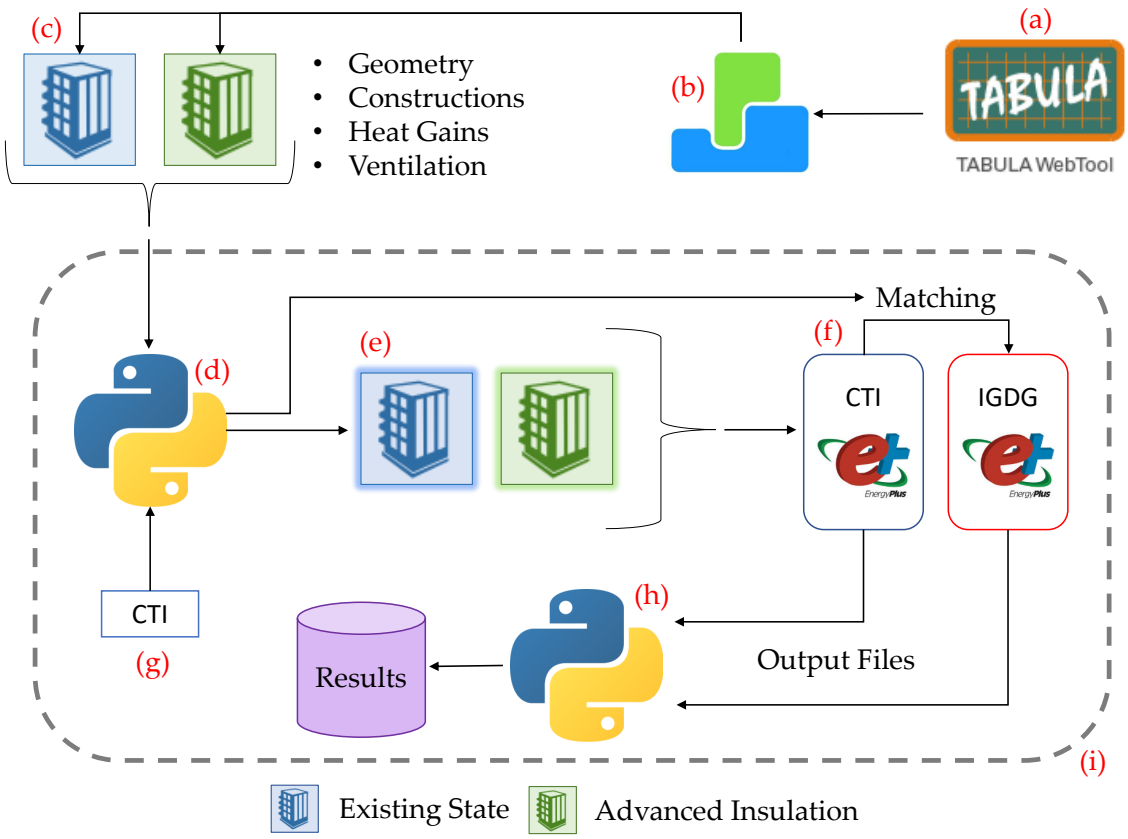

Figure 4.1: Workflow scheme

4.5 Building model description

Tabula web tool [135] is a web service where European building stock data are provided, divided by age, size and country. External surfaces areas and the related thermal transmittances are given, for the original building, along with usual and advanced refurbishments. In this analysis the insulated building corresponds to the advanced refurbishment solution of Tabula. Tabula information was used to develop the geometry and the construction model. Since architectural drawings are not provided, the building geometry was obtained solving an equation system. The stairwell areas were not modelled. Tabula gives different building typologies: single family house, terraced house, multifamily house and apartment block. This research focuses on Italian multifamily houses, divided into eight different periods, from the construction age before 1900 until today. Building characteristics are summarized in Table 4.1.

Construction period	Area [m^2]	WWR [%]	Volume [m^3]	HLS [m^2]	S/V [m^-1]
… - 1900	647	11.11	2684	1425	0.53
1921 - 1945	1165	11.99	4388	2243	0.51
1946 – 1960	961	20.84	3076	1551	0.50
1961 – 1975	934	9.33	3074	1667	0.54
1976 – 1990	1210	12.47	4136	1994	0.48
1991 - 2005	1120	14.56	3526	1763	0.50
2006 - …	915	13.92	2959	1357	0.46

Table 4.1: Buildings areas and characteristics

4.5.1 Heat Gains

Internal heat gains were modelled in accordance with EN ISO 13790:2008 technical standard, where time-varying internal gains are described for living room, bedroom and kitchen room types. Since no zoning was defined in the models, a fixed space distribution was set to calculate heat gains, as shown in Table 4.2.

Space Type Area	%
Bedroom	50
Kitchen and living room	35
No gain areas	15

Table 4.2: Space distribution within the thermal zones

Electric heat gains can be summarized into a maximum design power of 4.6 W/m^2. Occupancy was set to a maximum of 0.04 people/m^2 with metabolic heating rate set to 110 W/person during day and 85W/person at night. According to the Italian regulations, the heating period during the year and the relative switch-on hours during the day were set depending on the climatic zone, which was calculated directly from CTI climatic files, considering the HDD. The adopted schedules are shown in Table 4.3.

Zone	From HDD	To HDD	Working-hours	Start Date	End Date	Start Hour 1	End Hour 1	Start Hour 2	End Hour 2
A	0	600	6	01/12	15/03	8	11	19	22
B	601	900	8	01/12	31/03	8	12	18	22
C	901	1400	10	15/11	31/03	8	13	17	22
D	1401	2100	12	01/11	15/04	8	14	16	22
E	2101	3000	14	15/10	15/04	8	22	-	-
F	3001	-	-	-	-	0	24	-	-

Table 4.3: Climatic zone description with hour and date of heating system start-up and shutdown

Air temperature setpoint during the switch-on period was 20°C, while for the remaining hours, a set-back air temperature of 18°C was set. Cooling system availability

was modelled as always-on during the whole year. The air temperature was set to 26°C from 8 am to 10 pm: for the rest of the time, air temperature setpoint was set to 28°C. Heating and cooling schedules were modelled identically in both simulations, with CTI and IGDG weather files.

4.5.2 Heating and Cooling systems types

Heating and cooling systems types were modelled as ideal with 100% convective effects. It allowed the comparison of the energy consumption regardless the HVAC system typology. In order to model an ideal system, EnergyPlus [136] object ZoneHVAC:IdealLoadsAirSystem was used. It provides a model for an ideal HVAC system and it supplies cooling or heating air to a zone in sufficient quantity to meet the zone load. Cooling and heating thermal powers were modelled with unlimited capacity. Heating and cooling design supply conditions were modelled as shown in Table 4.4. Since cooling supply air conditions are far below zone internal air saturation conditions, latent gains were considered: the cooling system provides dehumidification. The ZoneHVAC:IdealLoadsAirSystem object is modelled as an ideal VAV terminal unit with variable supply air temperature and humidity. The supply air flow rate varies between zero and the maximum in order to satisfy the zone heating or cooling load.

	Air Temperature [°C]	Humidity Ratio [g_w/kg_{da}]
Heating	35	16
Cooling	12	8

Table 4.4: Heating and cooling air inlet conditions

4.5.3 Constructions

Building constructions include both opaque and transparent components. Tabula web tool provides construction overall thermal transmittances which is why layers conductivity, thickness specific heat and density were obtained accordingly. As regards the transparent surfaces, Tabula thermal transmittance was used while SHGC was set between 0.9 and 0.7 in accordance with the construction year. SHGC of 0.398 was set for all refurbished buildings. Window wall ratios are illustrated in Table 4.1. Opaque and transparent constructions characteristics are summarized from Table 4.5 to Table 4.7. The surface masses are reported in Table 4.6 for the uninsulated building only, since the values are not significantly affected by the application of an insulating material with low density. When two wall types were reported in Tabula web tool, the widest surface wall transmittance was selected: this case is highlighted with an asterisk (*) in Table 4.5 and Table 4.6. No shadings were modelled during simulations to avoid human behaviour influences.

OPAQUE U	… - 1900		1921 - 1945		1946 - 1960		1961 - 1975		1976 - 1990		1991 - 2005		2006 - …	
	B_U	B_I	B_U	B_I	B_U	B_I	B_U	B_I	B_U	B_I	B_U	B_I	B_U	B_I
U Wall [W/m^{2}K]	1.19	0.24	1.29*	0.21	1.42*	0.23	1.15*	0.23	0.77*	0.23	0.58*	0.21	0.33*	0.13
U Roof [W/m^{2}K]	1.28	0.21	1.48	0.21	1.10	0.21	1.10	0.21	0.75	0.21	0.57	0.21	0.28	0.13
U Floor [W/m^{2}K]	1.07	0.21	1.23	0.21	0.94	0.21	0.94	0.21	0.98	0.22	0.70*	0.21	0.30	0.20

Table 4.5: Opaque construction thermal transmittance for uninsulated and insulated models

OPAQUE M	… - 1900	1921 - 1945	1946 - 1960	1961 - 1975	1976 - 1990	1991 - 2005	2006 - …
M Wall [kg/m2]	1267	155	737	194	176	203	160
M Roof [kg/m2]	926	1210	406	406	276	277	278
M Floor [kg/m2]	1096	1454	459	478	276	276	278

Table 4.6: Opaque construction surface mass for uninsulated and insulated models

WINDOW	… - 1900		1921 - 1945		1946 - 1960		1961 - 1975		1976 - 1990		1991 - 2005		2006 - …	
	B_U	B_I	B_U	B_I	B_U	B_I	B_U	B_I	B_U	B_I	B_U	B_I	B_U	B_I
SHGC [−]	0.9	0.398	0.9	0.398	0.75	0.398	0.7	0.398	0.7	0.398	0.9	0.398	0.9	0.398
U_w [W/m^{2}K]	4.9	0.8	4.9	0.8	3.7	0.8	2.2	0.8	2.2	0.8	4.9	0.8	4.9	0.8

Table 4.7: Window characteristics for uninsulated and insulated models

4.5.4 Ventilation

Outdoor air flow rate, intended as intentionally or inadvertently introduced into the building, is strictly dependent on the building construction performance and windows' openings. A total outdoor air change rate of 0.3 ACH was modelled as constant for both uninsulated and insulated models, in order to allow a straight comparison among the results along with the simulation process. The analysis was maintained as objective as possible.

4.6 Weather files description

The two weather datasets, IGDG and CTI, not only differ for the considered period but also for the generation methodology. The IGDG weather files are available for download at EnergyPlus official web page [137], they are ready-to-use and do not need further data processing. However, even though CTI weather files are also freely available on the Italian thermo-technical committee website [138], they require additional processing to be used for dynamic building simulation. CTI files are provided with the following data, at an hour frequency:
In addition to the previous parameters, EnergyPlus requires dew point air temperature and direct normal solar radiation. Since two psychrometric variables are given (dry bulb air temperature and relative humidity), the dew point air temperature was calculated. Regarding solar data, EnergyPlus requires normal solar radiation in place of direct radiation on horizontal plane. However, the quantity is recorded using pyrheliometers. Such measuring instruments are rarely installed on weather

Dry bulb air temperature	[°C]
Relative humidity	[%]
Global solar radiation on horizontal plane	[W/m^2]
Direct solar radiation on horizontal plane	[W/m^2]
Diffuse solar radiation on horizontal plane	[W/m^2]
Vapor pressure	[Pa]
Wind speed	[m/s]

stations owing to their high cost. In literature, many efforts were therefore made to develop solar radiation models that allow splitting global horizontal radiation into its components. Once the direct horizontal radiation is calculated, the standard approach to obtain DNI envisages dividing the direct horizontal radiation by the cosine of the zenith angle. Gueymard [50] evaluated the performance of 140 separation models and carried out a statistical study of models' results. Pernigotto [58] investigated the impact of solar radiation models on building energy simulations in five European climates. Lupato [139] carried out a similar research with a 10-year dataset recorded in Trieste, studying the energy variability of each year. In this paper, the Perez model highlighted the best overall performance and was thus applied to obtain DNI from the global solar radiation of CTI weather files. In building energy simulations, ground temperature affects energy consumption, however the data are not provided by the weather files. A constant ground temperature of 18°C was set to maintain the simulation as objective as possible.

Figure 4.2: Weather file locations, CTI in blue and IGDG in red

4.6.1 IGDG Weather files, reference year methodology

The external air temperature data were collected in 68 weather stations, evenly distributed across the Italian territory. The data were recorded between 1951 and 1970. The procedure used to obtain the reference year was described by Mazzarella [140]. The identification of the single months that compose the reference year is based on the monthly mean air temperature and its variance, calculated for the twelve months for of the entire dataset. Later, the same parameters are calculated for every single month of the dataset. Finally , the selected months are the most representative, the selection of the representative month is based on the comparison between mean temperature and the variance [140]. Once the months are selected, the reference year is obtained combining the hourly values of the months.
The following data are included in the reference year, but they were not taken into consideration within the months' selection analysis:

- Wind speed
- Relative humidity
- Number of sunshine hours

The air temperature was recorded with a three-hour frequency: linear interpolation was used to obtain the hourly values. 30 of the 68 stations included daily total irradiation data: for the remaining 38, the data from another relatively close weather station were used. Dealing with solar data, as shown in chapter 2, is a difficult task due to the scarcity of historical measurements and the measuring tools spread across the territory. Therefore, the correlations [141], [48] and [142] were used to split the daily irradiation into its diffuse and direct components, and to obtain hourly values from daily data.
The correlations are:

- To split the daily total irradiation into direct and diffuse components: Erbs [141]
- To distribute the daily diffuse irradiation into hourly values: Liu-Jordan [48]
- To distribute the daily direct irradiation into hourly values: Collares-Pereira e Rabl [142]

4.6.2 CTI Weather files, reference year methodology

The CTI weather files were obtained applying the procedures of EN ISO 15927-4 [75] technical standard based on Finkelstein-Schafer statistic. The data used to generate the reference year were collected between 1989 and 2014.
The procedure is fully described in the standad [75] and can be summarized as follows:

1. the months' selection is based on three primary parameters: the air temperature, the relative humidity and the global solar radiation;
2. the daily mean values were calculated for each of the three parameters;
3. for each calendar month, the cumulative distribution function over all years was calculated, sorting the values in ascending order, with equation 4.1:

$$\phi_{(p,m,i)} = \frac{K(i)}{N+1} \tag{4.1}$$

   where $K(i)$ is the rank order within dataset;

4. for each year of the dataset, the cumulative distribution function over all months was calculated, sorting the values in ascending order, with equation 4.2:

$$F_{(p,y,m,i)} = \frac{J(i)}{n+1} \tag{4.2}$$

   where $J(i)$ is the rank order within the related month and year;

5. for each month of the dataset, the Finkelstein-Schafer statistic for all years was calculated, with equation 4.3:

$$F_{S(p,y,m)} = \sum_{i=1}^{n} \mid F_{p,y,m,i} - \phi_{p,m,i} \mid \tag{4.3}$$

   where $J(i)$ is the rank order within the related month and year;

6. for each calendar month, the results are ordered;

7. for the first three values o the ordered list, the wind speed standard deviation is calculated;

8. for every calendar month, the month with the lower wind speed standard deviation is selected;

9. the selected month are used to compose the reference year; an interpolation that covers the last 8 and the first 8 hours of each month was applied.

4.7 Weather files matching

First of all, building simulations were carried out with CTI weather files. CTI files locations are widespread on the Italian territory and can represent most of the Italian climatic conditions, as illustrated by blue dots in Figure 4.2. In literature, little research was carried out to define a method for weather files' selection. Briggs [143] developed a model to select the most representative weather files, considering HDD, CDD and the elevation difference between the building location and the weather station location. It was based on U.S. weather datasets and its application on Italian weather datasets led to poor outcomes: in some cases, northern locations were coupled to southern locations weather data. The poor results may be a consequence of the great diversity between the Italian and U.S. climatic conditions within the territory and country extensions. Moreover, the ASHRAE model refers to climatic parameters with a comparable record period which means that the assumption cannot be satisfied in the present case study. As highlighted in EnergyPlus official documentation [144], it is recommended to select a weather file within a range of 50 km and 100 m elevation difference between the building location and the weather station. Selecting a more distant weather station dataset, although corrected by adjustment techniques, is a practice also reported by other authors [36]. Therefore, a more restrictive limit of 50 km distance and 50 m elevation difference was set to select the related IGDG weather file. For every CTI location, distance and elevation difference related to IGDG dataset were calculated: all matchings that did not meet the requirements were rejected. This approach has been adopted possibly to replicate the choice a designer would operate in absence of local weather datasets. Fulfilling the previously described conditions allows multiple IGDG stations to be selected for a single CTI location: in this specific case, the closest station was chosen, considering the distance parameter only. The described method was applied to 108 CTI weather locations and resulted in a total of 52 valid matches which are shown in Figure 4.3. Matching results are shown in Table 4.8 and Table 4.9. In these tables, the CTI and the related IGDG station names are reported. Latitude, longitude, elevation, HDD and CDD are outlined for both weather files, as are distance, elevation, HDD and CDD difference between the two locations. HDD and CDD were calculated with the methodology described in the UNI –EN-ISO 15927-6:2008 technical standard [145] heating and cooling baseline air temperature were set to 20°C and 25°C respectively. During simulations, HDD and CDD calculations, no altitude correction was applied. The longitude of Olbia reported in the IGDG file was found incorrect and the correct value 9.5°was inserted.

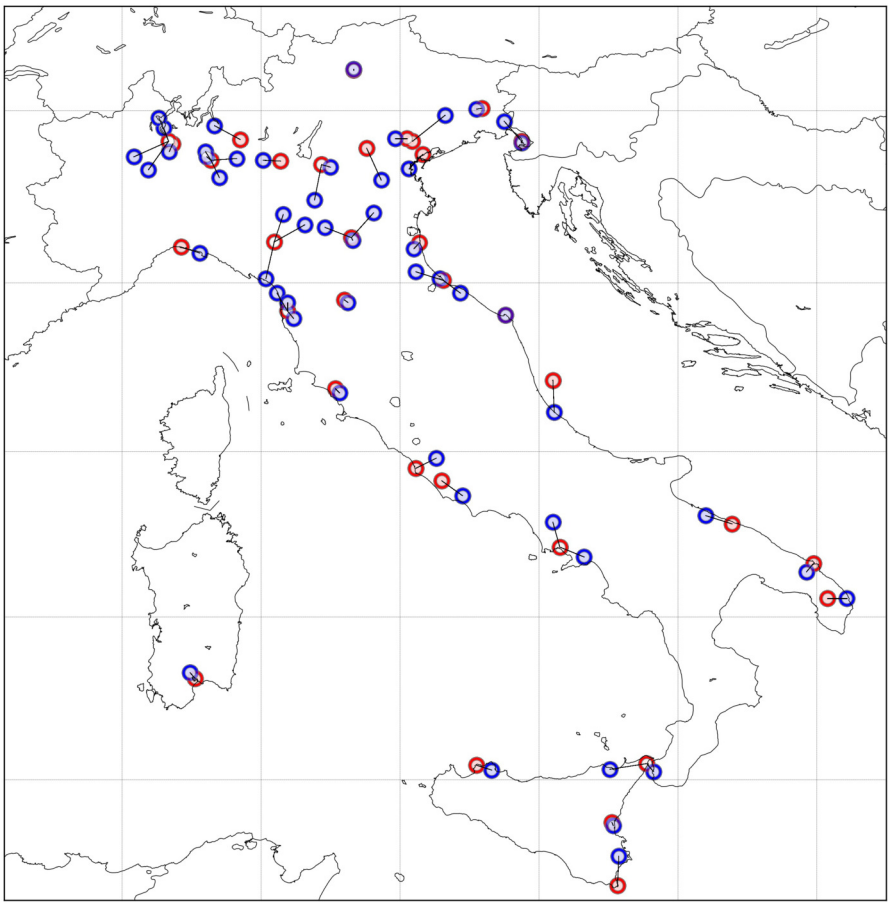

Figure 4.3: Weather file matchings

The inspection of Tables 4.8 and 4.9 shows, as a whole, a decrease in HDD between CTI and IGDG, which can be ascribed to an increase in external temperatures over the Italian territory, possibly due also to the climatic change. Though the TRY constitutes a form of average year [118], the energy consumption ensuing from the simulations is not always the average in the long term [6]. The TRYs are not the correct weather files to assess climate change. Indeed, in several cases, the test reference year leads to overestimation or underestimation of energy consumption or to a peak load demand [5]. However, the aim of choosing this methodology, is to compare the results that are achieved using TRY datesets calculated with different recording periods. Selecting the weather data location is always a critical aspect for performing an energy simulation, and this problem is even more critical if only a few dataset locations are available.

CTI Database						IGDG Database						Matching Values			
Station Name	Lat [°]	Lon [°]	Alt [m]	HDD [–]	CDD [–]	Selected Station Name	Lat [°]	Lon [°]	Alt [m]	HDD [–]	CDD [–]	Distance [km]	ΔHDD [–]	ΔCDD [–]	ΔAltitude [m]
Abruzzo_Pescara	42.47	14.22	5	2129	119	Pescara	42.85	14.2	16	2448	74	42	-319	45	-11
Calabria_Reggio Calabria	38.1	15.65	15	1268	194	Messina	38.2	15.55	59	1341	99	14	-73	95	-44
Campania_Battipaglia	40.73	14.65	55	1745	147	Napoli-Capodichino	40.85	14.3	72	2036	92	32	-291	55	-17
Campania_Vitulazio	41.15	14.2	65	1923	191	Napoli-Capodichino	40.85	14.3	72	2036	92	34	-113	98	-7
Emilia Romagna_Bologna	44.5	11.32	48	2696	87	Bologna-Borgo.Panigale	44.53	11.3	49	3000	126	4	-305	-38	-1
Emilia Romagna_Cesena	44.13	12.23	42	2708	74	Rimini	44.03	12.62	13	2917	44	33	-209	30	29
Emilia Romagna_Ferrara	44.82	11.62	6	2860	124	Bologna-Borgo.Panigale	44.53	11.3	49	3000	126	41	-140	-2	-43
Emilia Romagna_Modena	44.65	10.92	37	2873	120	Bologna-Borgo.Panigale	44.53	11.3	49	3000	126	33	-127	-5	-12
Emilia Romagna_Parma	44.8	10.32	57	2812	137	Parma	44.48	10.19	68	3194	68	37	-383	69	-11
Emilia Romagna_Ravenna	44.4	12.2	2	2772	69	Marina.di.Ravenna	44.47	12.28	2	2762	45	10	10	24	0
Emilia Romagna_Reggio Emilia	44.68	10.63	56	2876	129	Parma	44.48	10.19	68	3194	68	41	-319	61	-12
Emilia Romagna_Rimini	44.05	12.57	7	2764	49	Rimini	44.03	12.62	13	2917	44	5	-153	5	-6
FVG_Gradisca d'Isonzo	45.88	13.5	30	2684	124	Trieste	45.65	13.75	20	2418	79	32	266	45	10
FVG_Pordenone	45.95	12.65	30	2804	96	Treviso-S.Angelo	45.65	12.18	18	2982	60	49	-178	36	12
FVG_Trieste - Molo Bandiera	45.63	13.75	2	2034	71	Trieste	45.65	13.75	20	2418	79	2	-384	-8	-18
FVG_Udine	46.02	13.1	80	2811	107	Udine-Campoformido	46.03	13.18	92	2977	73	6	-167	35	-12
Lazio_Latina	41.47	12.9	23	1760	178	Pratica.di.Mare	41.65	12.6	21	2222	41	32	-463	137	2
Lazio_Roma	41.92	12.52	32	1859	193	Roma-Fiumicino	41.8	12.23	3	2113	70	27	-255	124	29
Liguria_Recco - Polanesi	44.35	9.12	50	1706	75	Genova-Sestri	44.42	8.85	3	2055	37	23	-350	38	47
Lombardia_Bargnano	45.43	10.03	93	3038	115	Brescia-Ghedi	45.42	10.28	102	3199	83	20	-161	32	-9
Lombardia_Capralba	45.45	9.65	96	3159	111	Milano-Linate	45.43	9.28	103	3097	77	29	62	34	-7
Lombardia_Cinisello Balsamo	45.53	9.2	142	2815	165	Milano-Linate	45.43	9.28	103	3097	77	13	-282	88	39
Lombardia_Ispra	45.8	8.6	193	2974	59	Novara-Cameri	45.65	8.67	178	3475	55	18	-501	4	15
Lombardia_Milano - via Juvara	45.47	9.22	122	2562	119	Milano-Linate	45.43	9.28	103	3097	77	6	-535	42	19
Lombardia_Palidano di Gonzaga	44.97	10.77	22	3019	166	Verona-Villafranca	45.38	10.87	68	3125	73	46	-106	93	-46
Lombardia_S.Angelo Lodigiano	45.23	9.4	60	2965	148	Milano-Linate	45.43	9.28	103	3097	77	24	-131	71	-43

Table 4.8: Weather file matching results

CTI Database						IGDG Database						Matching Values			
Station Name	Lat [°]	Lon [°]	Alt [m]	HDD [–]	CDD [–]	Selected Station Name	Lat [°]	Lon [°]	Alt [m]	HDD [–]	CDD [–]	Distance [km]	ΔHDD [–]	ΔCDD [–]	ΔAltitude [m]
Lombardia_Valmadrera	45.83	9.33	237	2616	111	Bergamo-Orio.al.Serio	45.67	9.7	238	3208	48	34	-592	64	-1
Marche_Ancona - Regione	43.62	13.52	91	2155	96	Ancona	43.62	13.52	105	2302	38	0	-146	58	-14
Marche_Villa Fastiggi	43.88	12.87	20	2379	140	Rimini	44.03	12.62	13	2917	44	26	-538	96	7
Piemonte_Cameri	45.53	8.68	173	3514	68	Milano-Malpensa	45.62	8.73	211	3487	50	11	27	17	-38
Piemonte_Massazza	45.47	8.17	226	3220	63	Novara-Cameri	45.65	8.67	178	3475	55	44	-255	8	48
Piemonte_Pallanza	45.92	8.53	202	2799	97	Novara-Cameri	45.65	8.67	178	3475	55	32	-676	41	24
Piemonte_Vercelli	45.32	8.38	132	2984	124	Novara-Cameri	45.65	8.67	178	3475	55	43	-491	68	-46
Puglia_Ver_3.1_Mesagne	40.55	17.85	53	1797	227	Brindisi	40.65	17.95	10	1707	90	14	89	137	43
Puglia_Ver_3.1_Otranto	40.23	18.43	24	1704	121	Lecce	40.23	18.15	48	1875	136	24	-171	-15	-24
Puglia_Ver_3.1_Trani	41.23	16.4	63	1872	181	Bari-Palese.Macchie	41.13	16.78	49	1941	101	34	-69	79	14
Sardegna_Decimomannu	39.32	8.98	20	1869	168	Cagliari-Elmas	39.25	9.05	18	1740	81	10	129	87	2
Sicilia_Catania	37.43	15.07	10	1467	216	Catania-Fontanarossa	37.47	15.05	17	1643	155	5	-177	60	-7
Sicilia_Palermo	38.12	13.32	50	1264	241	Palermo-Punta.Raisi	38.18	13.1	21	1164	77	20	100	164	29
Sicilia_Patti	38.13	15.02	70	1451	197	Messina	38.2	15.55	59	1341	99	47	110	97	11
Sicilia_Siracusa	37.05	15.15	90	1706	344	Cozzo.Spadaro	36.68	15.13	51	1286	119	41	420	226	39
Toscana_Carrara	44.05	10.07	90	2033	68	Parma	44.48	10.19	68	3194	68	49	-1162	0	22
Toscana_Collesalvetti	43.58	10.47	15	2369	131	Pisa-S.Gusto	43.67	10.38	1	2424	70	12	-54	61	14
Toscana_Firenze	43.77	11.25	70	2143	266	Firenze-Peretola	43.8	11.2	38	2535	126	5	-393	140	32
Toscana_Lido di Camaiore	43.88	10.23	5	2284	116	Pisa-S.Gusto	43.67	10.38	1	2424	70	26	-139	46	4
Toscana_Rispescia	42.7	11.13	40	2110	193	Grosseto	42.75	11.07	7	2337	123	7	-227	70	33
Toscana_San Giuliano Terme	43.77	10.38	5	2272	87	Pisa-S.Gusto	43.67	10.38	1	2424	70	11	-151	17	4
Trentino Alto Adige_Bolzano	46.48	11.33	265	2780	99	Bolzano	46.47	11.33	241	3663	65	1	-882	34	24
Veneto_Buttapietra	45.35	11	39	2829	129	Verona-Villafranca	45.38	10.87	68	3125	73	11	-296	56	-29
Veneto_Campagna Lupia	45.33	12.13	0	2751	113	Venezia-Tessera	45.5	12.33	10	2837	62	25	-86	51	-10
Veneto_Castelfranco Veneto	45.68	11.93	50	2922	140	Treviso-Istrana	45.68	12.1	45	3148	65	13	-226	76	5
Veneto_Monselice - Ca' Oddo	45.2	11.73	6	2864	111	Vicenza	45.57	11.52	39	3078	86	44	-215	24	-33

Table 4.9: Weather file matching results

4.8 Discussion and results analysis

Since not all the results and graphs can be reported for each building type, only multifamily-house results from 1961 to 1975 are shown below. According to ISTAT data, this period is representative for the majority of the existing Italian buildings. As previously explained, an ideal system was modelled. The system provides 100% convective heating and cooling: it allows to maintain the results as objective as possible, moving away from the system typology influence. Data analysis focuses on ideal energy consumption: no analysis of energy-cost or peak demand was carried out since the results are strictly related to HVAC systems. The main results are shown in Table 4.11 and Table 4.12, related to uninsulated and insulated cases respectively. In Tables 4.11 and 4.12, the first column reports the CTI station name while the remaining columns report heating and cooling energy for both weather files and their absolute difference. The purpose of the following discussion is to analyse the weather file impact in terms of: Cooling and heating energy difference (kWh/m^2) between the two datasets; Cooling and heating energy difference (kWh/m^2) between the two datasets and the distribution across the Italianterritory; Cooling and heating energy (kWh/m^2) related to CTI: its variability within the datasets; Refurbishment energy saving difference (kWh/m^2) between the two datasets.

4.8.1 Cooling and heating difference

Ideal heating and cooling energies were obtained using the two weather files for both uninsulated and insulated buildings thus allowing evaluating the energy difference, expressed in kWh/m^2. It was computed using the CTI and IGDG databases respectively, calculated in accordance with equations 4.4 and 4.5.

$$\Delta Q_C = Q_{C,CTI} - Q_{C,IGDG} \tag{4.4}$$

$$\Delta Q_H = Q_{H,CTI} - Q_{H,IGDG} \tag{4.5}$$

Results for uninsulated and insulated models are shown in Figure 4.4 and Figure 4.5 and the cooling and heating results are reported in blue and red respectively. Regarding the uninsulated building, as can be noticed in Figure 4.4, almost all the cooling energy differences are positive, while the heating differences are negative. Cooling energy consumption achieves a maximum increase of 26.5 kWh/m^2, mostly for southern locations. In accordance with cooling data, simulation results show heating energy consumption reduction, with a maximum decrease of almost 41.5 kWh/m^2. Regarding the results for the insulated building, a similar trend can be noticed in Figure 4.5, but it is characterized by lower energy reductions. The cooling and heating variations show a maximum of 11.7 kWh/m^2 and 14.3 kWh/m^2 respectively.

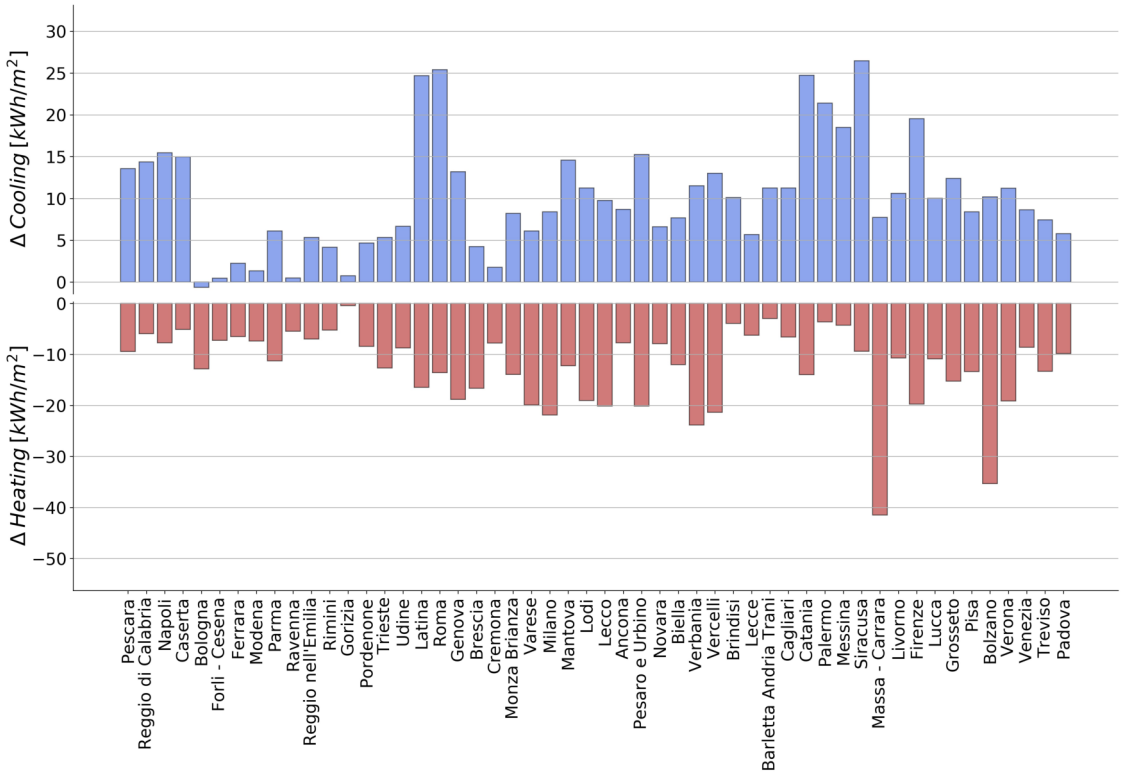

Figure 4.4: Heating and cooling energy difference between CTI and IGDG weather files, uninsulated building

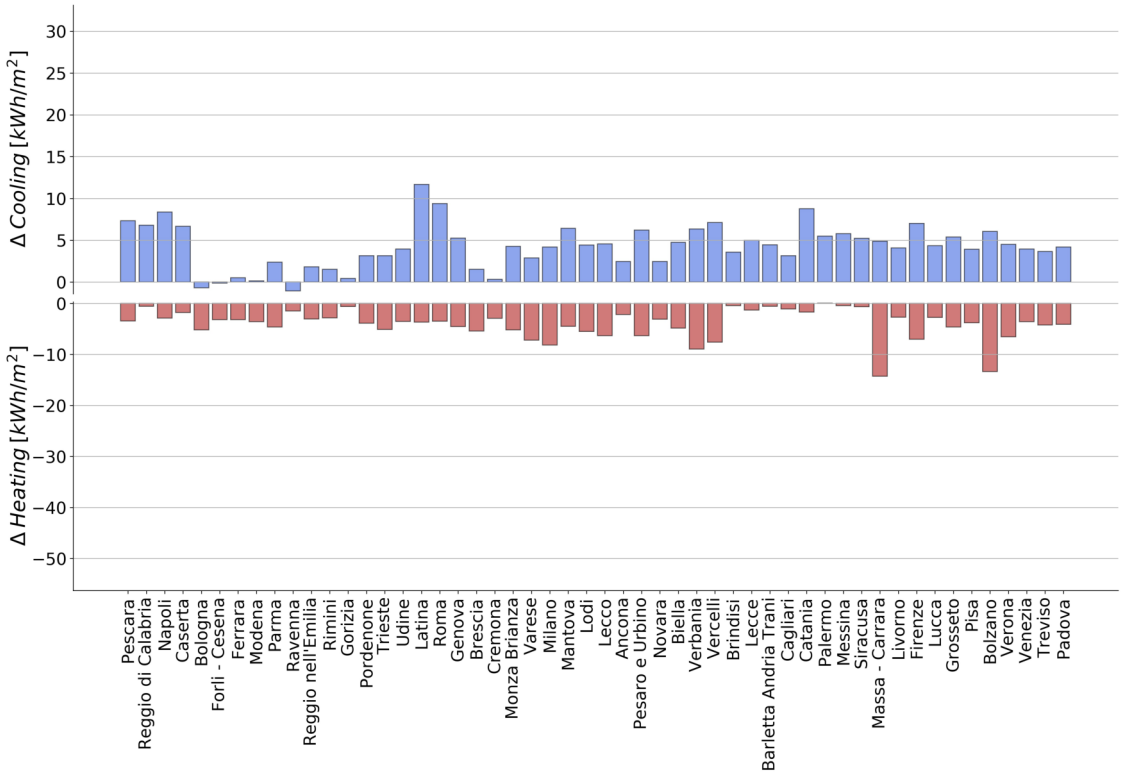

Figure 4.5: Heating and cooling energy difference between CTI and IGDG weather files, insulated building

4.8.2 Maps

Energy consumption differences between CTI and IGDG datasets are shown from Figure 4.9 to Figure 4.12. They were calculated in accordance with equations 4.4 and 4.5. The dot colour intensity represents the energy difference. Different scales were used for uninsulated and insulated buildings. Representing such data on the map allows analysing their trends, also considering the territory distribution. As for cooling energy differences, they are more pronounced in southern areas, with a maximum along the Tyrrhenian coast and Sicily: the highest value is 26.5 kWh/m^2. Conversely, the differences are less significant in the Po Valley area. Regarding heating, northern Italian areas are more affected by the dataset selection; the inspection of Figures 4.10 and 4.12 shows higher energy differences. However, Figure 4.10 and 4.12 illustrate the presence of two outliers, characterized by a strong energy variation. They correspond to the locations of Massa-Carrara and Bolzano. Monthly solar irradiation (kWh/m^2) and mean air temperature were studied to assess the results of Bolzano and Massa Carrara. Their CTI and IGDG values were compared to the entire CTI dataset, which, in this analysis includes all the data, not only those identified by the matching method. Regarding Bolzano mean air temperature, no remarkable variations were appreciated: an overall increase was registered, comparable with other weather station data. Instead, as can be seen in Figure 4.6, the global solar irradiation on horizontal plane, reported in the CTI dataset for Bolzano during winter, appears to be very high, both in terms of absolute and increasing value compared to the old IGDG data. Concerning the summer period, the opposite effect takes place: the irradiation is one of the lowest of the entire dataset. The direct component, presented in Figure 4.7, leads to a quite astonishing result: irradiations are the highest within the dataset during winter and January and March irradiations stand above all the other data.

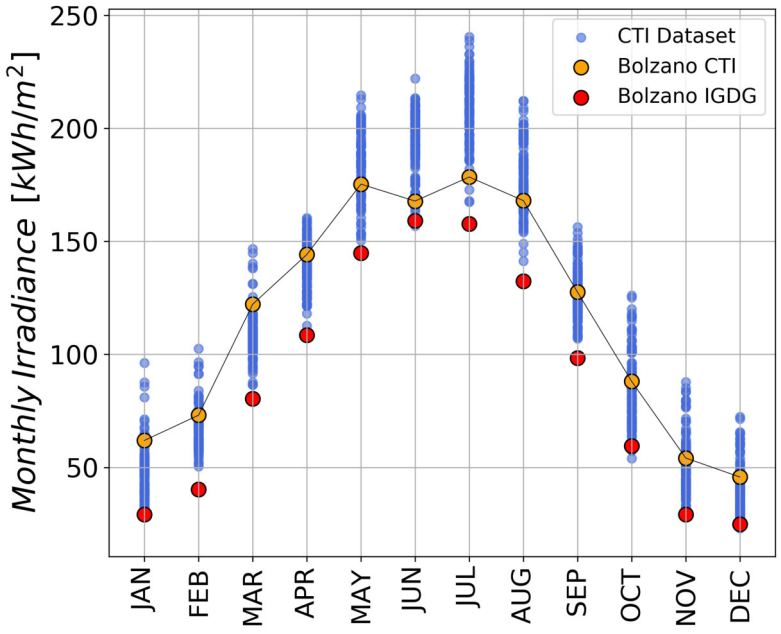

Figure 4.6: Monthly global irradiance

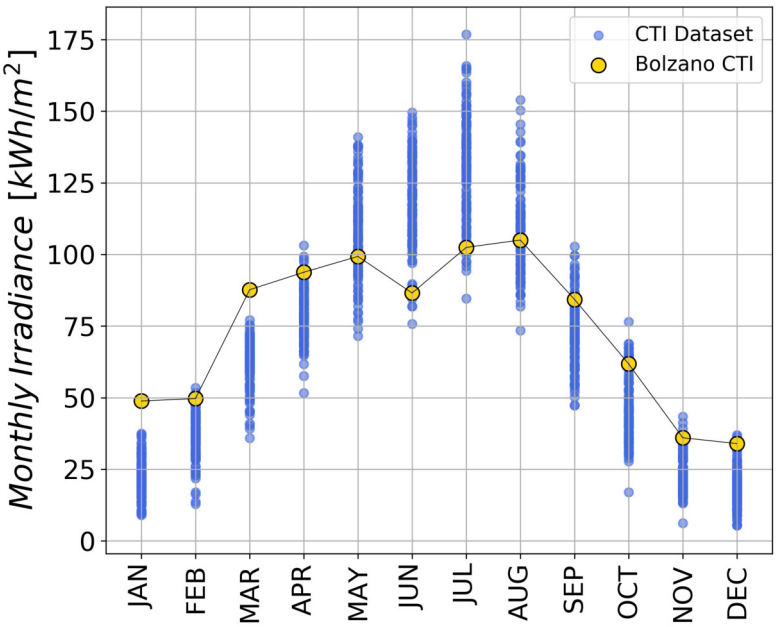

Figure 4.7: Monthly direct irradiance

As for Massa Carrara, solar radiation increase is comparable to the dataset trend. Instead, a great increase of mean air temperature is shown in Figure 4.8 during winter, while during summer the difference is moderate. The worst-case scenario is reported in December, when the mean air temperature moves from 0.7°C to 8.7°C. This variation explains the great heating energy reduction which could also be noticed analyzing the HDD variation. Their values are 2033 and 3194 for CTI and IGDG, respectively. Nevertheless, not all the air temperature increase is to be attributed to global warming: in this case the matching method linked a coastal city with an inland one. Furthermore, the Appennino Tosco-Emiliano National Park, located between the weather stations, contributes to the air temperature decrease. The territory topography thus affects the simulation outcomes highlighting the potential risk that can ensue by choosing the closest weather file from a less widespread and outdated dataset as the IGDG.

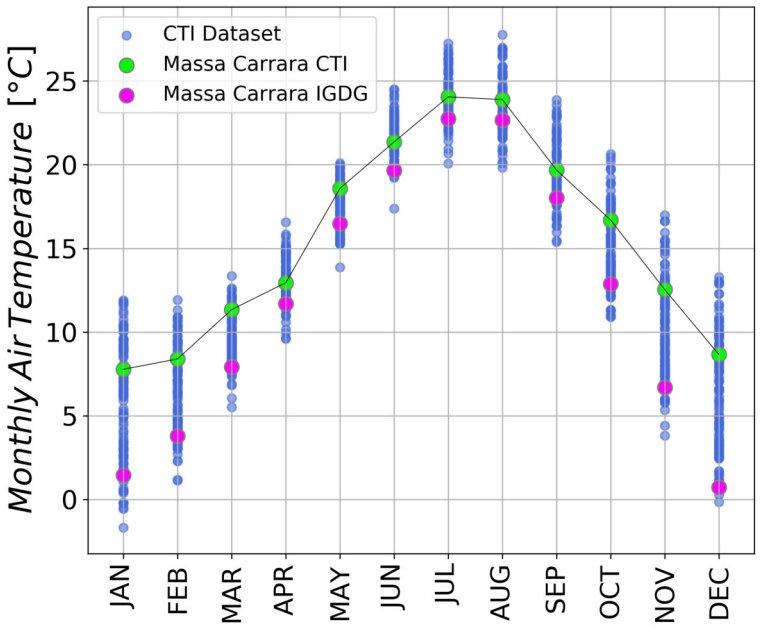

Figure 4.8: Monthly dry-bulb air temperature

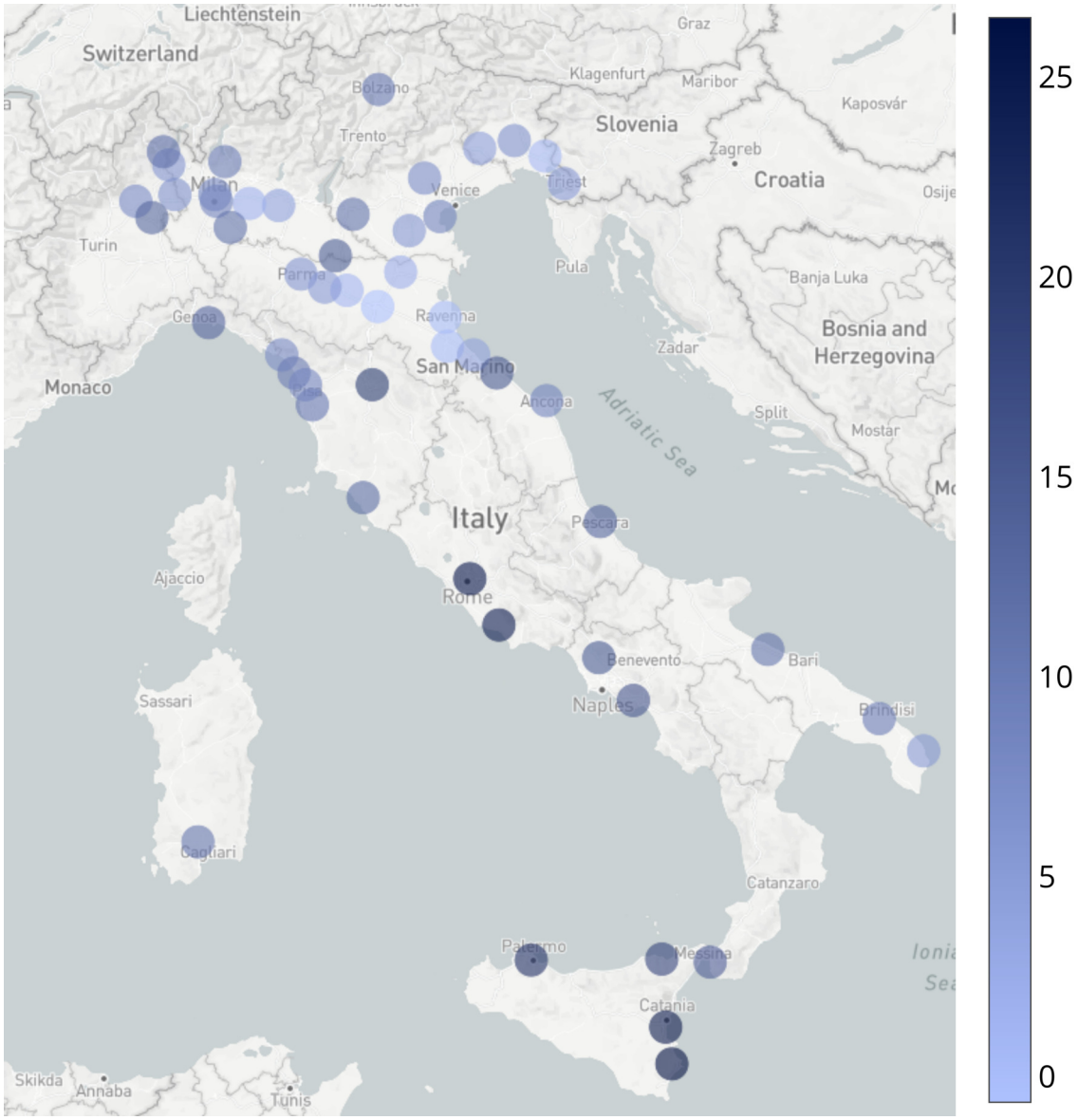

Figure 4.9: Annual cooling energy difference per area between CTI and IGDG weather files, uninsulated building [kWh/m^2]

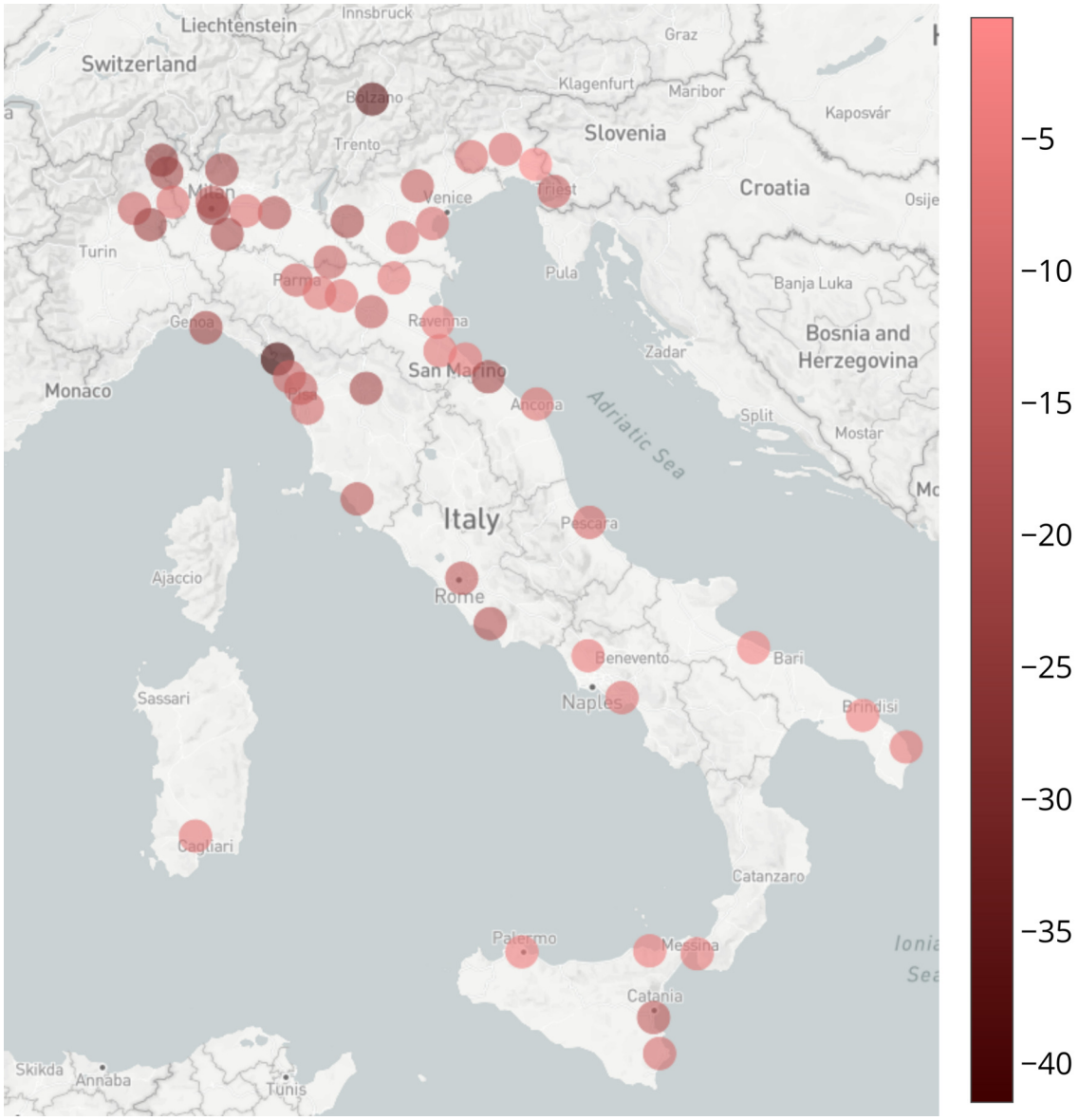

Figure 4.10: Annual heating energy difference per area between CTI and IGDG weather files, uninsulated building [kWh/m^2]

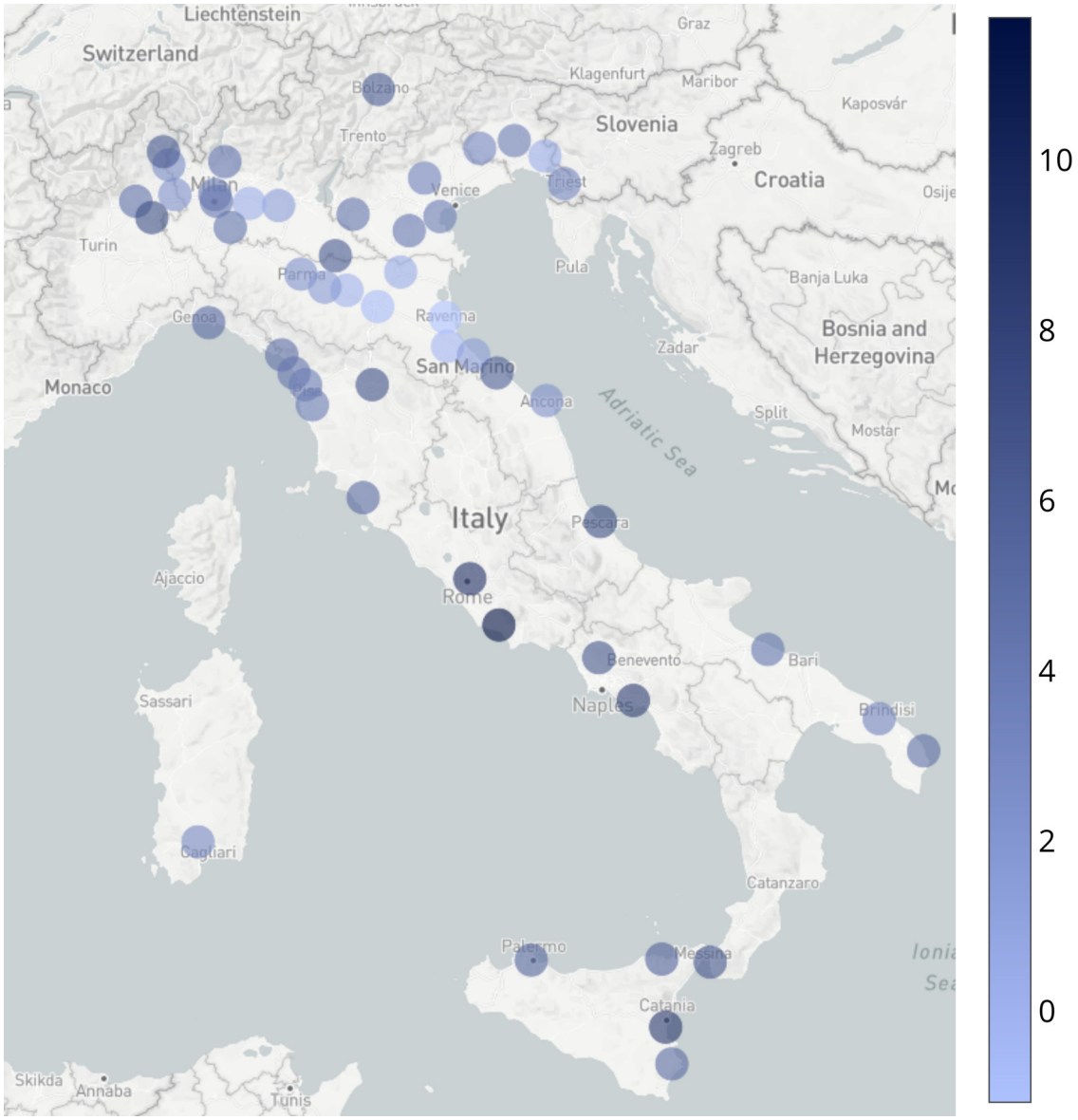

Figure 4.11: Annual cooling energy difference per area between CTI and IGDG weather files, insulated building [kWh/m^2]

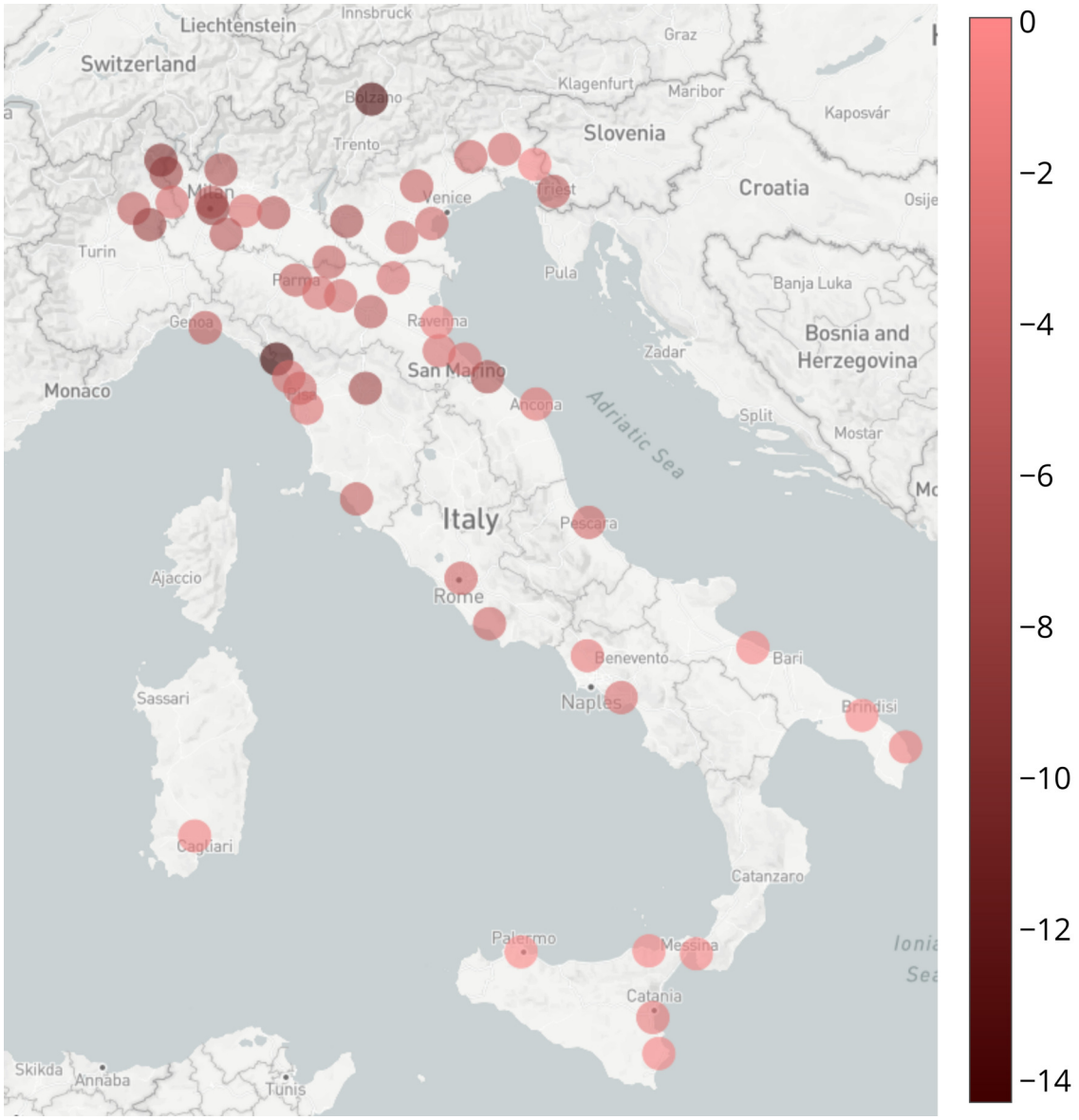

Figure 4.12: Annual heating energy difference per area between CTI and IGDG weather files, insulated building [kWh/m^2]

4.8.3 Cooling and heating distribution

Heating (red) and cooling (blue) energies related to CTI weather files are shown in Figure 4.13 and Figure 4.14: they include all year construction models' results. The same data are reported in Figure 4.15 and Figure 4.16 for the reference model. The plots are reported in pairs, for the uninsulated and the insulated models, respectively. The energy data are presented with the related IGDG consumptions on the x-axis: the continuous line represents the space where no energy variation occurred selecting a weather file or the other. As shown in the figures below, blue dots are placed above the line while the red lie below. It implies that, with more recent weather data, the cooling energy increases and the heating decreases. Different axes' scales between uninsulated and insulated figures were set to maintain the figures' legibility. On the contrary, identical x-axis and y-axis scales were set within each figure. As highlighted in Figure 4.15, cooling data are concentrated owing to

the heating-based scale: cooling energy is lower than heating energy for uninsulated building. Nevertheless, the green dotted rectangle that contains cooling data shows a significantly greater height compared to its base: it indicates that the new weather files enhance energy consumption variability. The opposite occurs when considering insulated building data in Figure 4.16: cooling energy is predominant while heating and cooling variabilities are similar (height and base of the orange rectangle are comparable). The insulated model energy consumption is less dependent on climatic conditions and internal gains constitute a large part of the cooling load. The energy consumption variabilities for insulated and uninsulated buildings (the green and orange boxes in Figure 4.15 and 4.16) are analysed with standard deviation: the results are shown in Table 4.10 and were calculated using equation 4.6.

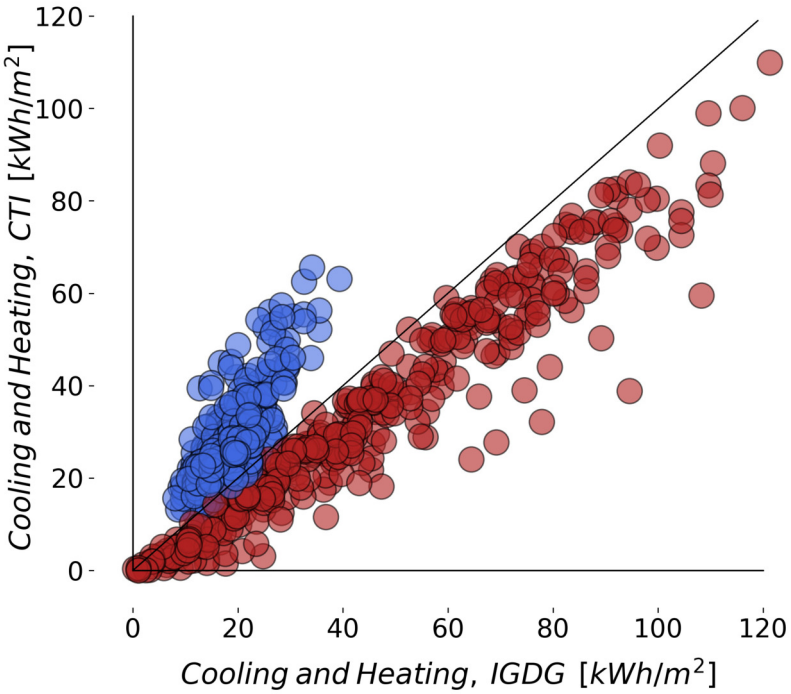

Figure 4.13: CTI files heating and cooling energy: uninsulated building (all models)

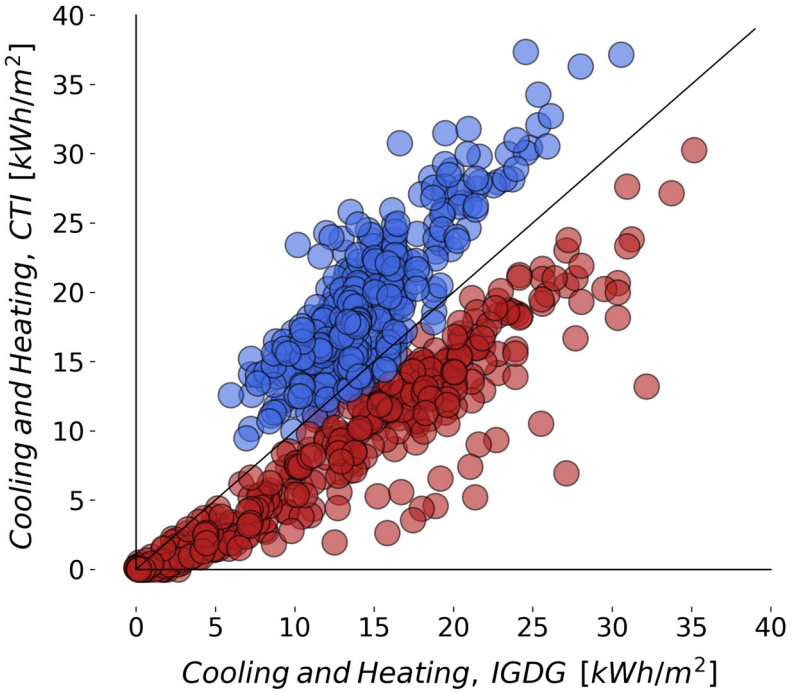

Figure 4.14: CTI files heating and cooling energy: insulated building (all models)

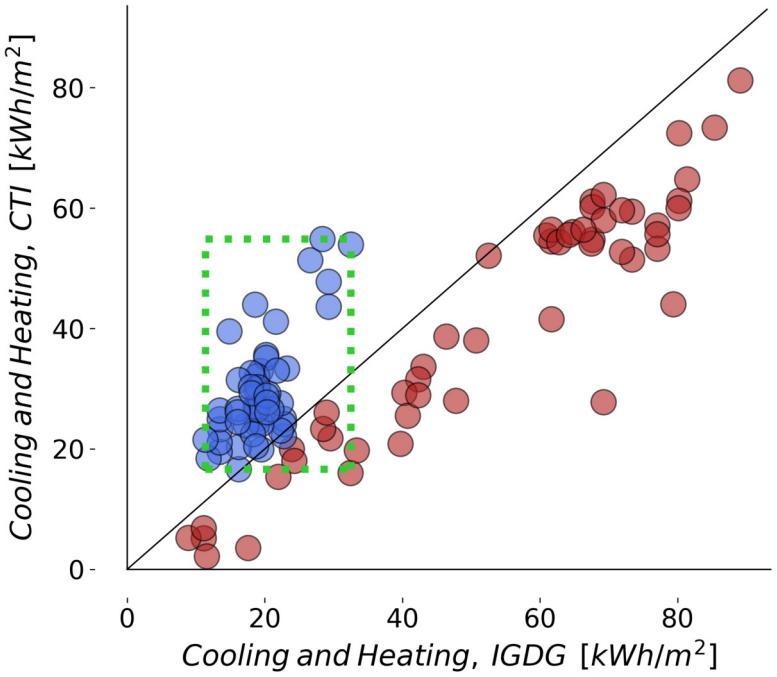

Figure 4.15: CTI files heating and cooling energy: uninsulated building (reference models)

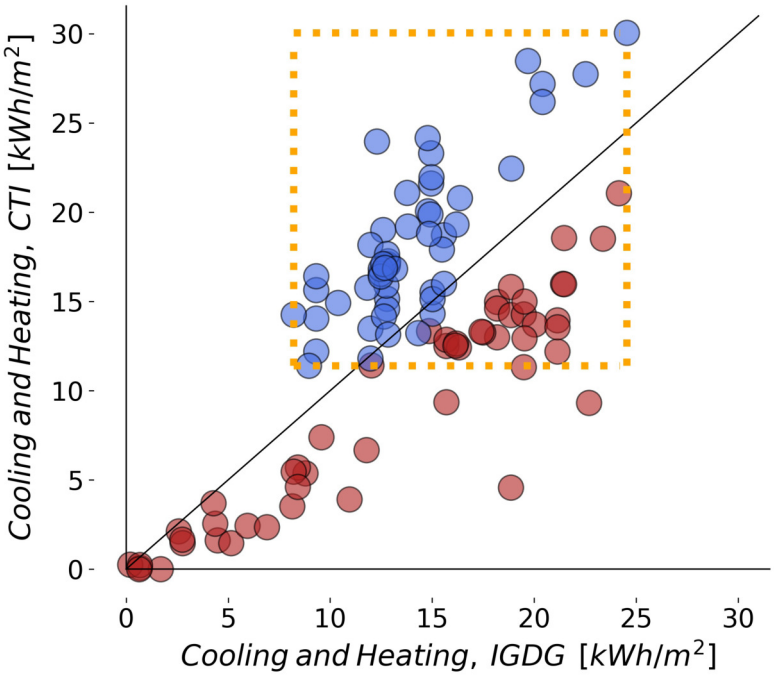

Figure 4.16: CTI files heating and cooling energy: insulated building (reference models)

	… - 1900 [kWh/m²]	1921 - 1945 [kWh/m²]	1946 - 1960 [kWh/m²]	1961 - 1975 [kWh/m²]	1976 - 1990 [kWh/m²]	1991 - 2005 [kWh/m²]	2006 - … [kWh/m²]
B_U IGDG	4.47	4.39	5.09	4.39	3.29	3.7	4.02
B_U CTI	9.84	9.42	10.38	8.93	6.23	7.03	6.81
B_I IGDG	3.56	3.48	3.83	3.3	3.16	3.36	3.3
B_I CTI	4.9	4.62	5.43	4.42	4.18	4.82	4.38

Table 4.10: Cooling energy variability: standard deviation

$$SD = \sqrt{\frac{\sum_1^n (x_i - \bar{x})^2}{n-1}} \tag{4.6}$$

4.8.4 Cooling and heating energy savings

Figures 4.17 and 4.18 represent the energy savings in kWh/m^2 calculated as the difference between uninsulated and insulated energy consumption. Therefore, the renovation energy savings variation that could be achieved using a weather file or the other can be analysed. Energy savings are calculated in accordance with equation 4.7 and 4.8.

$$\Delta Q_{Sav,C} = Q_{unins,C} - Q_{ins,C} \tag{4.7}$$

$$\Delta Q_{Sav,H} = Q_{unins,H} - Q_{ins,H} \tag{4.8}$$

With regard to cooling energy saving, while for the Po Valley area a slight difference is shown, higher differences are identified in southern locations. The ideal energy

saving for Catania, Palermo, Messina and Syracuse ranges from 5.9 kWh/m^2 to 8.9 kWh/m^2 using the IGDG database and from 21.6 kWh/m^2 to 27.1 kWh/m^2 with the CTI files. Although for energy quantification an HVAC-system model is required, these variations are expected to affect the economic analyses significantly, which might include pay-back time and net present value. Various cities of central Italy highlight non-negligible differences: the values of Latina, Rome and Florence are 2.6 kWh/m^2, 3.8 kWh/m^2 and 6.7 kWh/m^2 for IGDG and increase to 15.6 kWh/m^2, 19.8 kWh/m^2 and 19.2 kWh/m^2 for CTI. As for heating savings, the differences are less remarkable than those regarding the cooling scenario. Massa-Carrara and Bolzano present values of 50.4 kWh/m^2 and 56.7 kWh/m^2 for the IGDG file and of 23.2 kWh/m^2 and 34.7 kWh/m^2 for the CTI. However, these locations represent the outliers as reported in Section 4.8.2. Other significant results are recorded in Milan, Varese, Lecco, Pesaro and Urbino, Verbania, Vercelli, Florence and Verona. In general, refurbishment investments for heating energy savings would be less convenient when using the new CTI weather files instead of the older IGDG.

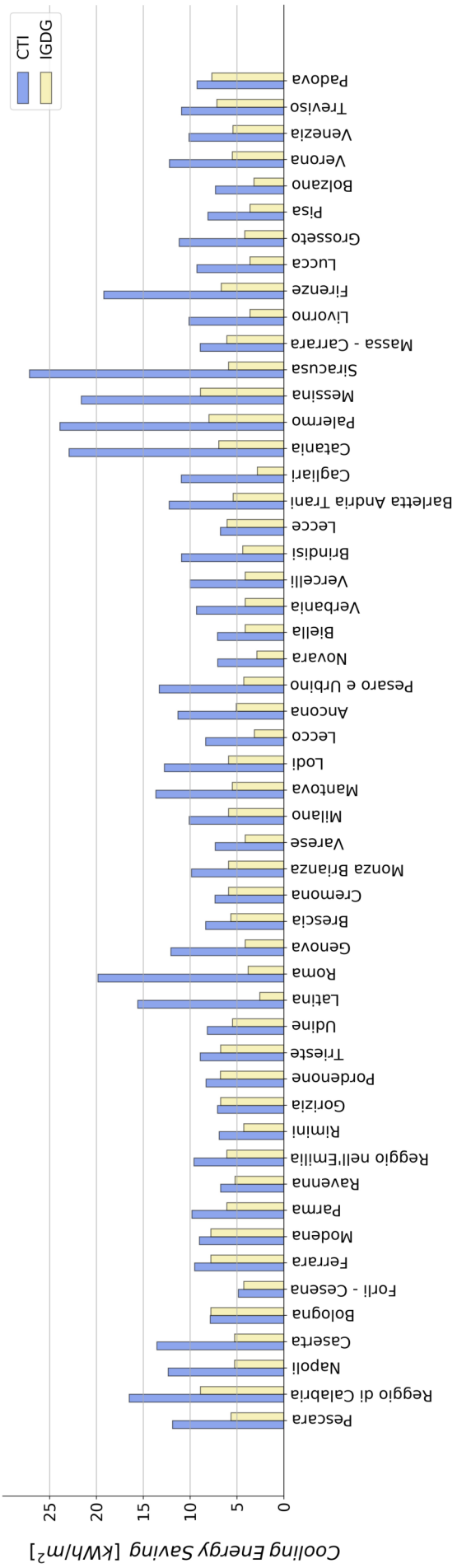

Figure 4.17: Cooling energy savings for CTI and IGDG files

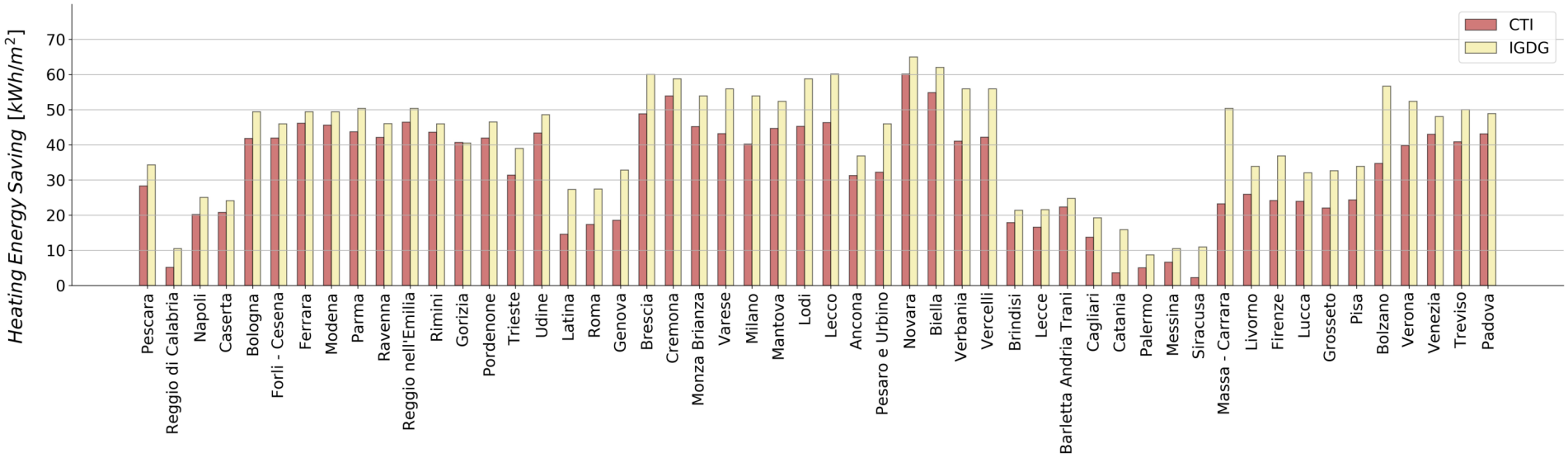

Figure 4.18: Heating energy savings for CTI and IGDG files

4.9 Final remarks

The building performance is extremely affected by the choice of the weather dataset: in general, heating energy decreases while cooling energy increases. However, energy need difference across the Italian territory showed a non-uniform distribution. The highest cooling energy differences occur in southern regions, especially along the Tyrrhenian coast. Regarding heating energy differences, northern locations generally result more affected by the weather file selection. No significant trend difference was identified for uninsulated and insulated buildings. The analysis allowed the identification of two outliers, Bolzano and Massa Carrara with a high decrease in heating energy. The Bolzano new weather file presents very high direct solar irradiance during the heating period which leads to a reduction of heating needs. For Massa Carrara, located on the shore, the matching algorithm selected an inland weather station, with lower temperatures not mitigated by the sea effect. The last result highlights the importance in choosing the weather files: the selection of the closest station, according to EnergyPlus documentation, can lead to significant errors in energy simulations. The problem draws attention to the risk that occurs selecting the weather file from the IGDG dataset, which is outdated and less widespread in the Italian territory. Regarding cooling energy consumption, the results show that using the updated dataset for the uninsulated building entails an increase of energy consumption variability, which does not occur for insulated buildings. Instead, for heating energy, the variability remains unaffected. Energy savings underline that, both for heating and cooling energy, the weather file selection could involve high differences. It emerged that the use of the outdated dataset leads to cooling savings underestimation and heating savings overestimation.

CTI Station	Heating CTI [kWh]	Heating IGDG [kWh]	Cooling CTI [kWh]	Cooling IGDG [kWh]	Δ Heating [kWh]	Δ Cooling [kWh]
Abruzzo_Pescara	31415	40200	30758	18095	-8785	12664
Calabria_Reggio Calabria	4840	10377	40758	27333	-5536	13425
Campania_Battipaglia	20362	27579	33265	18830	-7217	14435
Campania_Vitulazio	21787	26568	32810	18830	-4781	13980
Emilia Romagna_Bologna	51139	63099	20669	21266	-11960	-598
Emilia Romagna_Cesena	50831	57575	15552	15134	-6743	418
Emilia Romagna_Ferrara	57033	63099	23359	21266	-6066	2092
Emilia Romagna_Modena	56206	63099	22523	21266	-6892	1256
Emilia Romagna_Parma	54120	64615	23290	17581	-10495	5709
Emilia Romagna_Ravenna	51766	56840	18632	18190	-5075	442
Emilia Romagna_Reggio Emilia	58079	64615	22568	17581	-6537	4986
Emilia Romagna_Rimini	52691	57575	19014	15134	-4884	3879
FVG_Gradisca d'Isonzo	48658	49048	21506	20805	-391	701
FVG_Pordenone	50752	58597	22564	18208	-7845	4356
FVG_Trieste - Molo Bandiera	35530	47348	25776	20805	-11818	4971
FVG_Udine	52290	60452	22338	16123	-8162	6215
Lazio_Latina	14930	30293	36898	13859	-15363	23039
Lazio_Roma	18458	31118	41046	17333	-12660	23713
Liguria_Recco - Polanesi	19486	37058	29950	17627	-17572	12323
Lombardia_Bargnano	60467	75996	20991	17041	-15529	3949
Lombardia_Capralba	67629	74894	19116	17465	-7265	1652
Lombardia_Cinisello Balsamo	55497	68487	25135	17456	-12990	7679
Lombardia_Ispra	53330	71932	18216	12524	-18602	5692
Lombardia_Milano - via Juvara	48075	68487	25287	17456	-20413	7831
Lombardia_Palidano di Gonzaga	55709	67098	30468	16864	-11389	13604
Lombardia_S.Angelo Lodigiano	57142	74894	27976	17465	-17751	10512
Lombardia_Valmadrera	56016	74795	21714	12594	-18779	9120
Marche_Ancona - Regione	36097	43298	27257	19151	-7201	8106
Marche_Villa Fastiggi	38790	57575	29362	15134	-18785	14228
Piemonte_Cameri	75812	83177	17194	11021	-7365	6173
Piemonte_Massazza	68494	79685	19699	12526	-11191	7173
Piemonte_Pallanza	49701	71932	23281	12524	-22231	10758
Piemonte_Vercelli	51988	71932	24663	12524	-19944	12140
Puglia_Ver_3.1_Mesagne	18672	22350	31133	21694	-3679	9438
Puglia_Ver_3.1_Otranto	16843	22660	24859	19548	-5817	5312
Puglia_Ver_3.1_Trani	24299	27066	30806	20290	-2767	10516
Sardegna_Decimomannu	14338	20496	28236	17727	-6158	10508
Sicilia_Catania	3346	16378	47949	24850	-13033	23099
Sicilia_Palermo	4896	8285	50343	30355	-3389	19988
Sicilia_Patti	6396	10377	44599	27333	-3980	17266
Sicilia_Siracusa	2056	10810	51218	26492	-8754	24726
Toscana_Carrara	25909	64615	24790	17581	-38706	7209
Toscana_Collesalvetti	29502	39474	24893	14996	-9973	9897
Toscana_Firenze	26174	44595	38423	20173	-18421	18250
Toscana_Lido di Camaiore	27413	37574	24346	14996	-10161	9350
Toscana_Rispescia	23845	38053	28329	16763	-14207	11566
Toscana_San Giuliano Terme	27006	39474	22848	14996	-12469	7852
Trentino Alto Adige_Bolzano	41114	74099	20104	10605	-32986	9499
Veneto_Buttapietra	49256	67098	27345	16864	-17842	10482
Veneto_Campagna Lupia	51861	59899	26970	18906	-8039	8064
Veneto_Castelfranco Veneto	50549	62983	25890	18950	-12435	6940
Veneto_Monselice - Ca' Oddo	52693	61873	24384	18977	-9180	5406

Table 4.11: Heating and cooling energy consumption for CTI and IGDG weather files, B_U

CTI Station	Heating CTI [kWh]	Heating IGDG [kWh]	Cooling CTI [kWh]	Cooling IGDG [kWh]	Δ Heating [kWh]	Δ Cooling [kWh]
Abruzzo_Pescara	5007	8206	19689	12853	-3200	6836
Calabria_Reggio Calabria	71	616	25384	19040	-545	6343
Campania_Battipaglia	1505	4179	21763	13945	-2674	7818
Campania_Vitulazio	2389	4064	20181	13945	-1676	6235
Emilia Romagna_Bologna	12125	16973	13366	14013	-4847	-647
Emilia Romagna_Cesena	11688	14652	11035	11163	-2964	-129
Emilia Romagna_Ferrara	13988	16973	14494	14013	-2985	481
Emilia Romagna_Modena	13635	16973	14137	14013	-3338	123
Emilia Romagna_Parma	13298	17604	14158	11929	-4306	2229
Emilia Romagna_Ravenna	12461	13858	12357	13355	-1396	-998
Emilia Romagna_Reggio Emilia	14762	17604	13630	11929	-2842	1701
Emilia Romagna_Rimini	12015	14652	12595	11163	-2637	1432
FVG_Gradisca d'Isonzo	10659	11215	14929	14536	-556	393
FVG_Pordenone	11612	15223	14838	11905	-3611	2932
FVG_Trieste - Molo Bandiera	6234	10988	17477	14536	-4754	2941
FVG_Udine	11808	15090	14729	11031	-3283	3698
Lazio_Latina	1371	4801	22377	11478	-3431	10899
Lazio_Roma	2280	5551	22550	13794	-3271	8756
Liguria_Recco - Polanesi	2208	6429	18716	13800	-4221	4916
Lombardia_Bargnano	14931	19990	13214	11781	-5059	1433
Lombardia_Capralba	17332	20040	12279	11973	-2708	306
Lombardia_Cinisello Balsamo	13327	18186	15959	11970	-4859	3988
Lombardia_Ispra	13014	19734	11391	8690	-6719	2701
Lombardia_Milano - via Juvara	10565	18186	15887	11970	-7621	3916
Lombardia_Palidano di Gonzaga	14009	18215	17750	11753	-4206	5996
Lombardia_S.Angelo Lodigiano	14912	20040	16104	11973	-5127	4131
Lombardia_Valmadrera	12806	18700	13938	9685	-5895	4253
Marche_Ancona - Regione	6913	8929	16730	14435	-2016	2294
Marche_Villa Fastiggi	8736	14652	16962	11163	-5916	5799
Piemonte_Cameri	19663	22539	10637	8352	-2876	2285
Piemonte_Massazza	17294	21817	13115	8691	-4523	4425
Piemonte_Pallanza	11388	19734	14609	8690	-8346	5919
Piemonte_Vercelli	12652	19734	15332	8690	-7082	6642
Puglia_Ver_3.1_Mesagne	1989	2403	20951	17620	-413	3331
Puglia_Ver_3.1_Otranto	1370	2571	18570	13924	-1202	4646
Puglia_Ver_3.1_Trani	3450	3987	19413	15262	-538	4152
Sardegna_Decimomannu	1545	2560	18038	15108	-1015	2930
Sicilia_Catania	1	1575	26580	18382	-1574	8198
Sicilia_Palermo	235	183	28052	22912	52	5140
Sicilia_Patti	213	616	24439	19040	-403	5399
Sicilia_Siracusa	6	600	25890	21015	-593	4875
Toscana_Carrara	4269	17604	16490	11929	-13334	4561
Toscana_Collesalvetti	5321	7845	15462	11648	-2524	3815
Toscana_Firenze	3650	10223	20503	13959	-6574	6545
Toscana_Lido di Camaiore	5109	7664	15706	11648	-2555	4058
Toscana_Rispescia	3298	7601	17929	12891	-4304	5038
Toscana_San Giuliano Terme	4306	7845	15317	11648	-3539	3669
Trentino Alto Adige_Bolzano	8710	21176	13314	7655	-12466	5659
Veneto_Buttapietra	12087	18215	15966	11753	-6128	4213
Veneto_Campagna Lupia	11703	15061	17551	13860	-3358	3692
Veneto_Castelfranco Veneto	12395	16333	15718	12305	-3938	3414
Veneto_Monselice - Ca' Oddo	12426	16258	15758	11837	-3832	3921

Table 4.12: Heating and cooling energy consumption for CTI and IGDG weather files, B_I

Chapter 5

Wheather file impact: optimization

5.1 Problem introduction

It is well known that the energy consumption in residential sector represents the highest share of the final energy use in industrialized countries. These figures highlight the undeniable urgency to reduce the energy requirement for heating and cooling of buildings. The highest share of energy is due to the poor building fabric insulation. In order to reduce the building consumption for heating, large investments are focused on refurbishment activities, however, a balance should always be searched between investment costs and energy savings. In this scenario, optimization tools are instruments particularly suited to fulfil investment cost analysis and widely used from designers and researchers. Nevertheless, the optimization process is usually developed with annual simulation: it implies that it is affected by weather file selection, as introduced in chapter 3.

5.2 Literary review

In literature, several authors studied the impact of weather files on building energy simulation, analysing investment costs and energy savings. Pernigotto [104] analysed six methodologies for the TRY definition and studied their applications to optimization, focusing on Pareto frontier results. The author used two datasets recorded in Trento and Monza: he showed that, by referring to the recommended insulation thickness, the impact of TRYs is low. However, the author also highlighted that the uncertainty related to energy and economic efficiency is relevant. Hosseini (2018) applied a prediction model to generate future weather conditions files and he used them in roof design optimization. Huws and Jankovic (2014) analysed the effect of retrofit measures for current and future climate showing an increase in carbon emissions in the future. Ciulla [125] used a similar approach performing a Design of Experiments (DOE) for a social housing stock in Italy, they highlighted the cost optimality of moderate refurbishing measures.

5.3 Analysis scope

To study weather the file effect on building energy optimization, a case-study was carried out. Three weather files were selected to accomplish the optimizations: they were recorded from weather station in proximity to each other, in Trieste, but their datasets were recorded in different periods. This analysis aims to study the optimization outcomes' differences obtained from the selection of the three weather files, applied to a residential test building refurbishment activity.

5.4 Building description

An existing building in Trieste was chosen to run the optimization: it is a historical building and it is composed of four sections with apartments adjacent to each other. Every section is formed by four floors, each one with two small flats. The ground floor apartments consist of a kitchen, a bathroom and a bedroom. Every level above the ground floor has two apartments that contain one and two bedrooms respectively, a bathroom and a kitchen. The ground level floors and the third level ceilings are adjacent to aerated crawl spaces. The base building was built with massive structures (no insulation was present): due to its historical importance, all the refurbishments were designed to preserve the facades. Therefore, all the vertical insulation layers were placed in the internal part of the structures, while no cooling system is installed. Figure 5.1 represents the distribution on each floor and a typical flat.

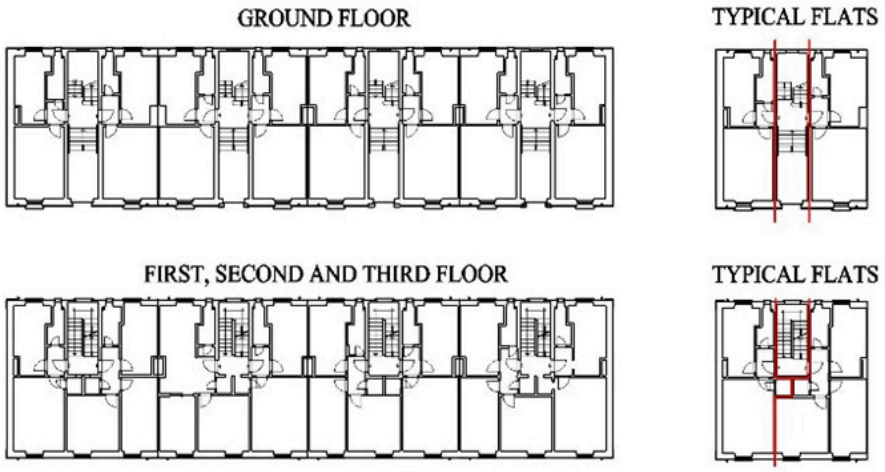

Figure 5.1: Buildings plant

Figure 5.2: Building satellite picture

5.5 Building model description

The building was firstly modelled with DesignBuilder (2017), a software interface that uses EnergyPlus [136] as calculation engine. The model replicates the state of the building before the refurbishment.

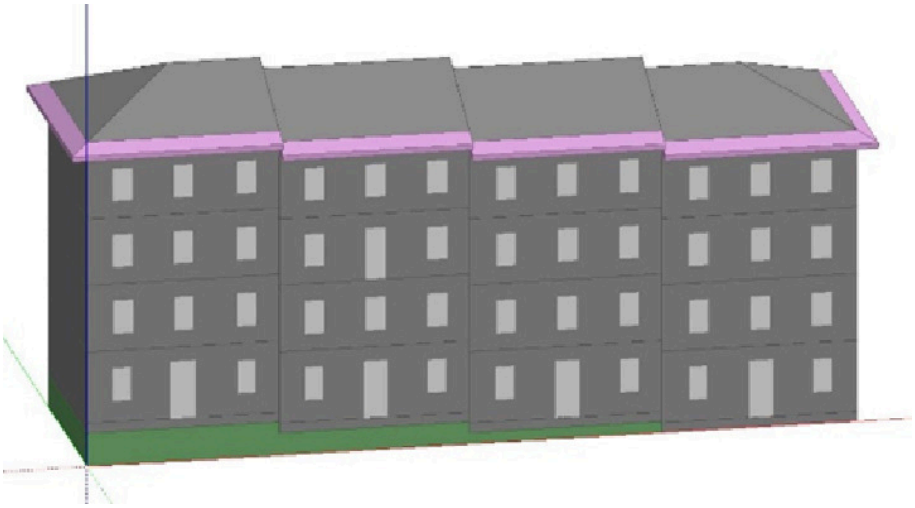

Figure 5.3: Model image

Opaque constructions and external fenestrations performance values are reported in Table 5.2. Ventilation was modelled as time-varying to take into account voluntary window opening for fresh air purposes and involuntary infiltration. Figure 5.4 reports the air change rated used in occupied zones and stairwells. Infiltration in crawl spaces and unoccupied roof-spaces was modelled as constant, with a value of 0.6 ACH for the base model and 0.3 ACH for the insulated model.

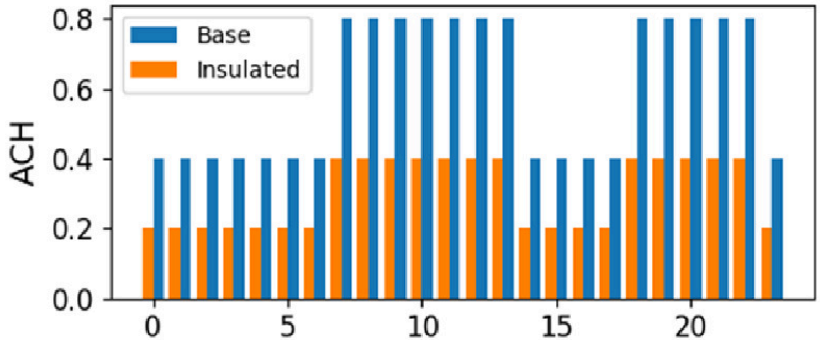

Figure 5.4: Air changes per hour

The external wall is a massive construction and it is mainly composed of two layers of full-bricks, each 25 cm thick. The ground floor, the roof and the third level ceilings are composed of a concrete structure whose thickness varies from 15 cm to 22 cm. External fenestrations consist of a single-layer glass with high SHGC and thermal transmittance. Internal gains and occupancy patterns do not change between the original and the insulated models and are variable according to the destination of each space. Electric gains correspond to a maximum of 400 W for kitchens and 100 W for bedrooms. These gains are time-varying according to the space type as shown in Figure 5.5. No gains were modelled for entrances, circulation spaces and bathrooms. Lighting gains were considered as included in internal gains.

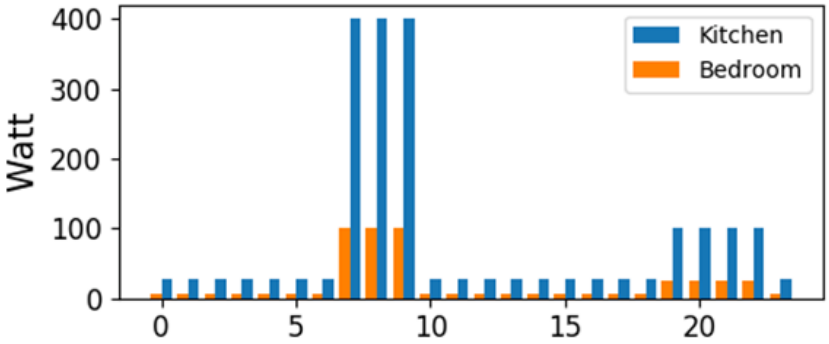

Figure 5.5: Internal electric gains

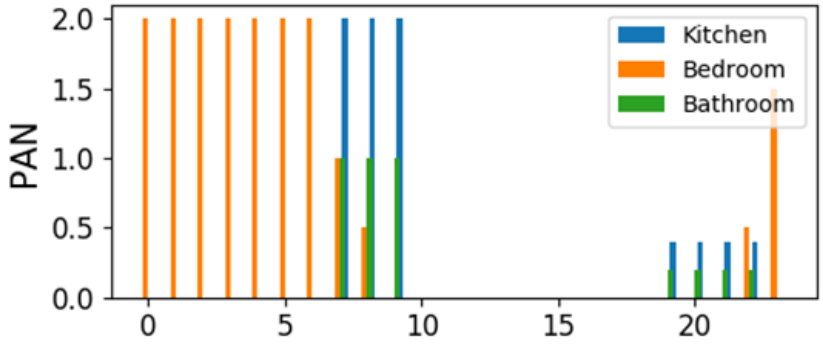

Figure 5.6: Persons absolute number

Occupancy was modelled with a maximum of two persons for kitchen and bedroom and one person for bathrooms. Occupancy is time-varying as shown in Figure 5.6. Heating setpoint temperature is 20°C from 7 am to 2 pm and from 4 pm to 11 pm. During the remaining time a setback temperature of 18°C was set. Each building was modelled with an HVAC system composed of a gas boiler (E+ object Boiler:HotWater) and water radiators as terminals (E+ object ZoneHVAC:Baseboard:RadiantConvective:Water). Pumps were modelled as variable speed pumps (E+ object Pump:VariableSpeed). Both pumps and boilers power have been set as "Autosize", an EnergyPlus key word that allows the software to calculate the design power based on sizing calculations. According to Italian law for climatic zone E, the boiler availability was set from the 15th of October until the 15th of April. The heating system water temperature was modelled as modulating through outdoor air temperature sensor. Circulation spaces and entrances were modelled as unconditioned spaces, thus without heating terminals. Finally, no cooling system was modelled since Italian social housing panorama is often provided with heating system only.

5.6 Weather files

Three weather files were selected to accomplish the optimizations. The first was obtained from EnergyPlus weather data source and it was derived from the "Gianni De Giorgio" weather file collection. This TRY was created from measurements recorded from 1951-1070. The second TRY has recently been elaborated by Italian Thermo-Technical Committee and it is based on measurements from the early 2000s. Since the solar radiation is reported as global radiation on horizontal plane in the CTI file, the Perez model was chosen to extract its components: direct normal radiation and diffuse horizontal radiation, Lupato [63]. The third data was recorded by the University of Trieste, and it reports all weather quantities at 10 minutes interval, in this case also the measured direct horizontal radiation is available, the data has been recorded between 2001 and 2010. According to the latitude and longitude reported in the weather files, the three weather stations are distant 1 km from each other with no relevant elevation differences. The IGDG, and CTI datasets have been recorded at the same place on a dock surrounded by the sea, while the UNITS data has been collected on the roof of a building located less than two hundred meters from the sea. The weather datasets aim to test the differences in TRYs obtained from different recording periods. Therefore, the impact of rising temperatures in building energy optimization was analysed. In Table 5.1, cooling degree-day and heating degree-day are reported for the three datasets.

Weather file	Recording period	CDD18	HDD18
IGDG	1951-1970	594	1882
CTI	1995-2017	733	1553
UNITS	2001-2010	704	1671

Table 5.1: Weather files degree-days

The weather stations' location is illustrated in Figure 5.7 below.

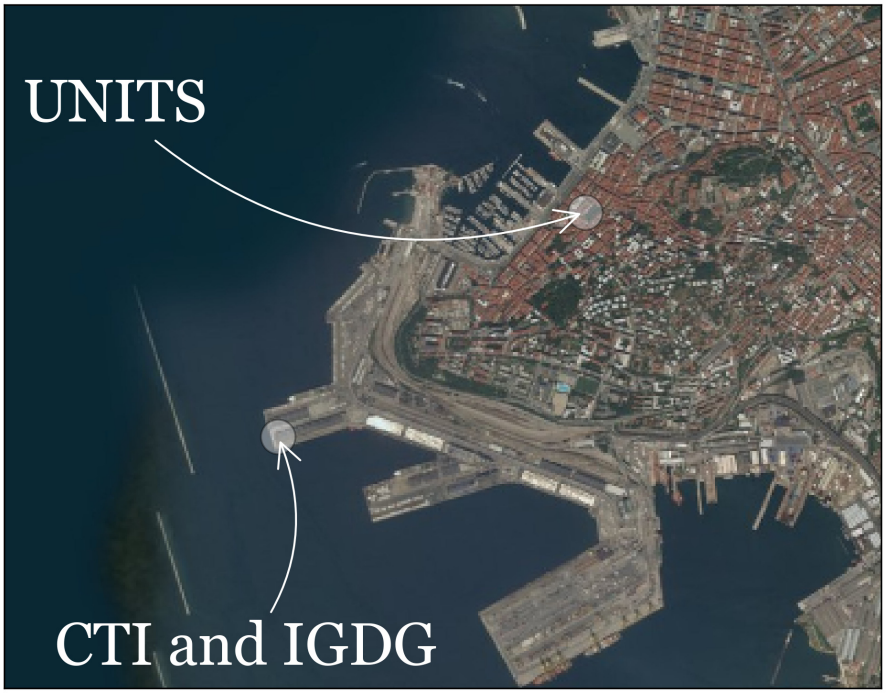

Figure 5.7: Weather stations' location

5.7 Methodology

The optimization was carried out with modeFRONTIER software [146] an optimization environment that can be coupled with third-party engineering tools. modeFRONTIER is a commercial code developed in Trieste by a ESTECO a spin-off of the University. Different algorithms can be applied using numerical codes as computational cores for performing optimization. The program takes care of the whole optimization process. It starts by generating the parameters defined by the user, runs the simulation code directly or using user defined scripts, reads the outputs applying the chosen optimization algorithm to define new designs. For the present case a python script has been created in order to allow modeFRONTIER to drive the optimization. The python script implements the "eppy" library using the parameters provided by the optimizer. It modifies the building model characteristics (IDF objects), runs the EnergyPlus simulation, and reads the results of a single run post processing the data. The script takes care also of the economical side of the problem by computing the investment costs and the net present value. Primary energy and net present value are used as optimization objectives by modeFRONTIER in order to define new designs. The computation workflow is represented in Figure 5.8.

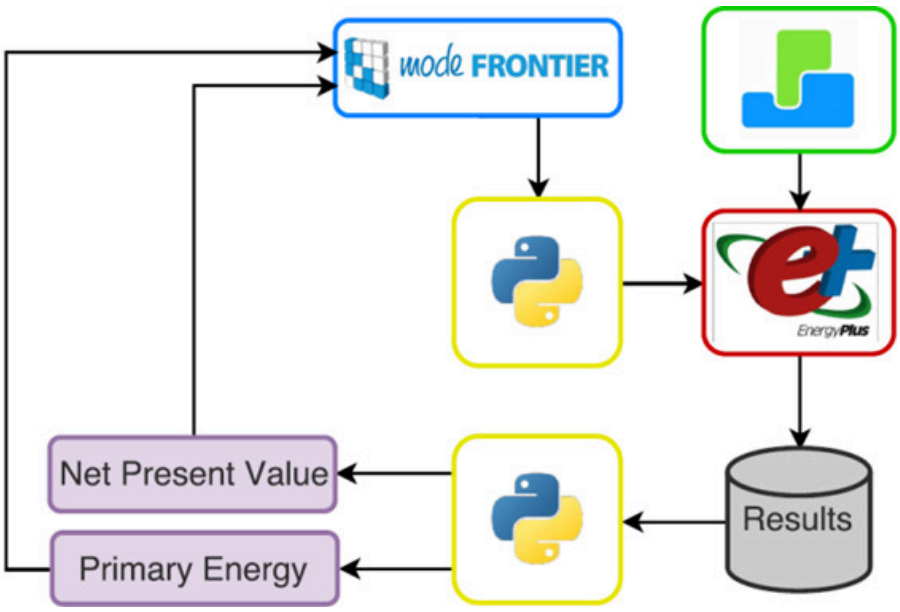

Figure 5.8: Workflow representation

The multi-objective optimization aims to minimize the primary energy and the net present value of the refurbishment investment. Similar design objectives has been used by Pierangioli [147], but they used a Design of Experiments (DOE) approach, while Huws and Jankovic [124] used DesignBuilder to perform a genetic optimization but the objectives were the reduction of carbon emissions and thermal comfort indices.

5.8 Design choices

Ten optimization variables were defined: seven variables are related to the opaque surfaces and three are related to transparent ones. The opaque variables are the insulation thickness of the four external walls with different exposition plus floor, roof and ceiling that separates heated areas to unheated roof space. The variables related to transparent surfaces are the thermal characteristics of the north and south exposed windows. Southern façade consists of two different windows dimensions that were treated as separate variables. Table 5.2 reports the base and the lower and higher ranges of overall thermal transmittances for opaque surfaces, along with the insulation layer characteristics (conductivity, density, specific heat and thickness). Base thermal transmittance values are highlighted in grey. In Table 5.3, the window glass and frame thermal transmittances are reported. Three different types of windows were chosen: a double-glass with air gap, a double-glass with argon filled gap and a triple-glass with argon filled gaps. Solar performance values and prices are reported as well. Base thermal transmittance values are highlighted in grey. Design choices costs The costs of insulation layers were calculated as gross prices, considering also the cost of installation. Prices were obtained from the public regional administration price list Prezziario Regionale dei Lavori Pubblici [148]. The equations for price calculation, expressed in EUR/m2, are hereafter reported in equations from 1 to 4. The variable t represents the insulation thickness expressed in centimetres:

$$p_{ceil} = 1.508 \cdot t + 1.914 \tag{5.1}$$

$$p_{floor} = 2.448 \cdot t + 4.527 \tag{5.2}$$

$$p_{roof} = 3.2271 \cdot t + 6.611 \tag{5.3}$$

$$p_{wall} = 2.614 \cdot t + 4.007 \tag{5.4}$$

Window prices were instead acquired from real quotes, the price comprises transport and installation costs.

5.9 Optimization settings

When dealing with optimization the computational cost can become a limiting factor. For instance, genetic algorithms require hundreds of simulations, the speed of modern computers and the availability of multicore systems can help in reducing the computational burden. Yet, when the time spent for a single simulation increases, alternative methods can help designers to obtain optimized solutions in reasonable times. Response Surface Methods (RSM) are gaining popularity since only a limited number of direct evaluations are required, and the optimization is performed indirectly on mathematically constructed surfaces as performed in Hiyama (2015) for daylighting calculation. However, the solutions heavily depend on the mathematical form used to interpolate the real computation results. Manzan and Clarich [149] adopted the FAST algorithm of modeFRONTIER, comparing the results with standard genetic NSGA II algorithm for a daylighting problem, showing how the same Pareto front can be obtained with a fraction of the simulations and substantially lower computational time. In the present case, the same approach was applied. The FAST algorithm starts from a Design of Experiments and trains a Response Surfaces. For each objective a different set of RSM is trained, then the complete virtual optimization can be performed in a few instants without using the numerical codes. The solutions pertaining to the Pareto frontier are then validated through real time simulations, in this case EnergyPlus, updating the database used for RSM training. In this way, more and more accurate RSM is built in an adaptive and interactive way. Sixteen individuals compose the initial population and the optimization was carried out for 15 generations, for a total of 240 solutions. Each run of EnergyPlus lasted approximately one hour on a XEON X5650 cpu at 2.67 GHz with 24 cores. Using 16 simulations in parallel each optimization could be accomplished in about 16 hours.

5.10 Net present value

The net present value of the investment was calculated over 30 years with the equation 5.

$$NPV = -C_0 + \sum_{1}^{30} C_i \cdot \left(\frac{1+f}{i+r}\right)^i \tag{5.5}$$

Where:
f is the inflation rate, set to 0.7%
i is the time of the cash flow
r is the discount rate, set to 1.17%
C_0 is the cost of the investment expressed in EUR
C_i is the cash flow, calculated with equation 5.6.

$$C_i = Cost_{base} - Cost_{insulated} \tag{5.6}$$

Where: Costbase and Costinsulated are the annual operational costs considering both natural gas and electricity, for base and insulated models, respectively. Primary energy and conversion factors Conversion factors to primary energy were set to 2.42 and 1.05 for electricity and natural gas, respectively. Operational and energy costs Standard cubic meters of natural gas were calculated considering the lower heating value of natural gas and were set to 9.94 kWh/sm^3. The costs of natural gas and electricity were considered as constant and were set to 0.98 EUR/sm^3 and 0.25 EUR/kWh, respectively.

5.11 Discussion and results analysis

Optimizations results are reported from Figures 5.9 to 5.14 with bubble-plots. Bubbles diameters are proportional to the external walls thermal transmittance, south and north oriented, that covers most of the heat losses. Bubble colours represent window types that is blue Type 0, green Type 1 and red Type 2. NPV and primary energy represent x and y-axes, respectively. The Pareto frontiers are generally composed by low wall thermal transmittances (lower diameter bubbles) while south- and north-oriented windows are usually different: northern fenestrations are characterized by low transmittance and SGHC, plotted with red colour in figures. South exposed windows instead show higher transmittances and SGHC, green and red colours in figures. An unsurprising result, since high SGHC windows increase solar gains and no cooling system was simulated. The pattern is common to all TRY files. Figure 5.15 presents the three Pareto frontiers obtained with different TRYs at the same time. The different position of the results represents the impact of the weather files in the optimization. Finally, a weighted coefficients method was used to choose three design combinations, among those of the Pareto frontier, for each optimization run. The coefficients used, applied to NPV and PE objectives are NPVc = 1 and PEc=0, which means maximum net Present value, NPVc=0.5 PEc=0.5 mean value NPVc=0, PEc=1 minimum primary energy. The results for each solution are reported in Tables 5.5, 5.6 and 5.7. In Figure 5.15, the three solutions for the three cases are also highlighted for each Pareto frontier. An additional information is given by primary energy analysis, for instance for the three weather files the same pattern is replicated, the difference among minimum primary energy consumption and mean values is low. On the contrary the values of NPV increase substantially from the optimum energy solutions to the mean-weighted one (0.5 coefficient for both optimization variables). The behaviour is reversed if the mean solution and the maximum NPV ones are compared. In this case large differences in PE are evident for a limited variation of NPV, indicating that with a little more investment

substantial energy savings could be obtained.

Construction	U_{min}	U_{max}	Insulation
Wall	0.14	0.49	2 to 14
Ceiling	0.14	1.61	2 to 25
Roof	0.21	0.81	2 to 20
Floor	0.17	0.68	2 to 20

Table 5.2: Windows solar properties, prices and glass and frame thermal transmittances are reported

	Window 113*165 cm			
Windows Types	U_g [W/m^{2}K]	SHGC [–]	U_f [W/m^{2}K]	Price [€]
Type 0	1.4	0.66	1.3	365
Type 1	1.2	0.425	1.3	370
Type 2	0.8	0.398	1.1	438

Table 5.3: Windows solar properties, prices and glass and frame thermal transmittances are reported

	Window 40*90 cm			
Windows Types	U_g [W/m^{2}K]	SHGC [–]	U_f [W/m^{2}K]	Price [€]
Type 0	1.4	0.66	1.3	113
Type 1	1.2	0.425	1.3	113
Type 2	0.8	0.398	1.1	122

Table 5.4: Windows solar properties, prices and glass and frame thermal transmittances are reported

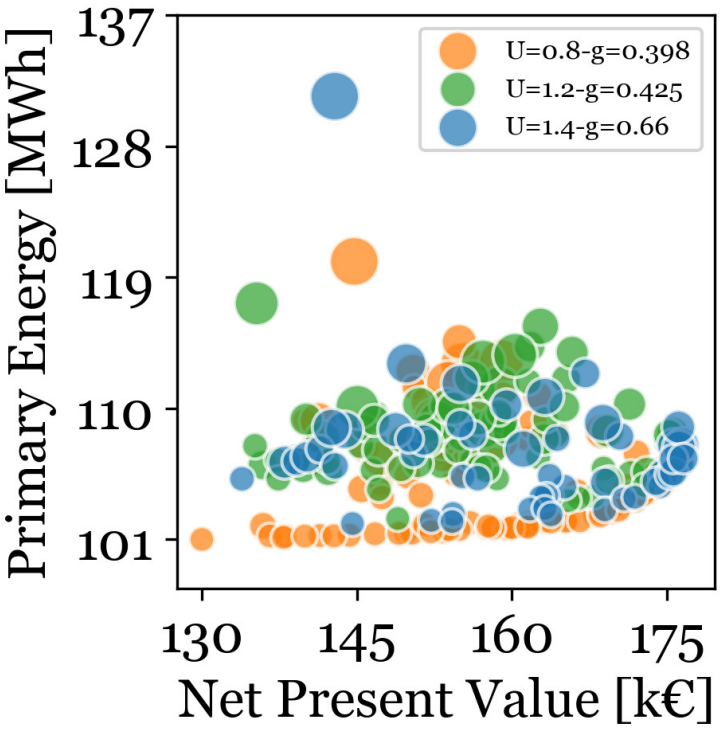

Figure 5.9: Solutions with IGDG weather file and southern wall transmittance

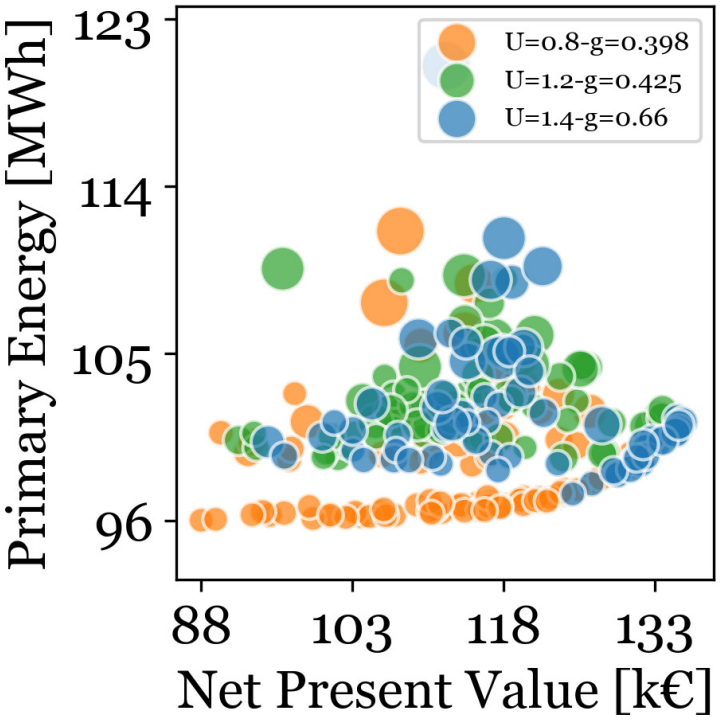

Figure 5.10: Solutions with CTI weather file and southern wall transmittance

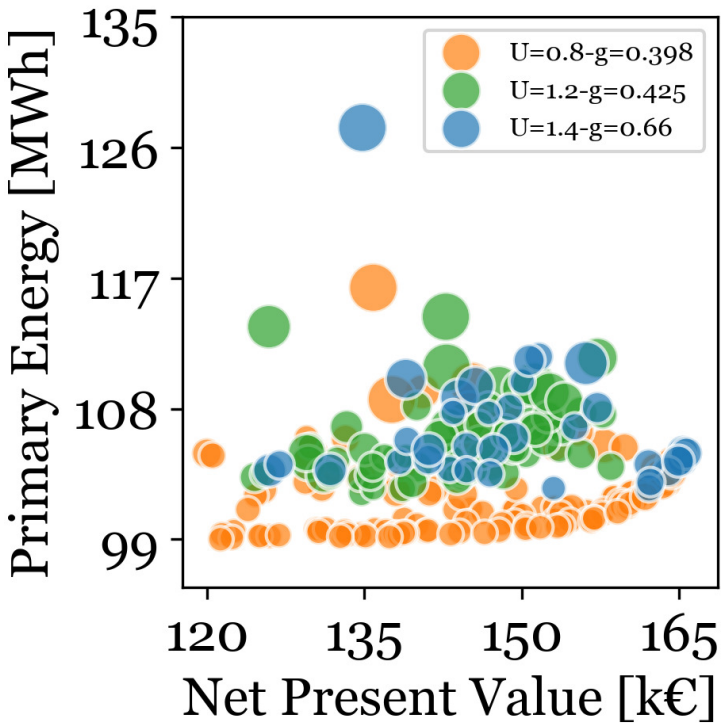

Figure 5.11: Solutions with UNITS weather file and southern wall transmittance

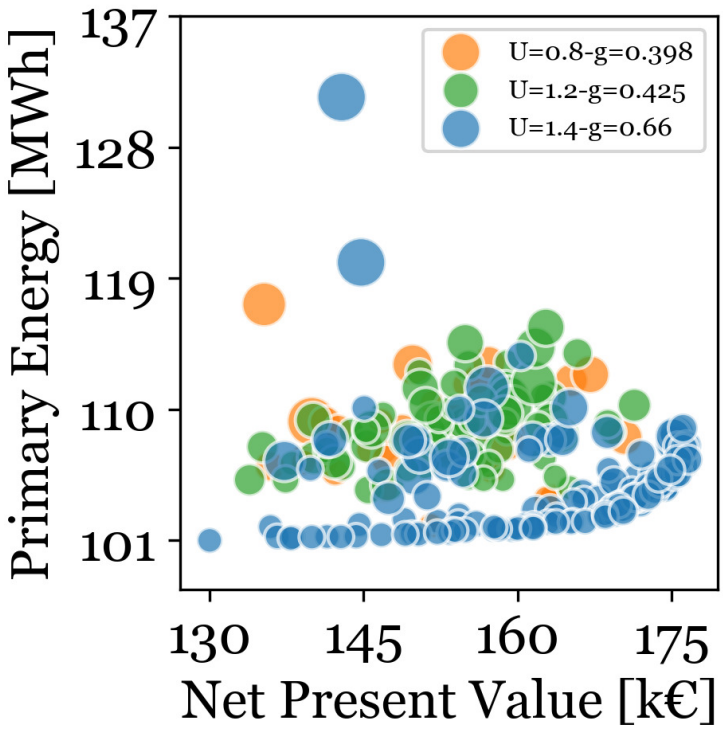

Figure 5.12: Solutions with IGDG weather file and northern wall transmittance

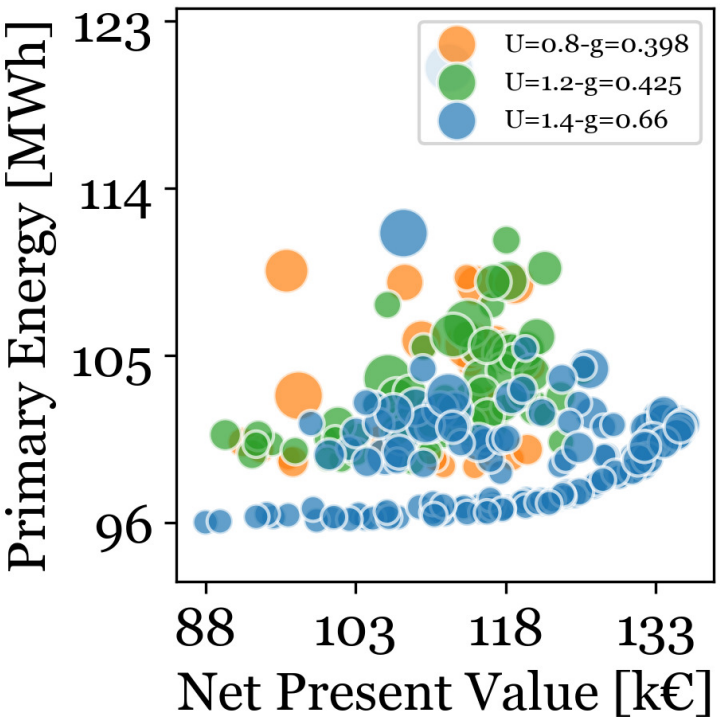

Figure 5.13: Solutions with CTI weather file and northern wall transmittance

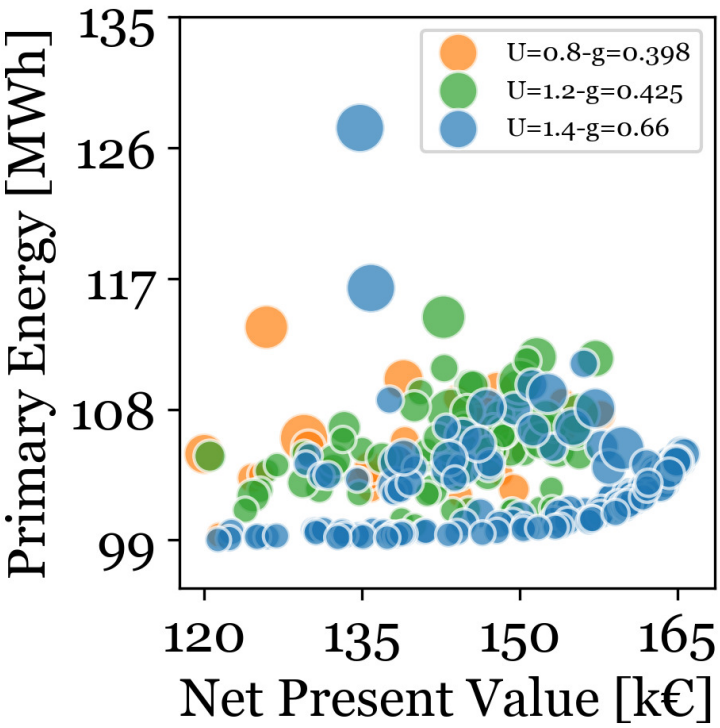

Figure 5.14: Solutions with UNITS weather file and northern wall transmittance

NPVc=1, PEc=0	IGDG	UNITS	CTI
Uwall - south	0.282	0.337	0.337
Uwall – north	0.307	0.337	0.307
Uwall – east	0.282	0.282	0.282
Uwall – west	0.243	0.307	0.282
Uceiling	0.222	0.197	0.272
Uroof	1.347	1.347	1.347
Ufloor	0.489	0.489	0.489
Win(1.13x1.65) N	Type1	Type1	Type1
Win(1.13x1.65) S	Type1	Type1	Type1
Win(0.4x0.9) S	Type3	Type1	Type1
PE (MWh)	107.0	105.7	101.3
NPV (kEUR)	177.0	165.7	135.9
Investment (kEUR)	96.4	92.8	91.6
Pay-back (years)	10.2	10.3	11.4

Table 5.5: Pareto Solution with NPVc=1 and PEc=0

NPVc=0, PEc=1	IGDG	UNITS	CTI
Uwall - south	0.214	0.214	0.214
Uwall – north	0.214	0.214	0.214
Uwall – east	0.227	0.227	0.227
Uwall – west	0.227	0.227	0.214
Uceiling	0.143	0.155	0.143
Uroof	0.188	0.17	0.179
Ufloor	0.139	0.217	0.204
Win(1.13x1.65) N	Type3	Type3	Type3
Win(1.13x1.65) S	Type1	Type1	Type1
Win(0.4x0.9) S	Type1	Type1	Type1
PE (MWh)	101.5	99.7	96.0
NPV (kEUR)	130.4	121.3	88.1
Investment (kEUR)	157.5	152.7	153.3
Pay-back (years)	15.9	16.26	18.27

Table 5.6: Pareto Solution with NPVc=0 and PEc=1

NPVc=0.5, PEc=0.5	IGDG	UNITS	CTI
Uwall - south	0.214	0.227	0.214
Uwall – north	0.214	0.214	0.214
Uwall – east	0.227	0.243	0.227
Uwall – west	0.243	0.243	0.214
Uceiling	0.149	0.143	0.143
Uroof	1.347	1.347	1.347
Ufloor	0.345	0.489	0.489
Win(1.13x1.65) N	Type3	Type3	Type3
Win(1.13x1.65) S	Type1	Type1	Type1
Win(0.4x0.9) S	Type3	Type1	Type1
PE (MWh)	102.7	101.0	97.1
NPV (kEUR)	167.0	156.7	122.5
Investment (kEUR)	117.6	114.1	116.3
Pay-back (years)	11.9	12.2	13.8

Table 5.7: Pareto Solution with NPVc=0.5 and PEc=0.5

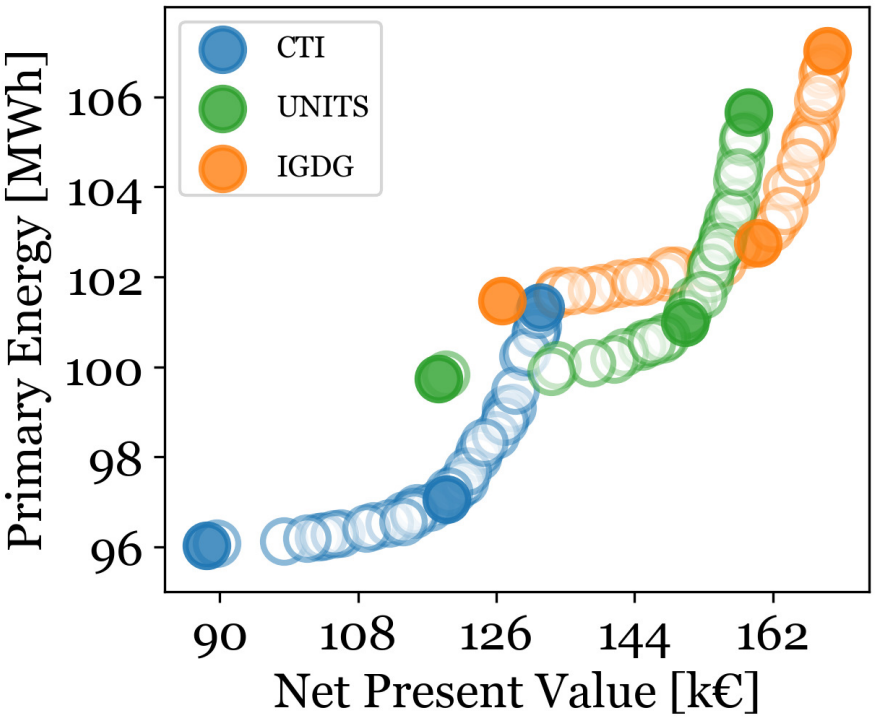

Figure 5.15: Pareto frontier for each weather file and selected individual for the analysis

5.12 Final remarks

Building energy optimization was carried out with three different weather files and applied to a social house in Trieste. Although two of the weather measurements

tested were recorded in the same period and position, Pareto frontiers showed remarkable differences. The CTI and IGDG datasets generate quite different Pareto fronts with lower PE for the former, due to the rise of temperatures. The UNITS Pareto front shows higher PE than the CTI dataset, since is less influenced by the sea. As expected the increase in PE also lead to an increase of NPV as more expensive solution are searched by the optimization. In applying multi-objective optimization, attention should be paid to the choice of the weather file since it could greatly affect the optimization results, leading to optimal solutions for a specific climate, but that can be less performant if climate change effects are taken into account. Despite the NPV, primary energy differences cannot be ignored. In this specific case, the design choices are very similar, as can be noticed from the analysis of Tables from 5.5 to 5.7. For instance, though the opaque and transparent constructions performances are similar in most cases, great NPV differences must be highlighted that can greatly influence the decision makers in adopting selected solutions. Further analysis should be carried out to investigate on:

- deeper economic analysis, taking into account national incentives and facilitations;
- weather file differences at hourly frequency;
- Cooling systems impact on optimizations.

Chapter 6

Wheather file impact: cooling system sizing

This chapter aims to focus on cooling design calculations and the effect of climatic design conditions on its results. In general, sizing procedures of a residential HVAC system involves the design to meet the accurate predicted heating and cooling loads of a house [150].
Variations in the characteristics of residential buildings can lead to complex load calculations [42]. The heat flows are time-varying so that the related system load is time-varying as well. The variation of the heat flows are to be reconducted to building characteristics, both as regard the envelope performance, the building usage and the exposure. The identification of the peak demand on HVAC system is based on design-day or short period calculations using near-extreme conditions [36]. Hourly or sub-hourly analysis is frequently carried out to determine the load trend and to identify its peak.
During heating system sizing, in order to analyse the worst-case scenario, the following assumptions are usually taken:

- No solar gain
- No occupancy (if it may take place, according to building usage)
- No process internal gains (if it may take place, according to building usage)

Therefore, the total heating thermal power is mainly evaluated calculating ventilation and transmissione heat losses with the equations:

$$q_t = A \cdot U \cdot \Delta\Theta \tag{6.1}$$

$$q_v = \dot{m}_v \cdot C_p \cdot \Delta\Theta \tag{6.2}$$

$$q_i = \dot{m}_i \cdot C_p \cdot \Delta\Theta \tag{6.3}$$

where:

q_t: transmission heat loss
q_v: ventilation heat loss
q_i: infiltration heat loss
A: the surface area
U: the surface thermal transmittance

$\Delta\Theta$: the temperature difference
$\dot{m}$: the air mass flow rate
C_p: the air specific heat

Equations 6.2 and 6.3 consider only sensible heat loss because in the residential case studies humidification is rarely considered at system level, depending on the climate. On the other hand, the cooling sizing process involves time-varying internal heat gains, solar gains on opaque and transparent surfaces and latent gains: the problem is more complex, even more because the variables involved may have non-coincident peaks. Accordingly, this chapter investigates the impact of climate conditions on cooling design.

6.1 Cooling load metodologies

In literature, several load calculation methods were developed [42] and the ASHRAE method is one of the most widely used [150]. Theoretically, different types of structures require the same calculation procedures, both as regards residential and commercial buildings. However, in practice, simplifications are used if contextualized into a specific building typology. Therefore, load calculation methods can be used specifically with residential or commercial buildings [151].
Mao [152] compared all the cooling load methods published in Ashrae from 1967 to 2013. The author carried out a literary review, dividing the methods in four groups, based on the period: "Pre 1945", "1946-1969", "1970-1989" and "1990-Present": the last group is summarized below.
The first wide-spread computer-oriented method for dynamic calculations for building in the U.S. was published in 1972 [153, 152]: the Transfer Function Method (TFM). It uses weighting factors to calculate the heat gains from the surfaces. The TFM method was developed by Rudoy and Duran [154] and, in 1974, the Cooling Load Temperature Difference/Cooling Load Factor Method (CLTD/CLF) was published. It was included in the 1977 Ashrae Book of Fundamentals and it contains tabulated values to estimate cooling load calculations through the structures: this method aims to simplify the TFM methodology. The CLTD coefficients were recalculated and updated by Edward Sowell in 1988 [155].
The CLTD procedure was updated again in 1993, when the Solar Cooling Load Method (SCL) was introduced. The new term calculates the cooling loads due to solar radiation transmitted through windows. In the CLTD previous versions, the solar load was inaccurate if used with latitudes and dates other than 40°N/July 21 [156].
Curtis Pedersen developed, in 1997, the Heat Balance method (HBM)[157]: it requires the calculations of four processes: outside surface heat balance, wall conduction process, inside surface heat balance and zone air heat balance.
Spitler based his method on the HBM and presented, in 1997, the Radiant Time Series Method (RTSM). The author simplified the methodology and used one-dymensional time-varying conduction [152].
Charles Barnaby [158] developed, in 2004, two cooling loads methods: the Residential Heat Balance (RHB) and the Residential load calculations (RLF). The former was designed to be implemented in computer algorithms, while the latter was simplified and it is suitable for manual calculations.

Nigusse improved the RTSM method in 2007 [159], introducing the solar heat gain factor to evaluate the solar load through transparent surfaces.
The simulations carried out in this analysis were developed with EnergyPlus simulation software, which is based on heat balance method: it uses the HBM sizing method [157] to calculate the zone loads [160].

6.2 Boundary condition definition

The cooling load methodologies described in section 6.1 require setting the external boundary conditions. They are a series of data which define the solar and thermo-hygrometric parameters of the climate. Therefore, they affect the heat gain terms and the cooling load results: weather is an important factor when sizing an HVAC system [5]. The climate parameters used could be obtained with different statistical methodologies and they represent extreme conditions, assessed with confidence levels. In this analysis, we applied two methodologies, the UNI EN 15927 [145] and the Ashrare design conditions [161], which can be found in the Ashrae Handbook of Fundamentals 2009 [42].

6.2.1 UNI EN 15927-2

The UNI EN 15927 is divided into six parts: the second part is dedicated to the calculation methodology for hourly data necessary to determine the building design cooling load [145].
The aim is to define individual days for each calendar month with confidence levels of 5%, 2% and 1%. Daily mean dry-bulb temperature and daily total global solar radiation are required, while other parameters are optional. In this analysis, all of the five proposed parameters were used and are summarized in Table 6.1.

Parameter	**Band**	**Unit**
Daily man dry-bulb temperature	±0.5	[°C]
Total global solar irradiation	±0.05	[kWh/m^2]
Daily mean dew-point temperature	±0.5	[°C]
Daily dry-bulb temperature swing	±0.5	[°C]
Daily mean wind speed	±0.5	[m/s]

Table 6.1: Climate parameters used to identify the design day

The standard aims to identify extreme condition days from a dataset. First, the parameters in Table 6.1 are obtained from the dataset hourly value. The procedure uses the percentile to identify the related confidence levels. Finally, it adds or subtracts the predefined values, showed in the second column of Table 6.1, defining the search bands. It subsequently searches for a day of the dataset that "falls" within the intervals. If no day is identified, the bands are progressively increased. If more than one day is identified, the bands are progressively reduced. The dimension of the dataset is relevant: the standard recommends to apply the procedure to at least 10-year datasets.
The design day can not include missing values, which is why fitting methodologies

may be included as pre-process. The selection of five parameters highlights another critical aspects: not only the dataset is required to be adequately extended but each of the parameter should to be uniform, in terms of low missing data. In other words, if even one values include several data gap, the procedure may not produce good results.
As described in the UNI EN 15927-2, one design day are obtained for each calendar month and confidence level, for a total of 36 design days. This may be useful when sizing a building system that does not require cooling during the hottest months. For example, the schools in Italy are closed in July and August: sizing a cooling system for the hottest month could lead to an over-sized system. On the other hand, if the procedure has to be applied to a building that needs to be conditioned the whole year, the hottest month design day is appropriate. However, in the standard, no indication is given on how to select the most extreme month. Therefore, two criteria were used to identify the extreme month: the maximum mean air temperature and the maximum total global irradiation were individually used to identify one design day for each confidence level over the 12 calendar months, for a total of 6 design days. This procedure is not described in the UNI EN 15927-2 and aims to identify one design day to be used when sizing a cooling system available all the year: the choice between the design day based on temperature and total irradiation is closely related to the characteristics of building under examination.
A similar concept was highlighted by Pernigotto, Cui and Hensen [68, 5, 22], but applied to reference year weighing factors selection, that is explained in section 3.3. These authors highlighted that the reference years are mostly composed by actual month measurements, selected with weighing factors, that enhance the importance of some variables over the others. The typical meteorological year assumes "an average building [22]" without considering the various sensitive variables of different building types and systems [5]. Accordingly, the same argument can be applied to cooling design, where the building characteristics are fundamental to select appropriate climate design conditions.

6.2.2 ASHRAE Design Conditions

According to Ashrae Handbook Fundamentals 2009, Chapter 17 [42], outdoor design conditions heating and cooling should be selected from location-specific climate. As regards cooling, two psychometric variables are required: the design dry-bulb temperature and mean coincident wet bulb temperature are given for 3 confidence levels: 0.4%, 1% and 2% where the 1% level is indicated as appropriate. The hottest-month dry-bulb temperature daily range and the related wind speed are also required. As highlighted in Ashrae Chapter 14, the hottest month generally is suitable for middle latitudes. This pattern does not always hold: buildings with high performance horizontal shadings or wide south-oriented windows may have a cooling peak in different periods due to the sun position. It is recommended to carry out the procedure several times of the year.

The matching method Since the CTI weather station do not coincide with the Ashrae reports' weather station, a matching method was applied to be able to select the corresponding Ashrae report, obtained from a weather station within 50 km distance and 50 m height difference from the CTI dataset. The methodology was

developed to be able to replicate a practitioner's selection and it is kept simplified on purpose: further details can be found in section 4.7. The imposed limits are 50 km distance and 50 m height difference between the two weather stations. All the matchings that do not fall within these limits were rejected. 109 CTI datasets were made available from the CTI while the Italian Ashrae reports are 103: the matching method returned 53 valid comparisons. The matching method results are shown in Figure 6.1.

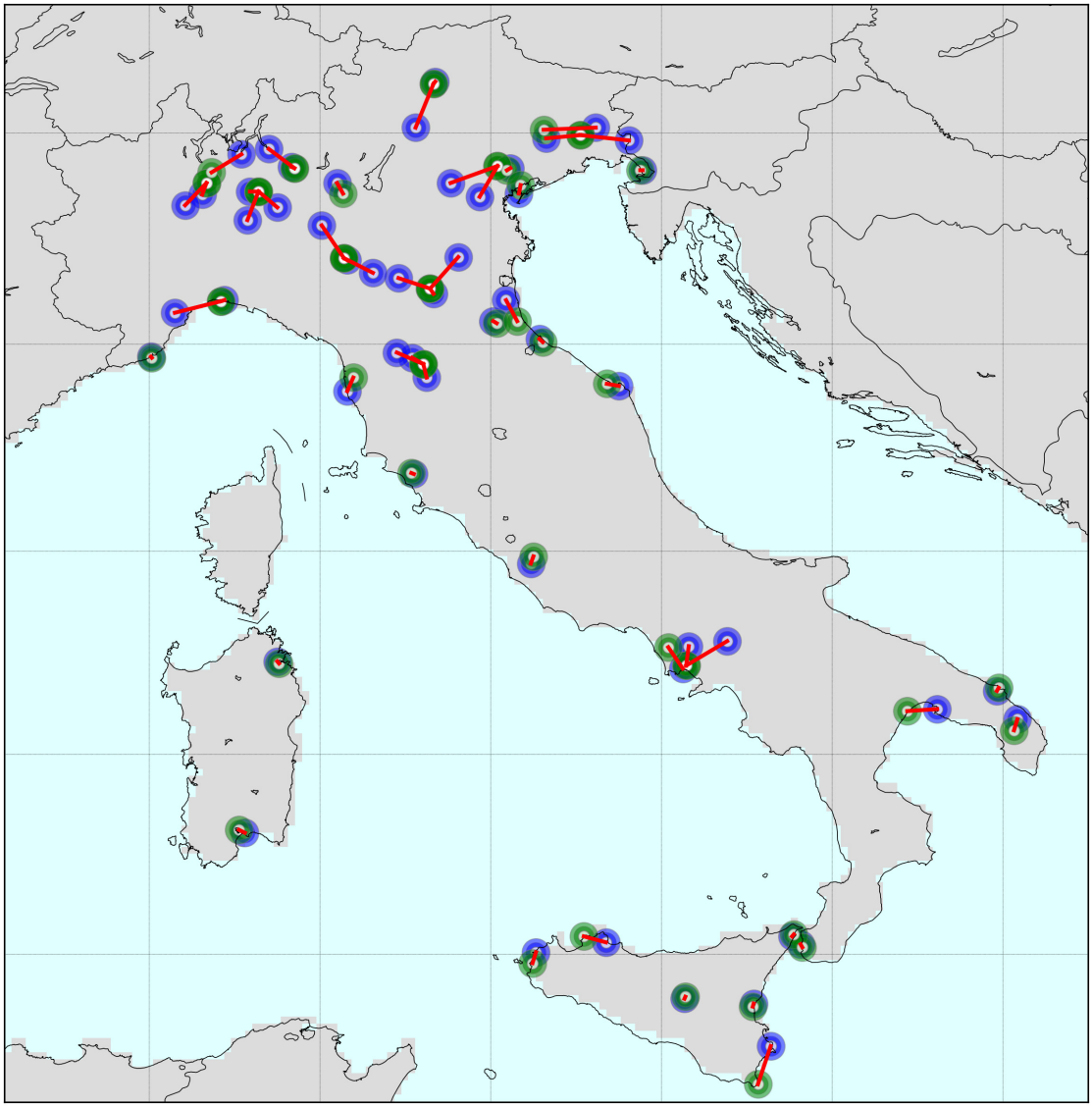

Figure 6.1: Matching method map, CTI stations (blue) and Ashrae stations (green)

6.3 Case study introduction

In this section, a brief case study introduction is given. The analysis aims to test the weather-related design methods with a test building model, for each dataset available when allowed by the matching method described in section 6.2.2. The methodologies are applied to different period recordings and weather stations and thus results are not directly comparable. The aim is to highlight the differences between using one

method or the other, considering the data available for the Italian territory. The major objective of this analysis is to highlight the differences a practitioner can obtain in choosing one design method or another.
Design procedures were applied to one typology of building which can be considered representative of the residential scenario for the whole Italian territory. This choice could be considered restrictive, but it allows a direct comparison of the results. For instance the proposed method could be efficiently applied to different models using different window to wall ratio and building usages, but losing the generalization of the results. The project is ongoing and further investigations are described in section 6.9.

6.4 Data source

The data are provided by CTI and were collected from several third-party weather stations. Therefore, datasets informations are confidential and were used for research purposes only. The data and design day results can not be illustrated.

6.5 Outdoor conditions design comparison

The aim of this analysis is to compare the application of the Ashrae procedures, with data collected from Ashrea Climate Conditions 2017 [161] with the results of the UNI EN 15927-2, applied to the CTI datasets.

UNI EN 15927-2 methodology provides three confidence levels to identify the design days: 99%, 98% and 95%. Similarly, the Ashrae Design Climatic Conditions [161] reports contain three maximum dry-bulb temperature levels: 99.6%, 98% and 95%. The methodologies are completely different: it is not possible to simply select the same confidence level to compare each other. Thus, the methods were compared with the highest confidence levels, 99% for UNI EN 15927-2 and 99.6% for Ashrae. As regard solar radiation data in the design day method, global radiation data at hourly frequency are identified and converted into direct normal radiation with the Perez model [52], that shows high performance [63]. For the Ashrae methodology, a *Clear Sky* model is instead needed and has to be applied to obtain solar radiation. Therefore, three different solar models were applied:

- Ashrae *Clear Sky* model [162, 163]
- Ashrae *Tau* model [42]
- *Zhang Huang* model [164, 165]

The models are EnergyPlus built-in functions and, to input them, it is sufficient to select the option within the EnergyPlus interface. When applying the Ashrae *TAU* model, the *taub* and *taud* coefficients are required: these values are related to beam and diffuse solar radiation respectively and were obtained from the Ashrae climate conditions reports.
Finally, five methods were tested and simulated, the methods are summarized in Table 6.2 where the source of the psychometric and solar parameters are illustrated.

The fourth column in Table 6.2 represents the ID for each combination and will be reported in the graphs' legends of the following figures. The key words "tb" and "rb" stand for temperature based and radiation based respectively and were defined in section 6.2.1.

Dry-bulb temperature	Second psychometric variable	Solar radiation	ID
15927 tb	Relative humidity 15927 tb	15927 tb	*DD_t*
15927 rb	Relative humidity 15927 rb	15927 rb	*DD_r*
Ashrae Report	Wet-bulb Ashrae Report	Ashrae *Clear Sky*	*CS*
Ashrae Report	Wet-bulb Ashrae Report	Ashrae *Tau*	*TAU*
Ashrae Report	Wet-bulb Ashrae Report	*Zhang Huang*	*ZH*

Table 6.2: Summary of the sizing method selected

6.5.1 ASHRAE Clear Sky Solar Model

According to EnergyPlus documentation [62], the ASHRAE Clear Sky Solar model is suitable to estimate hourly solar radiation for any month of the year. The direct normal radiation is calculated with equation 6.4.

$$DNI = \frac{A}{exp\left(\frac{B}{\sin\beta}\right)} \tag{6.4}$$

Where A is the apparent solar irraiation at air mass m=0 and B is the atmospheric extinction coefficient. A and B are obtained from Table 6.3.

	I_0[W/m^2]	Equation of time [minutes]	Declination [°]	A [W/m^2]	B [-]
Jan	1416	-11.2	-20.0	1202	0.141
Feb	1401	-13.9	-10.8	1187	0.142
Mar	1381	-7.5	0.0	1164	0.149
Apr	1356	1.1	11.6	1130	0.164
May	1336	3.3	20.0	1106	0.177
Jun	1336	-1.4	23.45	1092	0.185
Jul	1336	-6.2	20.6	1093	0.186
Aug	1338	-2.4	12.3	1107	0.182
Sep	1359	7.5	0.0	1136	0.165
Oct	1380	15.4	-10.5	1166	0.152
Nov	1405	13.8	-19.8	1190	0.144
Dec	1417	1.6	-23.45	1204	0.141

Table 6.3: A and B coefficients

6.5.2 ASHRAE Tau Solar Model

The *Ashrae Tau Model* is a revision of the Clear Sly model [62], introduced in Ashrae 2009 Handbook of Fundamentals [42]. The model uses beam and diffuse optical depths that are obtained from Ashrae Climatic Design Data. The model uses equations 6.5, 6.6, 6.7, 6.8 and 6.9.

$$E_b = E_0 \cdot exp[-\tau_b \cdot m^{ab}] \tag{6.5}$$

$$E_d = E_0 \cdot exp[-\tau_d \cdot m^{ad}] \tag{6.6}$$

$$m = \frac{1}{\sin\beta + 0.50572 \cdot (6.07995 + \beta)^{-1.6364}} \tag{6.7}$$

$$ab = 1.219 + 0.043 \cdot \tau_b - 0.151 \cdot \tau_d - 0.204 \cdot \tau_b \cdot \tau_d \tag{6.8}$$

$$ad = 0.202 + 0.852 \cdot \tau_b - 0.007 \cdot \tau_d - 0.357 \cdot \tau_b \cdot \tau_d \tag{6.9}$$

Where:

$E_b =$	Beam normal irradiance, [W/m^2]
$E_d =$	Diffuse horizontal irradiance, [W/m^2]
$E_0 =$	Extraterrestrial normal irradiance, [W/m^2]
m =	Air mass
$\tau_b =$	Beam optical depth
$\tau_d =$	Diffuse optical depth
$ab =$	Beam air mass exponent
$ad =$	Diffuse air mass exponent

6.5.3 Zhang-Huang Solar Model

The *Zhang-Huang Model*[165] uses weather parameters and constants to calculate the hourly solar radiation [62].

$$I = \frac{I_0 \cdot \sin h \cdot (c_0 + c_1 \cdot CC + c_2 \cdot CC^2 + c_3(T_n - T_{n-3}) + c_4 \cdot \varphi + c_5 \cdot V_\omega) + d}{k} \tag{6.10}$$

Where:

I	Estimated hourly solar radiation [W/m^2]
I_0	Global solar constant, 1355 [W/m^2]
CC	Cloud Cover
φ	Relative humidity [%]
T_n	Dry-bulb air temperature at current hour (n)
T_{n-3}	Dry-bulb air temperature at n-3 hour
V_ω	Wind speed [m/s]
c_0	Coefficient 0.5598
c_1	Coefficient 0.4982
c_2	Coefficient -0.6762
c_3	Coefficient 0.02842
c_4	Coefficient -0.00317
c_5	Coefficient 0.014
d	Coefficient -17.853
k	Coefficient 0.843

6.5.4 Temperature profile model

In Ashrae 2009 [42] Chapter 14 is illustrated a procedure to generate hourly air temperatures suitable as input for HVAC analysis. The authors, Hedrick [166] and Thevenard [167], have identified a representative profile for both dry-bulb and wet-bulb temperature on typical design-days. The $F(t)$ value is illustrated in Table 6.4.

$$\theta_t = \theta_{max} - F(t) \cdot \Delta\theta_{max} \tag{6.11}$$

Solar hour	Faction	Solar hour	Faction	Solar hour	Faction
1	0.88	9	0.55	17	0.14
2	0.92	10	0.38	18	0.24
3	0.95	11	0.23	19	0.39
4	0.98	12	0.13	20	0.50
5	1.00	13	0.05	21	0.59
6	0.98	14	0.00	22	0.68
7	0.91	15	0.00	23	0.75
8	0.74	16	0.06	24	0.82

Table 6.4: $F(t)$ coefficients, hourly values

In Figure 6.2, the value of $1 - F(t)$ is illustrated: it shows the daily temperature profile.

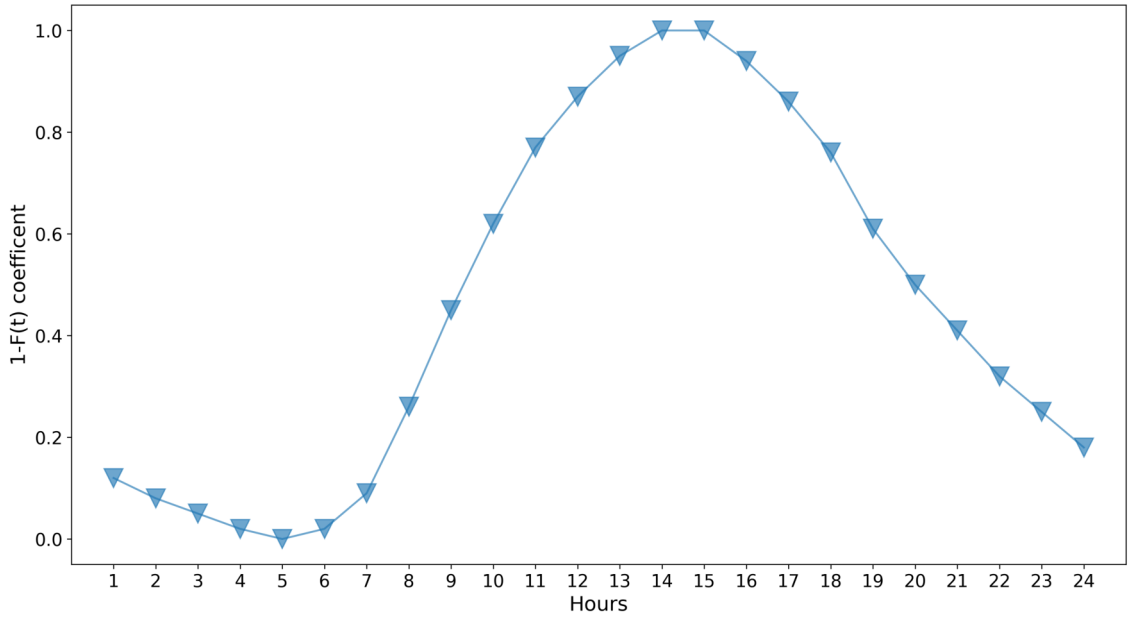

Figure 6.2: 1-F(t) coefficient

6.6 Test buildings

As already described in 4.8, according to ISTAT data, the period that goes from 1961 to 1975 is representative for the majority of the existing Italian buildings. Therefore, only the insulated and uninsulated buildings related to this period were analysed in this case-study.
The main characteristics of the building are summarized in the following tables. More details are reported in section 4.8.

Area [m^2]	WWR [%]	Volume [m^3]	HLS [m^2]	SV [m^-1]
934	9.33	3074	1667	0.54

Table 6.5: Building area and characteristics

The model was not divided into zones: a fixed space distribution was set (Table 4.2) and time-varying heat gains were modelled. Electric heat gains can be summarized into a maximum design power of 4.6 W/m^2. Occupancy was set to a maximum of 0.04 $people/m^2$. Cooling system availability was modelled as always-on during the whole year. The air temperature was set to 26°C from 8 am to 10 pm: for the rest of the time, air temperature setpoint was set to 28°C.
Heating and cooling systems types were modelled as ideal with 100% convective effects. In order to model an ideal system, EnergyPlus [136] object ZoneHVAC:IdealLoadsAirSystem was used. It provides a model for an ideal HVAC system and it supplies cooling or heating air to a zone in sufficient quantity to meet the zone load. Cooling design supply conditions were modelled as shown in Table 4.4, with $12°C$ air temperature and 8 g_w/kg_{da}. Since cooling supply air conditions are far below zone internal air saturation conditions, latent gains were considered: the cooling system provides dehumidification even if there is no dehumidification setpoint. The ZoneHVAC:IdealLoadsAirSystem object is modelled as an ideal VAV terminal unit with variable supply air temperature and humidity. The supply air flow rate varies between zero and the maximum in order to satisfy the zone cooling load. According to Ashrae 90.1, a sizing factor of 1.15 was set: it increases the design thermal power by 15%. Opaque constructions characteristics are illustrated from Table 6.6 to 6.8. Window wall ratios are illustrated in Table 6.5. When two wall types were reported in Tabula web tool, the widest surface wall transmittance was selected: this case is highlighted with an asterisk (*) in Table 6.6. No shadings were modelled during simulations to avoid human behaviour influences. Outdoor air flow rate, intended as intentionally or inadvertently introduced into the building, was set to 0.3 ACH.

OPAQUE U		1961 - 1975	
		B_U	B_I
U Wall	[W/m^{2}K]	1.15*	0.23
U Roof	[W/m^{2}K]	1.10	0.21
U Floor	[W/m^{2}K]	0.94	0.21

Table 6.6: Opaque construction thermal transmittance for uninsulated and insulated models

OPAQUE M		1961 - 1975
M Wall	[kg/m2]	194
M Roof	[kg/m2]	406
M Floor	[kg/m2]	478

Table 6.7: Opaque construction surface mass for uninsulated and insulated models

WINDOW		1961 - 1975	
		B_U	B_I
SHGC	[–]	0.7	0.398
U_w	[W/m^{2}K]	2.2	0.8

Table 6.8: Window characteristics for uninsulated and insulated models

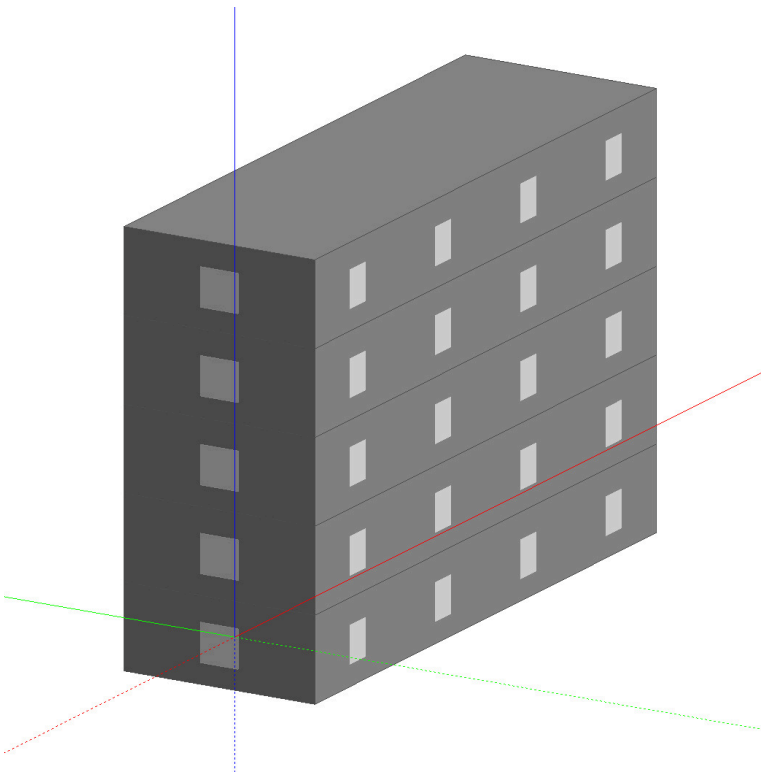

Figure 6.3: An image of the model

6.7 Results

Design power results for each weather condition are shown from Figure 6.4 to 6.6 and from 6.7 to 6.9 respectively. Since the middle floors presents the same characteristics and heat losses, the results are very close each other: an average value is shown in Figure 6.5 and 6.8 for insulated and uninsulated buildings.
Design days methods based on temperature and radiation are coloured in blue and orange, while *Clear Sky* (*CS*), *Zhang Huang* (*ZH*) and Tau (*TAU*) methods are green, red and purple. In addition, the vertical black lines represents the design power difference between the highest and the lowest value, for each station. The trends for uninsulated and insulated buildings, and from the three floor cases, are comparable. As regard the *ZH*, *CS* and *TAU* methodologies, that share identical hourly air temperatures, the *ZH* clearly shows the lowest results. Furthermore, *CS* and *TAU* methods are almost identical: the markers are predominantly overlapped. The reason of this result is that the *TAU* model is simply a revised version of the *CS* and it is based on location-specific optical depths for direct and diffuse radiation [62] with the coefficients tabulated by month for all the locations in 2009 ASHRAE handbook: Fundamentals [42, 161]. According to EnergyPlus documentation [62], the *TAU* model provide more physically plausible values compared to the *Clear Sky* model. As can be noticed from Figure 6.4 to 6.9, these improvements do not affect the simulation sizing results for this specific case-study. Finally, a specific trend is not identifiable for design day based on temperature (*DD_t*) and radiation (*DD_r*). *DD_r* appears to present several minimum values: the test building is characterized by a relatively low window wall ratio therefore this result may be justified by the fact that *DD_r* design day, during the procedure, can be selected outside of July and August that are the hottest months in terms of daily mean air temperature.
The outliers results are all owing to the *DD_t* and *DD_r* methods. The *CS*, *TAU* and *ZH* models share the same external air-conditions with different solar models. The *CS*, that usually over estimates the solar radiation[62], and the *TAU* models show similar results while the *ZH* presents always lower values.

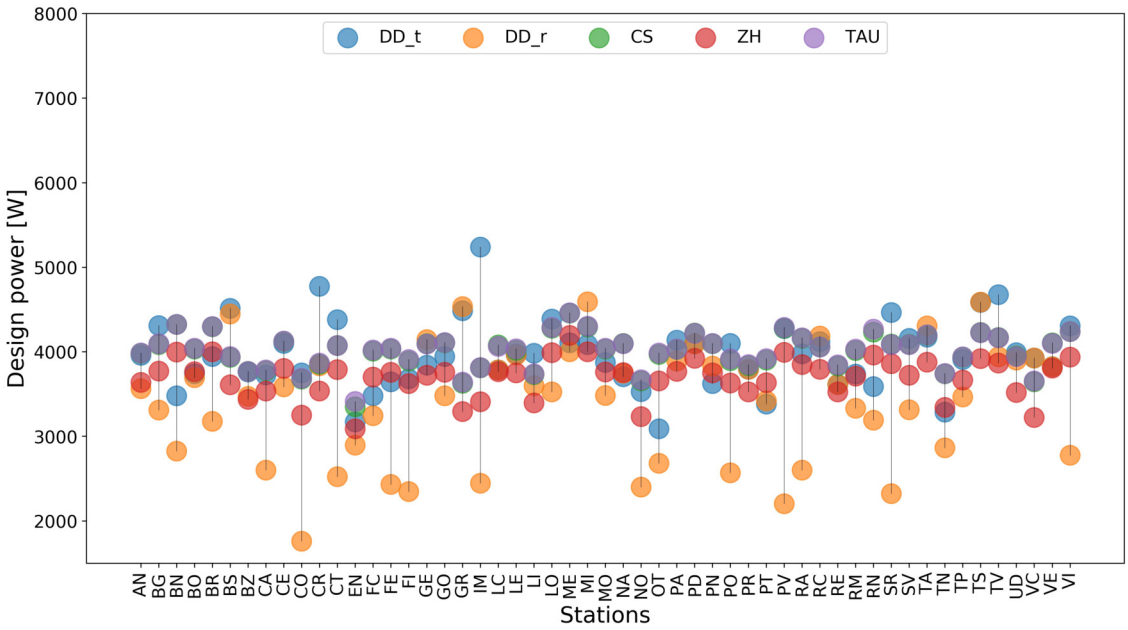

Figure 6.4: Design powers for the 5 methods: ground floor, insulated model

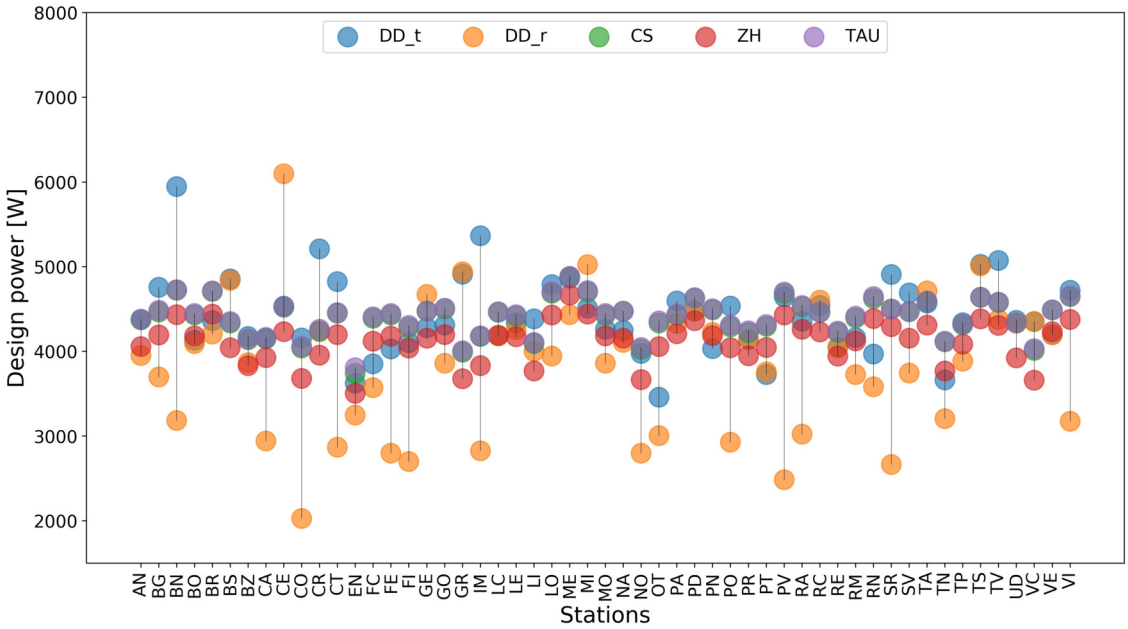

Figure 6.5: Design powers for the 5 methods: second, third and fourth floor (average), insulated model

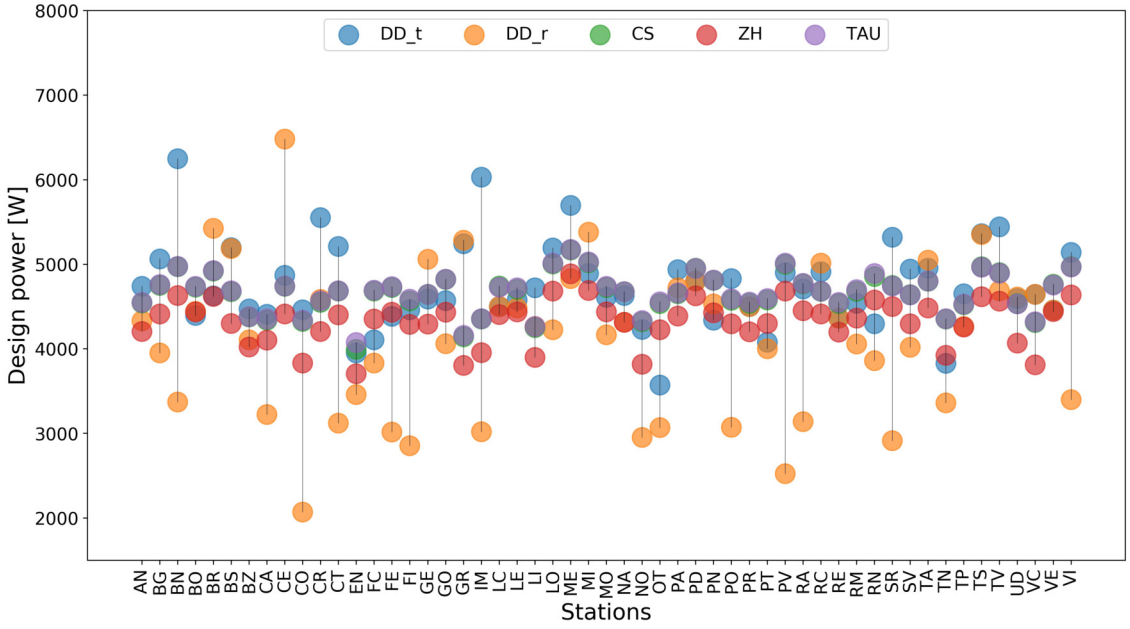

Figure 6.6: Design powers for the 5 methods: second, fifth floor, insulated model

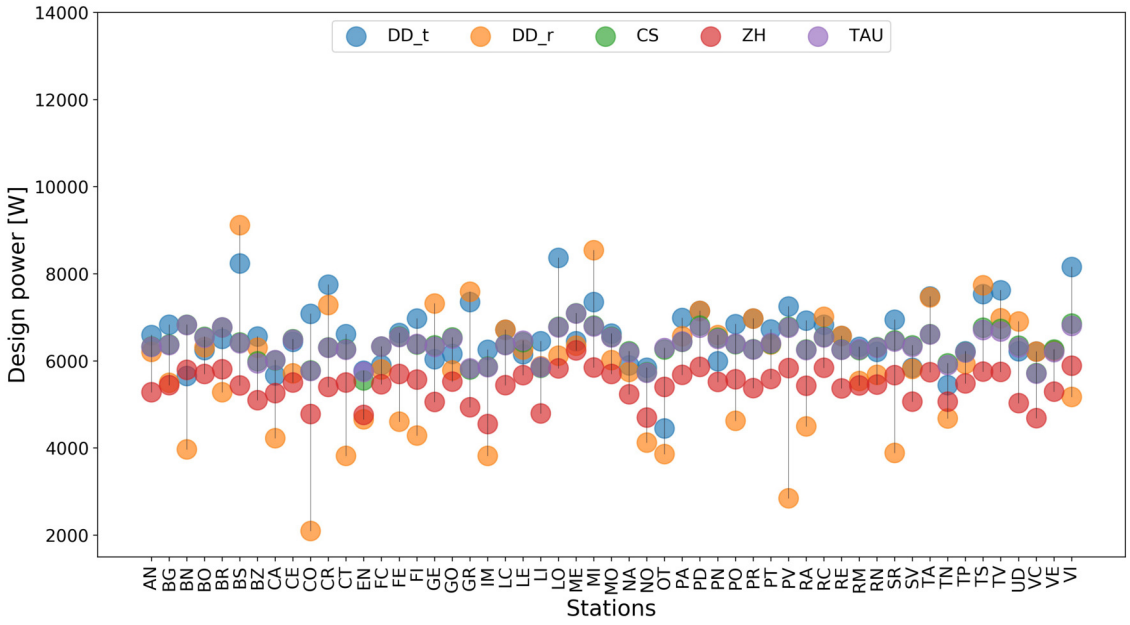

Figure 6.7: Design powers for the 5 methods: ground floor, uninsulated model

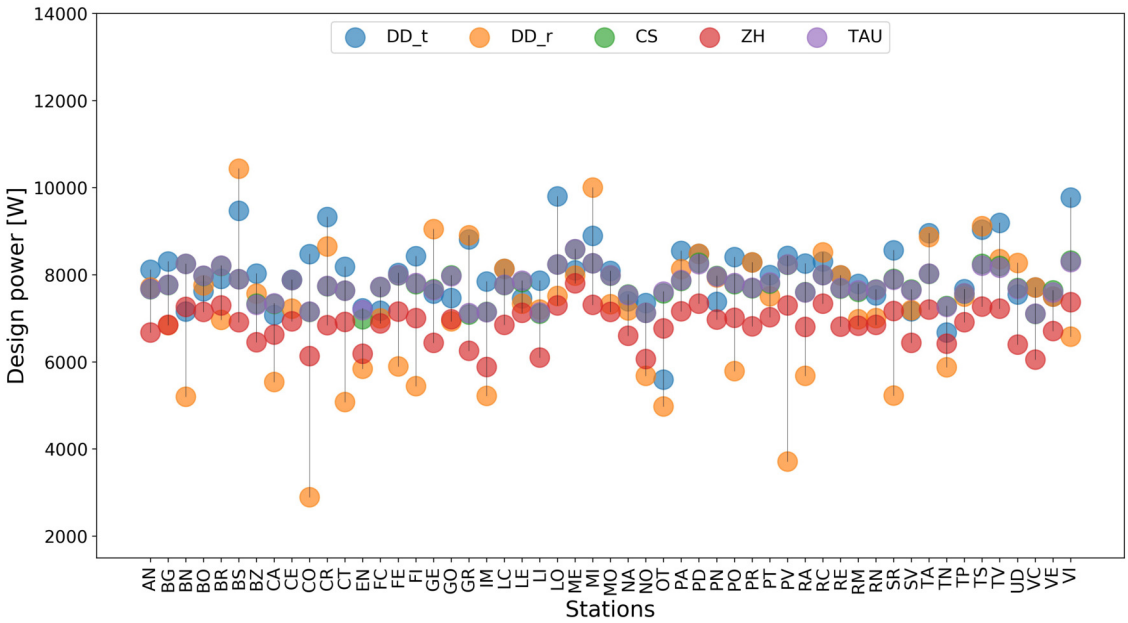

Figure 6.8: Design powers for the 5 methods: second, third and fourth floor (average), uninsulated model

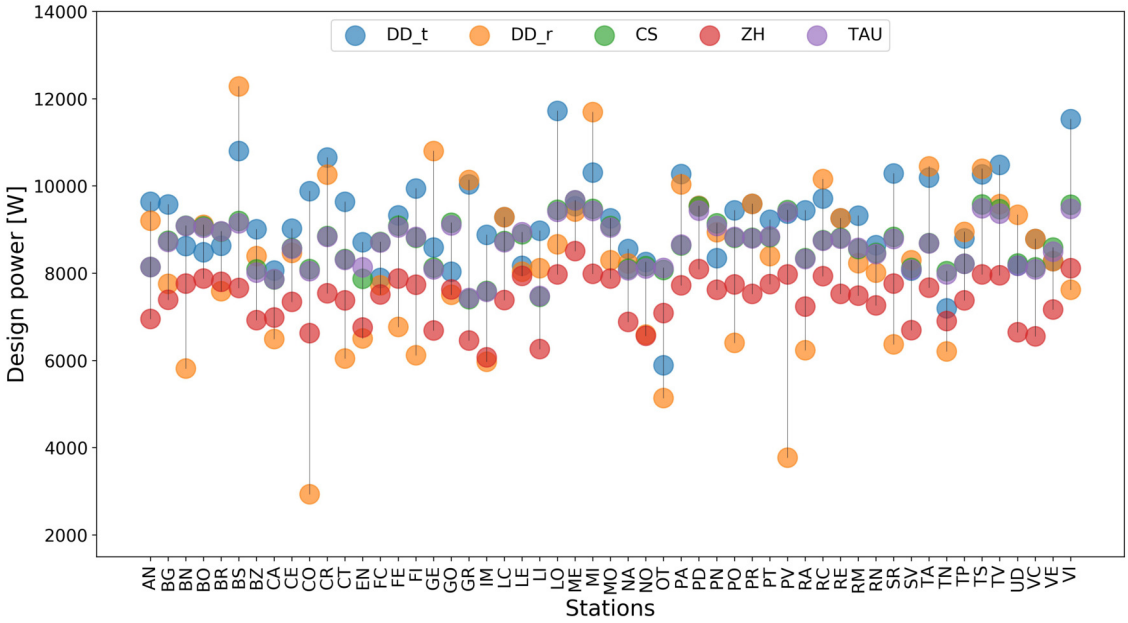

Figure 6.9: Design powers for the 5 methods: second, fifth floor, uninsulated model

In addition, the inspection of Figures from 6.4 to 6.9 reveals that some values stand above the others. In order to analyse these outliers, the percentage differences between the highest value and the *CS* are studied. The *Clear Sky* method was selected for comparison because it is widely used. The Figures 6.10 and 6.11 represent the cases where the percentage differences are higher than 5%, for each floor.
Referring to Figure 6.10, the insulated case shows maximum percentage differences of 27.8%. In addition, for the insulated case, the numbers of stations identified increases moving from the ground floor to the top floor graph: they include 12, 15

and 21 elements. The top floor, with a higher external surface due to the roof, is more sensible to climate design conditions.
As for the uninsulated model, reported in Figure 6.11, a maximum value of approximately 29% is shown. In this case the number of elements selected, for each floor scenario, is more uniform.

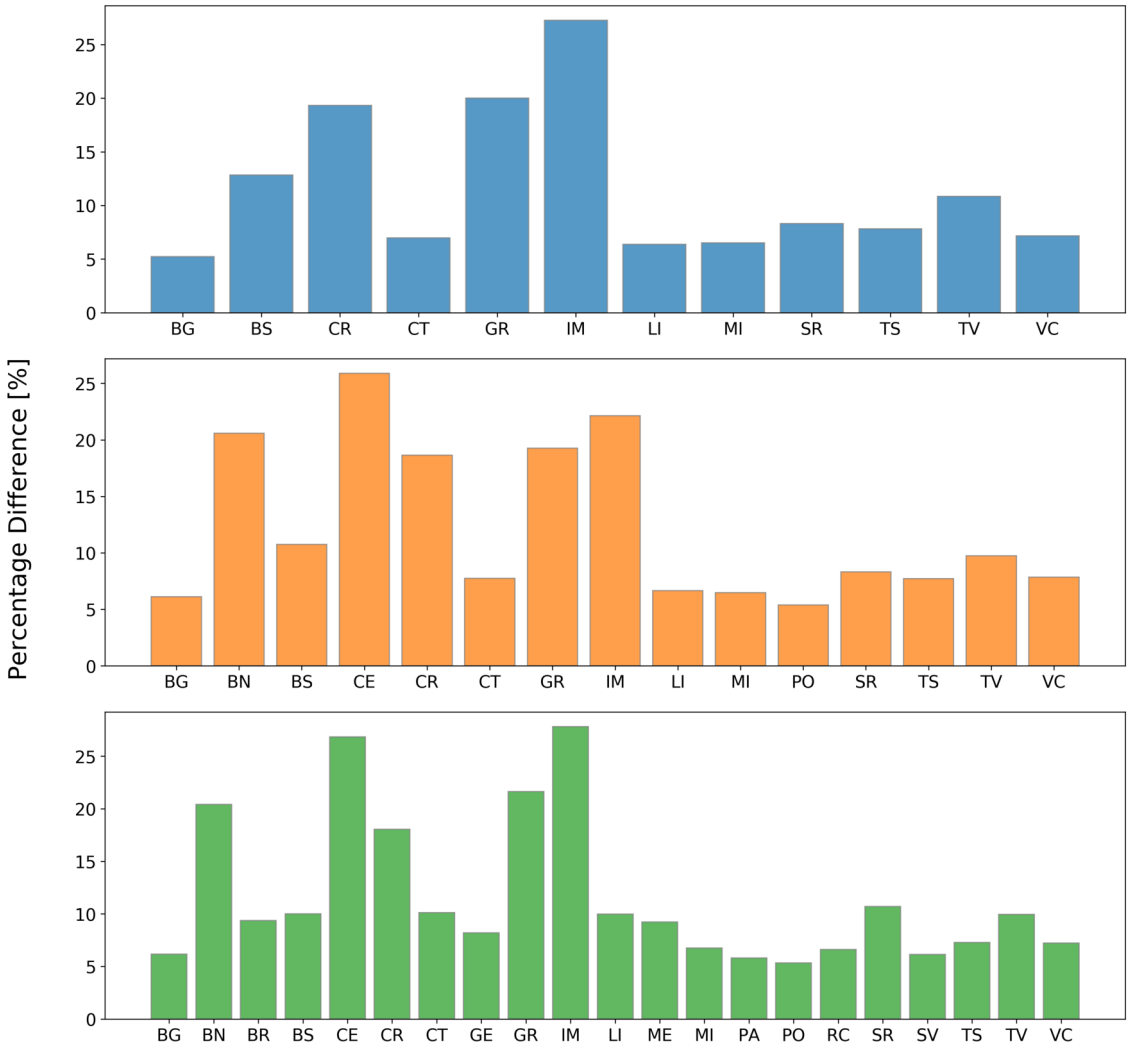

Figure 6.10: Percentage design power difference, insulated model. Ground floor (blue), middle floor (orange) and top floor (green).

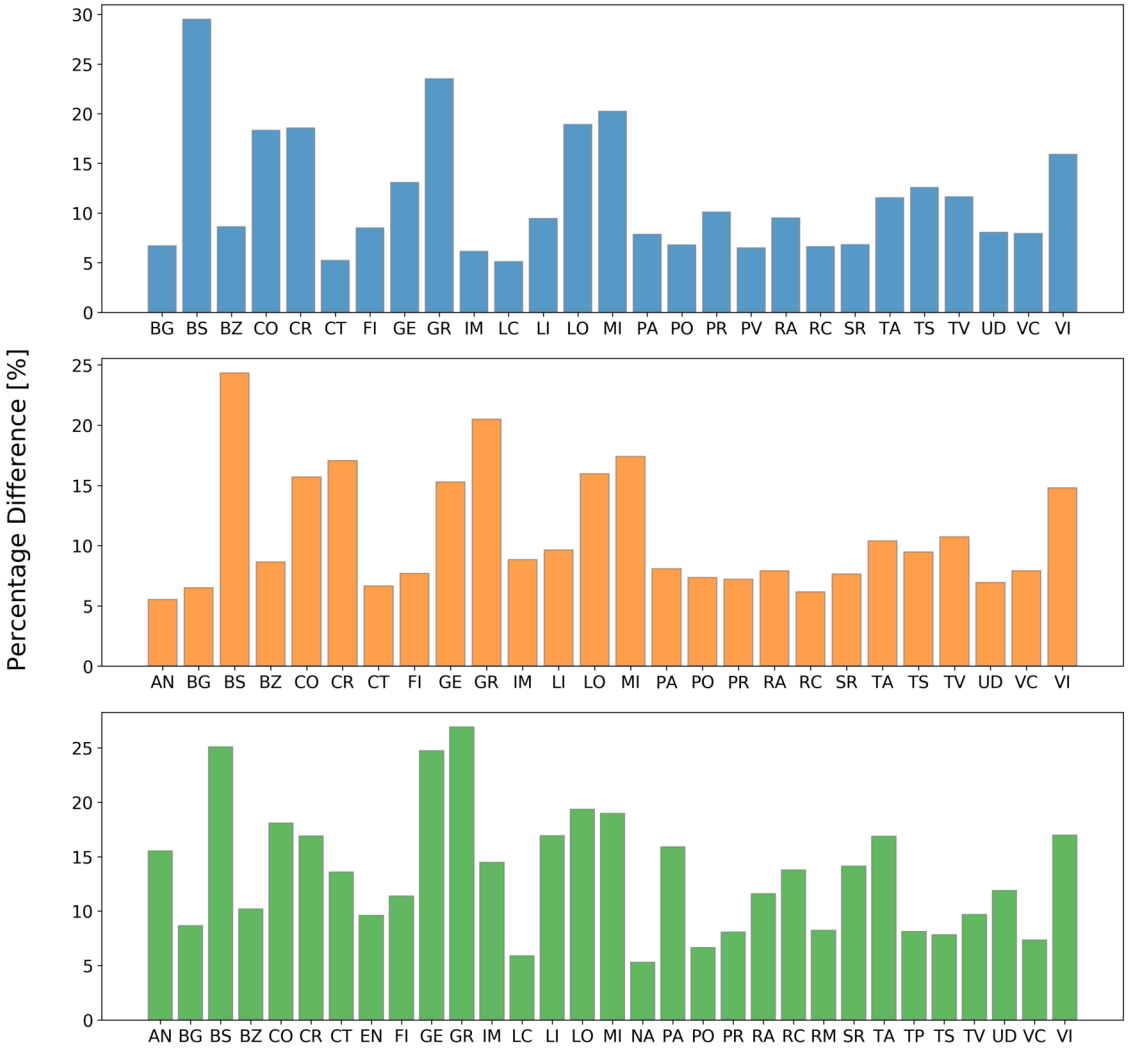

Figure 6.11: Percentage design power difference, uninsulated model. Ground floor (blue), middle floor (orange) and top floor (green).

The graphs included in Figures 6.10 and 6.11 illustrate the percentage difference between the highest model and the *CS* method but no information is provided about which method gave each specific result. To study the methods behaviour, pie charts are shown in Figure 6.10 and 6.11: the data represent, for the outliers cases, the percentage of which model caused the increase. In other words, for each floor, the pie represents the percentage of which method shows an high value, with respect to the *Clear Sky* method. The charts highlight that the design day method based on temperature gave the highest results: it caused from 71% to 80% of the outliers values which exceed the *CS* method. As already highlighted above, the result is affected by the building characteristics and it can not be generalized.

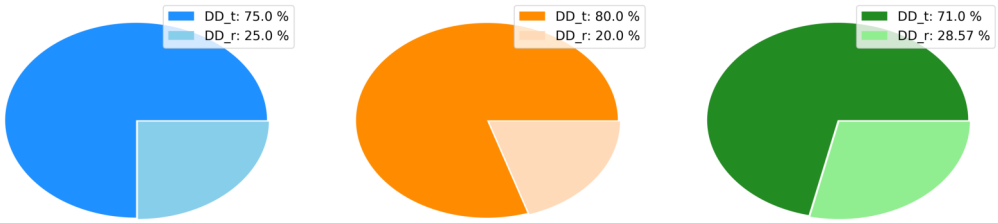

(a) Ground floor (b) Middle floor (c) Top floor

Figure 6.12: *DD_t* and *DD_r* occurrences percentage, insulated building

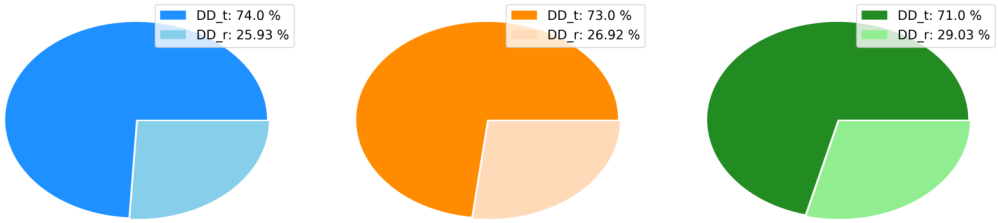

(a) Ground floor (b) Middle floor (c) Top floor

Figure 6.13: *DD_t* and *DD_r* occurrences percentage, uninsulated building

To test the sizing results, annual simulations were carried out. The weather file used are described in section 4.6 and were obtained from the same dataset provided from CTI. Therefore, the design day results and the TRY used are consistent and were derived from the same measurements. Conversely, the Ashrae climatic design conditions may be obtained from different measuring periods and weather station, within the limits explained at the end of section 6.2.2. The number the unmet hours were studied, derived from the annual simulations. An unmet hour is defined as an hour in which one or more zones is outside of the thermostat setpoint range [168]. A setpoint air temperature of 26°C and a thermostat range of 1.11°C were set. As highlighted in Figure 6.14 and 6.15, the unmet hours are relatively low, notably as concerns the uninsulated model. A maximum of 42 and 20 hours are shown for insulated and uninsulated models, respectively.

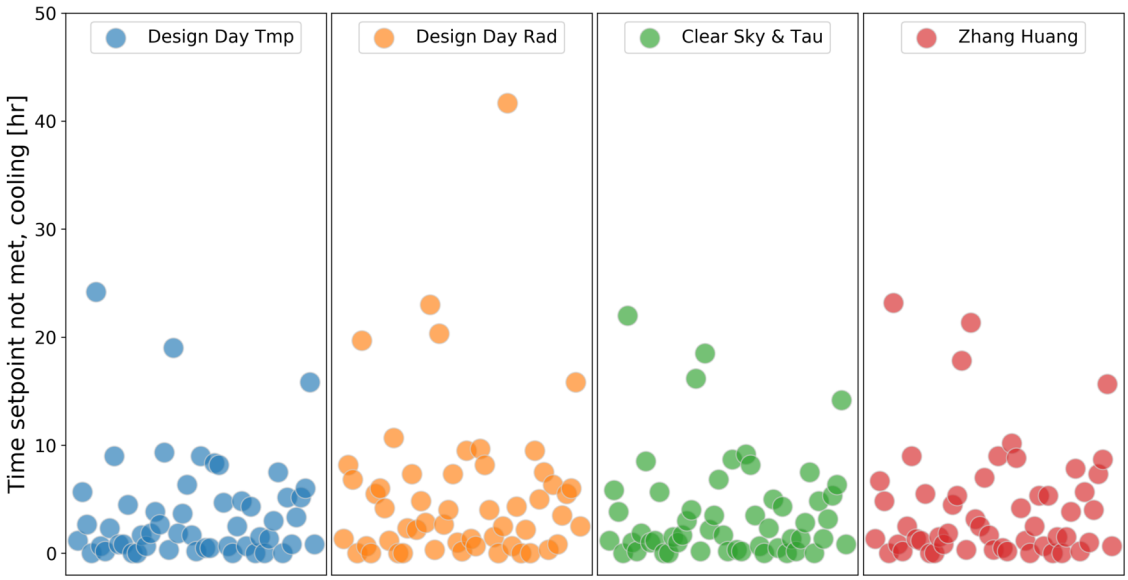

Figure 6.14: Time setpoint not met, insulated model

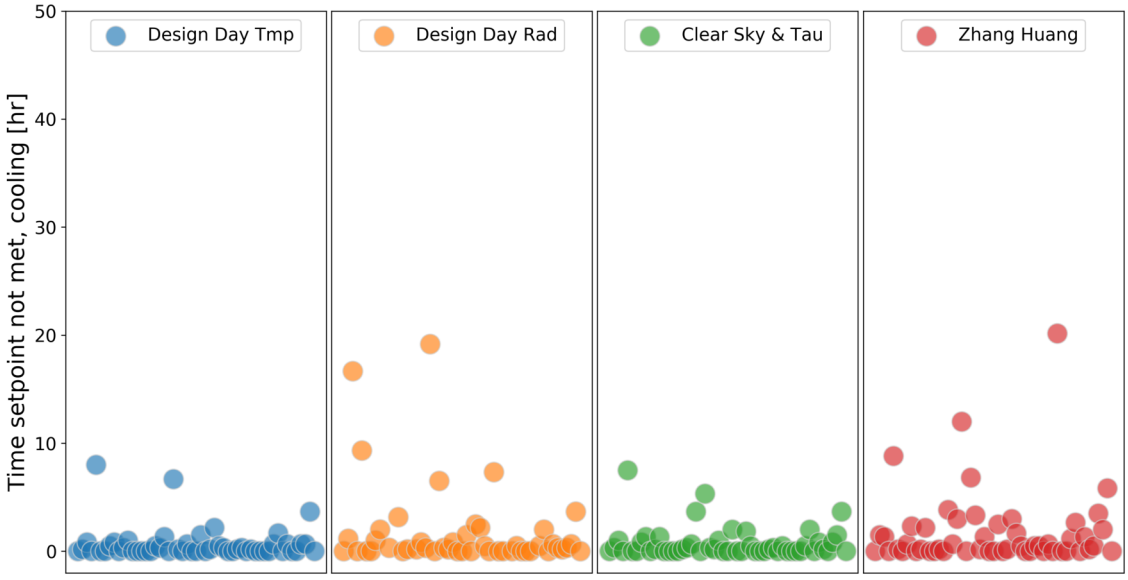

Figure 6.15: Time setpoint not met, uninsulated model

6.8 Final remarks

Several weather-related design methods were applied to a residential test building, insulated and uninsulated cases, to study sizing results and their effect of simulations. The design power difference reported from Figure 6.4 to 6.11 shows remarkable results with a maximum difference between the first and the second highest results of almost 28% and 20% for insulated and uninsulated buildings, respectively. However, unmet hours remain low, with a maximum of 42 hours for insulated building: the sizing factor of 1.15 involve adequate design power to maintain the internal cooling setpoint air temperatures for all the methods.

6.9 Further investigations

As highlighted in section 6.3, the project is ongoing. The following variations could be developed:

- Apply different building usage (e.g. commercial occupancy or internal gains)
- Apply different building characteristics. More specifically, varying the WWR, as proposed also by Pernigotto 2016 [58], could deepen the DD_r method study
- Apply different cooling systems.

Applying various cooling systems could allow to study the system effect and also energy consumption within the simulations. Moreover, the chiller part load ratio operation time, that is a critical aspect introduced by oversized systems, could be analysed.

Chapter 7

Conclusions

The thesis describes the effect of climatic data on building energy simulation.
Climatic data are fundamental to describe the simulation boundary conditions. The main weather data include the characteristics of hygrometer air, solar radiation and wind. These parameters affect several physic process models within the simulation: conduction heat transfer, convective heat transfer, solar heat gains, sensible and latent ventilation loads, system performance, renewable system performance and others.
Weather files are text files that contain climatic data of a specific location. In literature, several weather file typologies are defined and were described in chapter 3. The reference years are widely used: they are a sort of average year that aims to be representative of a climate.
Weather data, as previously mentioned, contain solar radiation data. However, the simulation codes require irradiation data to be provided in their components, the direct and diffuse radiation. Unfortunately, due to the measurement tool cost, in the majority of the stations only the global solar radiation is recorded: the data need to be post-processed to split the measure into its components. The procedure involves the use of numerical models therefore they introduce an element of uncertainty. In chapter 2, the impact of split algorithm was analysed. 33 split models were tested and their results were studied with statistical parameters. Finally, the outcomes of the highest three performance models were applied to building energy simulation of a test building to study the resulting energy difference between applying one model or another. The Perez model showed the best overall performance.
In the Italian panorama, the main source of weather files, the IGDG, is based on measure periods that span from 1951 to 1970. However, the CTI released new weather files in 2015, based on more modern recordings. The effect of the new dataset was studied for the Italian residential building stock, derived from the Tabula project: the new and the old datasets were tested and the energy differences were studied within the national territory. The results highlight that the introduction of more modern data increase the cooling energy consumption and decrease the heating energy consumption. More specifically, the cooling energy increase is more remarkable in southern regions, especially along the Tyrrhenian coast. As for heating energy, the decrease is more significant in northern locations. In addition, the CTI weather files enhanced the cooling energy consumption variability within the territory. Lastly, the critical aspects of the proposed matching method were discussed.

The weather file impact was studied also for optimization cases, with energy-cost analysis. A reference building was selected and a retrofit activity was analysed with an optimization process. In this case study, three weather files from Trieste, characterized from different recording periods, were tested. The approach aimed to maximize the net present value of the investment and minimize the primary energy consumption. The outcomes showed comparable results: the design choices for external walls, roof, ground floor and windows are similar. However, the economic indices of the investment highlighted significant differences, up to 16% and 48% for pay-back time and net present values, respectively.
Finally, the sizing design climate conditions were studied. The sizing of the systems is a crucial part for building energy analysis: it determines the maximum thermal power of internal units and generators that are required to provide or remove heat from the thermal zones. It is an important aspect, since undersized and oversized systems entail several issues such as occupants discomfort or energy waste. In collaboration with CTI, the methodology described in UNI EN 15927-2 was developed and applied to 109 datasets. The technical standard provides a method to identify 12 hourly-based day within the dataset that are suitable for cooling system sizing, one for each calendar month. From this methodology, two design days were identified: the first is characterized by the highest design day mean air temperature, the second from the highest daily total solar irradiance. These two design conditions were compared with other 3 methodologies, widely used in building energy simulations that require Ashrae reports. The five methodologies were applied to a test building and the outcomes were compared with each other: sizing runs and annual simulations were carried out. Annual simulations were carried out with reference years obtained from the same dataset used to identify the design day. The results illustrate that the temperature-based UNI EN 15927-2 design day provide results comparable with the Ashrae methods, that are occasionally higher with a maximum of almost 29%. However, considering the oversizing factor of 1.15 that is usually suggested in technical standards, all the sizing conditions illustrate positive results in terms of cooling unmet hours, with a maximum of 42. The result is strictly related to the test building case study characteristics and is representative of the Italian residential scenario.

Chapter 8

Nomenclature and Acronyms

8.1 Nomenclature

Symbols	Parameter	Unit
ACH	Air changes per hour	[h^{-1}]
AM	Air mass	[-]
C_p	Specific heat	[$Jkg^{-1}K^{-1}$]
DIF_h	Diffuse horizontal solar radiation	[Whm^{-2}]
DNI	Normal solar radiation	[Whm^{-2}]
DIR_h	Horizontal direct solar radiation	[Whm^{-2}]
E_0	Extraterrestrial solar radiation	[Whm^{-2}]
E_{0h}	Extraterrestrial solar radiation, horizontal	[Whm^{-2}]
$Elev$	Elevation	[m]
GLO_h	Global horizontal solar radiation	[Whm^{-2}]
HLS	Heat loss surface	[m^2]
I_{DIRINT}	Direct normal irradiance, Dirint model	[Whm^{-2}]
I_{DISC}	Direct normal irradiance, Disc model	[Whm^{-2}]
k_d	Diffuse fraction	[−]
k_t	Clearness index	[−]
k'_t	Kasten clearness index	[−]
M	Surface mass	[kgm^{-2}]
$Q_{C,CTI}$	Cooling energy, CTI weather file	[kWh]
$Q_{C,IGDG}$	Cooling energy, IGDG weather file	[kWh]
$Q_{H,CTI}$	Heating energy, CTI weather file	[kWh]
$Q_{H,IGDG}$	Heating energy, IGDG weather file	[kWh]
$Q_{ins,C}$	Cooling energy, insulated building	[kWh]
$Q_{ins,H}$	Heating energy, insulated building	[kWh]
$Q_{unins,C}$	Cooling energy, uninsulated building	[kWh]
$Q_{unins,H}$	Heating energy, uninsulated building	[kWh]
SHGC	Solar Heat Gain Coefficient	[-]
S/V	Surface area to volume	[m^-1]
t	Tickness	[cm]
T_d	Dew point temperature	[°]
U	Thermal transmittance	[$Wm^{-2}K^{-1}$]
Uf	Frame thermal transmittance	[$Wm^{-2}K^{-1}$]

Ug	Glass thermal transmittance	[$Wm^{-2}K^{-1}$]
Uw	Window thermal transmittance	[$Wm^{-2}K^{-1}$]
W	Atmospheric precipitable water	[cm]
Z	Zenith angle	[°]

Symbols	Parameter	Unit
λ	Thermal conductivity	[$Wm^{-1}K^{-1}$]
ρ	Density	[kgm^{-3}]
$\Delta k'_t$	Dynamic stability index	[-]
ΔQ_C	Cooling energy difference	[kWh]
ΔQ_H	Heating energy difference	[kWh]
$\Delta Q_{Sav,C}$	Cooling energy saving	[kWh]
$\Delta Q_{Sav,H}$	Heating energy saving	[kWh]

8.2 Acronyms

AMY	Actual meteorological year
B_I	Insulated building
B_U	Uninsulated building
CDD	Cooling degree-day
CTI	Italian thermo-technical committee
DNI	Direct normal solar radiation
E+	EnergyPlus
EPPY	EnergyPlus Python library
HDD	Heating degree-day
HVAC	Heating ventilation and air conditioning
IDF	EnergyPlus model files
IGDG	Gianni De Giorgio weather file database
ISTAT	Italian national institute of statistics
NPV	Net Present Value [kEUR]
NPVc	Net Present Value Coefficient
NZEB	Nearly zero energy building
p	Price (EUR)
PAN	People absolute number
PE	Primary Energy
Pec	Primary energy coefficient
PV	Photovoltaic system
SD	Standard deviation
TMY	Typical meteorological year
TRY	Test reference year
UNITS	University of Trieste
WWR	Window wall area ratio

CS	Ashrae *Clear Sky* model
DD_t	Design day based on air temperature (UNI 15927-2)
DD_r	Design day based on air solar radiation (UNI 15927-2)
TAU	Ashrae *TAU* model
ZH	*Zhang Huang* model

Bibliography

[1] International Energy Agency. Key world energy statistics. 2017. https://www.iea.org/publications/freepublications/publication/KeyWorld2017.pdf.

[2] Luis Pérez-Lombard, José Ortiz, and Christine Pout. A review on buildings energy consumption information. *Energy and Buildings*, 40(3):394 – 398, 2008.

[3] K Matsuura. Effects of climate change on building energy consumption in cities. *Theoretical and Applied Climatology*, 51:105–117, 03 1995.

[4] P. Papesch, J. Haberl, R. Koester, D. Proctor, and B. Berkebile. Buildings, climate change, education and action: The role of the building sector systems in climate change mitigation. http://www.susted.com/wordpress/content/buildings-climate-change-education-and-action-the-role-of-the-building-sector-systems-in-climate-change-mitigation_2011_03/.

[5] Cui Y., D. Yan, T. Hong, C. Xiao, X. Luo, and Q. Zhang. Comparison of typical year and multiyear building simulations using a 55-year actual weather data set from china. *Applied Energy, Volume 195, 890-904*, 2017.

[6] Tianzhen H., Wen-Kuei C., and Hung-Wen L. A sensitivity study of building performance using 30-year actual weather data. *Proceedings of BS2013: 13th Conference of International Building Performance Simulation Association, Chambéry, France, August 26-28*, 2013.

[7] G. Sorrentino, G. Scaccianoce, M. Morale, and V. Franzitta. The importance of reliable climatic data in the energy evaluation. *Energy, 48, 74–79*, 2012.

[8] Patrizia Ferrante, Maria La Gennusa, Stefania Nicolosi, Gianluca Scaccianoce, and Giancarlo Sorrentino. 320: Comparison of methodologies for test reference year (try) generation for mediterranean sites. 11 2018.

[9] Haojie Wang and Qingyan Chen. Impact of climate change heating and cooling energy use in buildings in the united states. *Energy and Buildings*, 82:428 – 436, 2014.

[10] Washington DC U.S. Department of Energy. *Buildings Energy Data Book, Department of Energy.* 2011.

[11] Drury Crawley. Estimating the impacts of climate change and urbanization on building performance. *Journal of Building Performance Simulation*, 1:91–115, 06 2008.

[12] David Claridge, Mingsheng Liu, Yeqiao Zhu, Mustafa Abbas, Aamer Athar, and Jeff Haberl. Implementation of continuous commissioning in the texas loanstar program: "can you achieve 15011 2018.

[13] United Nations. Convention on climate change, kyoto protocol to the united nations framework convention on climate change. 1997.

[14] The Guardian. What is the kyoto protocol and has it made any difference? https://www.theguardian.com/environment/2011/mar/11/kyoto-protocol.

[15] European Parliament. Directive 2002/91/ec of the european parliament and of the council of 16 december 2002 on the energy performance of buildings. 2002.

[16] EUR-Lex. Document 32002l0091. https://eur-lex.europa.eu/eli/dir/2002/91/oj.

[17] European Parliament. Directive 2009/28/ec of the european parliament and of the council of 23 april 2009 on the promotion of the use of energy from renewable sources and amending and subsequently repealing directives 2001/77/ec and 2003/30/ec. 2009.

[18] EUR-Lex. Document 32009l0028. https://eur-lex.europa.eu/legal-content/EN/ALL/?uri=CELEX:32009L0028.

[19] Brussels: European Committee for Standardization. En 15251:2007. indoor environmental input parameters for design and assessment of energy performance of buildings addressing indoor air quality, thermal environment, lighting and acoustics. 2007.

[20] J Clarke. *Energy simulation in building design*. 01 2007.

[21] Jos Schijndel. Bes with fem: Building energy simulation using finite element methods. 06 2016. https://arxiv.org/abs/1606.01243.

[22] Jan Hensen. Simulation of building energy and indoor environmental quality - some weather data issues. *Proceedings of the International Workshop on Climate Data and their Applications in Engineering*, pages 1–15, 01 1999.

[23] Tianzhen Hong, S.K. Chou, and T.Y Bong. Building simulation: An overview of developments and information sources. *Building and Environment*, pages 347–361, 05 2000.

[24] Michael Scott, LAURA E. WRENCH, and DONALD L. HADLEY. Effects of climate change on commercial building energy demand. *Energy Sources*, 16:317–332, 07 1994.

[25] Hiroshi Yoshino, Tianzhen Hong, and Natasa Nord. Iea ebc annex 53: Total energy use in buildings—analysis and evaluation methods. *Energy and Buildings*, 152:124 – 136, 2017.

[26] John Cook, Naomi Oreskes, Peter T Doran, William Anderegg, Bart Verheggen, Edward Maibach, J Stuart Carlton, Stephan Lewandowsky, Andy Skuce, Sarah Green, Dana Nuccitelli, Peter Jacobs, Mark Richardson, Baerbel Winkler, Rob Painting, and Ken Rice. Consensus on consensus: A synthesis of consensus estimates on human-caused global warming. *Environmental Research Letters*, 11:048002, 04 2016.

[27] Mohamed Hamdy, Salvatore Carlucci, Pieter-Jan Hoes, and Jan Hensen. The impact of climate change on the overheating risk in dwellings—a dutch case study. *Building and Environment*, 122, 06 2017.

[28] Intergovernmental panel on climate change. What is a gcm? `http://www.ipcc-data.org/guidelines/pages/gcm_guide.html`.

[29] Kevin K.W. Wan, Danny H.W. Li, Wenyan Pan, and C Lok. Impact of climate change on building energy use in different climate zones and mitigation and adaptation implications. *Applied Energy*, 97:274–282, 12 2011.

[30] Tony N.T. Lam, Kevin K.W. Wan, S.L. Wong, and C Lok. Impact of climate change on commercial sector air conditioning energy consumption in subtropical hong kong. *Applied Energy*, 87:2321–2327, 07 2010.

[31] Hassan Radhi. Evaluating the potential impact of global warming on the uae residential buildings - a contribution to reduce the co2 emissions. *Building and Environment*, 44:2451–2462, 12 2009.

[32] Donald H. Rosenthal, Howard Gruenspecht, and Emily A. Moran. Effects of global warming on energy use for space heating and cooling in the united states. *Energy Journal*, 16, 12 1995.

[33] Yusuke Arima, Ryozo Ooka, Hideki Kikumoto, and Toru Yamanaka. Near future weather data for building energy simulation in summer/winter seasons in tokyo developed by dynamical downscaling method. *ICUC9 - 9th International Conference on Urban Climate jointly with 12th Symposium on the Urban Environment*, 2015.

[34] Mark F. Jentsch, AbuBakr Bahaj, and Patrick A.B. James. Climate change future proofing of buildings—generation and assessment of building simulation weather files. *Energy and Buildings*, 40:2148–2168, 12 2008.

[35] Amélie Robert and Michaël Kummert. Designing net-zero energy buildings for the future climate, not for the past. *Building and Environment*, 55:150–158, 09 2012.

[36] C.S. Barnaby and D.B. Crawley. Weather data for building performance simulation, in: J.l.m. hensen, r. lamberts (eds.). *Building Performance Simulation-for Design and Operation, Taylor & Francis Group, New York, NY, pp.37–55*, 2011.

[37] David Sailor. Relating residential and commercial sector electricity loads to climate - evaluating state level sensitivities and vulnerabilities. *Energy*, 26:645–657, 07 2001.

[38] Thomas Wilbanks, Vatsal Bhatt, Daniel Bilello, Stanley Bull, James Ekmann, William Horak, Y Joe Huang, M Levine, Michael J. Sale, David Schmalzer, and Michael Scott. Effects of climate change on energy production and use in the united states. *US Department of Energy Publications*, 02 2008.

[39] Lund H. The design reference year users manual. 1995.

[40] World Meteorological Organization (WMO). International meteorological vocabulary. second edition, wmo-no. 182, geneva. 1992. https://library.wmo.int/index.php?lvl=notice_display&id=12407#.XIJ-GLh7lPZ.

[41] World Meteorological Organization (WMO). Guide to meteorological instruments and methods of observation. 2017.

[42] Refrigerating American Society of Heating and Inc. Air-Conditioning Engineers. *2009 ASHRAE handbook: Fundamentals*. 2009.

[43] Hadja Diagne, Mathieu David, Philippe Lauret, and John Boland. Solar irradiation forecasting: state-of-the-art and proposition for future developments for small-scale insular grids. 05 2012.

[44]

[45] Asit Bhattacharya and R Bhattacharya. Diffuse solar radiation and associated meteorological parameters in india. *Ann. Geophys.*, 14:1051–1059, 01 1996.

[46] D.R. Myers. Solar radiation modeling and measurements for renewable energy applications: Data and model quality. *International Expert Conference on Mathematical Modeling of Solar Radiation and Daylight—Challenges for the 21st Century Edinburgh, Scotland September 15–16*, 2003.

[47] P. Blanc, B. Espinar, N. Geuder, C. Gueymard, R. Meyer, R. Pitz-Paal, B. Reinhardt, D. Renné, M. Sengupta, L. Wald, and S. Wilbert. Direct normal irradiance related definitions and applications: The circumsolar issue. *Solar Energy*, 110:561 – 577, 2014.

[48] Benjamin Y.H. Liu and Richard C. Jordan. The interrelationship and characteristic distribution of direct, diffuse and total solar radiation. *Solar Energy*, 4:1–19, 07 1960.

[49] Lannini F., Wunderle S., Lehning M., and Fierz C. Division of global radiation into direct radiation and diffuse radiation. *Master's thesis, Faculty of Science, University of Bern*, 2010. http://occrdata.unibe.ch/students/theses/msc/34.pdf.

[50] Gueymard C. A. and Ruiz-Arias J. A. Extensive worldwide validation and climate sensitivity analysis of direct irradiance predictions from 1-min global irradiance. *Solar Energy, Volume 128, Pages 1-30, ISSN 0038-092X*, 2016.

[51] Alarcon-Padilla D. C. Blanco M. J. Computing solar vector. *Solar Energy*, 70(5):431–441, 2001.

[52] R. Perez, P. Ineichen, E. Maxwell, R. Seals, and A. Zelenka. Dynamic global-to-direct irradiance conversion models. *ASHRAE Transactions. 98(1):354-369*, 1992.

[53] E L. Maxwell. A quasi-physical model for converting hourly global horizontal to direct normal insolation. *Unknown*, 08 1987.

[54] Engerer N. A. Minute resolution estimates of the diffuse fraction of global irradiance for southeastern australia. *Solar Energy*, 116:215–237, 2015.

[55] Barbara Ridley, John Boland, and Philippe Lauret. Modeling of diffuse solar fraction with multiple predictors. *Renewable Energy*, 35:478–483, 02 2010.

[56] A. Skartveit, J. A. Olseth, and M. E. Tuft. An hourly diffuse fraction model with correction for variability and surface albedo. *Sol. Energy, vol. 63, no. 3, pp. 173–183*, 1998.

[57] F Kasten. A simple parameterization of the pyrheliometric formula for determining the linke turbidity factor. *Meteorologische Rundschau*, 33:124–127, 01 1980.

[58] G. Pernigotto, A. Prada, P. Baggio, A. Gasparella, and A. Mahdavi. Solar irradiance modelling and uncertainty on building hourly profiles of heating and cooling energy needs. *In Proceedings of the IV International High Performance Buildings Conference in Purdue, West Lafayette, IN, USA, 11–14 July*, 2016.

[59] Uni/ts 11300-1:2014 prestazioni energetiche degli edifici. *Parte 1: Determinazione del fabbisogno di energia termica dell'edificio per la climatizzazione estiva ed invernale.*

[60] Bird R. E. and Hultrom R. L. A simplified clear sky model for direct and diffuse insolation on horizontal surfaces. *SERI/TR-642-761, Solar Energy Research Institute, Golden, Colorado, USA*, 1981.

[61] Sengupta M. and Gotseff P. Evaluaton of clear sky models for satellite-based irradiance estimates. *Technical Report NREL/TP-5D00-60735, http://purl.fdlp.gov/GPO/gpo53784*, 2013.

[62] EnergyPlus. Engineering reference - the reference to energyplus calculations. `https://energyplus.net/sites/default/files/pdfs_v8.3.0/EngineeringReference.pdf`.

[63] Lupato G., Manzan M., and Cirilli S. Comparison of direct radiation split algorithms for energy simulation of buildings. *Proceedings of Building Simulation Applications BSA 2017, 8-10 February, Bolzano, Italy*, 2018.

[64] D. B. Crawley, , and Y. J. Huang. Does it matter which weather data you use in energy simulations? *User News, 18, 2–12*, 1997.

[65] J. Bilbao, A. Miguel, J. A. Franco, and A. Ayuso. Test reference year generation and evaluation methods in the continental mediterranean area. *Journal of Applied Meteorology, Volume 43*, 2003.

[66] Keeble E. Availability of uk climatic data for use in simulation. *BEPACTechnical Note 90/1, Building Research Establishment, Watford,UK*, 1990.

[67] The building enclosure. `https://builtenv.wordpress.com/2014/02/27/climate-data-for-building-simulations/`.

[68] G. Pernigotto, A. Prada, D. Cóstola, A. Gasparella, and J.L.M. Hensen. Multi-year and reference year weather data for building energy labelling in north italy climates. *Energy Build.*, 72:62–72, 2014.

[69] W. K. Chow and S. K. Fong. Typical meteorological year for building energy simulation in hong kong. *Architectural Science Review, 40(1): 11-15*, 1997.

[70] L. Yang, J. C. Lam, and J. Liu. Building energy simulation using multi-years and typical meteorological years in different climates. *Energy Conversion and Management, 49(1): 113-124*, 2008.

[71] T. Kershaw, M. Eames, and D. Coley. Comparison of multi-year and reference year building simulations. *Building Services Engineering Research and Technology, 31(4): 357-369*, 2010.

[72] Crawley D. B. Which weather data should you use for energy simulations of commercial buildings? *Transactions-American society of heating refrigerating and air conditioning engineers, Volume 104, Pages 498-515, Ashrae American Society Heating Refrigerating*, 1998.

[73] J Baltazar. Study of cubic splines and fourier series as interpolation techniques for filling in short period of missing building energy use and weather data. *Journal of Solar Energy Engineering*, 128, 01 2006.

[74] K. Skeiker. Comparison of methodologies for tmy generation using 10 years data for damascus, syria. *Energy Convers. Manag., 48, 2090–2102*, 2007.

[75] UNI EN ISO 15927-4:2005. Hygrothermal performance of buildings – calculation and presentation of climatic data – part 4: Hourly data for assessing the annual energy use for heating and cooling. 2005.

[76] T.L. Freeman. Evaluation of the "typical meteorological years" for solar heating and cooling system studies. *Final Report, Solar Energy Research Institute: Golden, CO, USA*, 1979. `https://www.nrel.gov/docs/legosti/old/8150-1.pdf`.

[77] A. Argiriou, S. Lykoudis, S. Kontoyianidis, C. A. Balaras, D. Asimakopoulos, M. Petrakis, and P. Kassomenos. Comparison of methodologies for tmy generation using 20 years data for athens, greece. *Sol. Energy, 66, 33–45*, 1999.

[78] Liping Wang, Paul Mathew, and Xiufeng Pang. Uncertainties in energy consumption introduced by building operations and weather for a medium-size office building. *Energy and Buildings*, 53:152–158, 10 2012.

[79] Mahabir Bhandari, Som Shrestha, and Joshua New. Evaluation of weather datasets for building energy simulation. *Energy and Buildings*, 49:109–118, 06 2012.

[80] C Lok, Kevin K.W. Wan, S.L. Wong, and Tony N.T. Lam. Principal component analysis and long-term building energy simulation correlation. *Energy Conversion and Management*, 51:135–139, 01 2010.

[81] Moncef Krarti, Donghyun Seo, and J Huang. Evaluation of typical weather year selection approaches for energy analysis of buildings (rp-1477). *ASHRAE Transactions*, 115, 01 2009.

[82] Meteonorm website. `http://www.meteonorm.com/en/features/features`.

[83] R. Perez, M. Kmiecik, K. Moore, S. Wilcox, R. George, D. Renne, F. Vignola, and P. Ineichen. Status of high resolution solar irradiance mapping from satellite data. *Proceedings of the ASES Annual Meeting, Portland, OR, pp. 265-270*, 2004.

[84] Tshewang Lhendup and Samten Lhundup. Comparison of methodologies for generating a typical meteorological year (tmy). *Energy for Sustainable Development*, 11:5–10, 09 2007.

[85] Ibraheem Almofeez, M.Y. Numan, Khalid A. Alshaibani, and Faris Almaziad. Review of typical vs. synthesized energy modeling weather files. *Journal of Renewable and Sustainable Energy*, 4, 01 2012.

[86] K.M. Knight, S.A. Klein, and J.A. Duffie. A methodology for the synthesis of hourly weather data. *Solar Energy*, 46:109–120, 12 1991.

[87] TRNSYS. Transient system simulation tool. `http://www.trnsys.com/`.

[88] Krista M. Knight. Development and validation of a weather data generation moledular. 11 1988.

[89] V.A. Graham, Kenneth Hollands, and T.E. Unny. Stochastic variation of hourly solar radiation over the day. pages 3796–3800, 12 1988.

[90] Larry Degelman. A weather simulation model for building energy analysis. *ASHRAE Transactions*, 82:435–447, 01 1976.

[91] L.O. Degelman. Monte carlo simulation of solar radiation and dry bulb temperatures for air conditioning purposes. *Report No. 70-9, sponsored by the National Science Foundation under Grant No. GK-2204*, 1970.

[92] Robert Adam Gansler. Assessment of generated meteorological data for use in solar energy simulations. 01 1993.

[93] Robert A. Gansler, S.A. Klein, and W.A. Beckman. Assessment of the accuracy of generated meteorological data for use in solar energy simulation studies. *Solar Energy*, 53:279–287, 09 1994.

[94] R.A. Gansler, S.A. Klein, and W.A. Beckman. Investigation of minute solar radiation data. *Solar Energy*, 55:21–27, 07 1995.

[95] V.A. Graham. *Stochastic Synthesis of the Solar Atmospheric Transmittance*. PhD thesis, University of Waterloo, 1985.

[96] TRNSYS: Transient system simulation tool. http://web.mit.edu/parmstr/public/trnsys/04-mathematicalreference.pdf. pages 303–306, 2018.

[97] Ali Celik. Long-term energy output estimation for photovoltaic energy systems using synthetic solar irradiation data. *Energy*, 28:479–493, 04 2003.

[98] Adnan Shariah and Bassam Shalabi. Optimal design for thermosyphon solar water heater. *Renewable Energy*, 11:351–361, 07 1997.

[99] Mo Chung, Jun-Un Park, and Hyung-Kee Yoon. Simulation of a central solar heating system with seasonal storage in korea. *Solar Energy*, 64, 12 1998.

[100] Gouri Datta. Effect of fixed horizontal louver shading devices on thermal perfomance of building by trnsys simulation. *Renewable Energy*, 23:497–507, 07 2001.

[101] Adel Ghoneim, Yusop Ahmad, and Ali H. Abdullah. Economic analysis of photovoltaic-powered solar domestic hot water systems in kuwait. *Renewable Energy*, 25:81–100, 01 2002.

[102] N Cardinale, F Piccininni, and Pietro Stefanizzi. Economic optimization of low-flow solar domestic hot water plants. *Renewable Energy*, 28:1899–1914, 10 2003.

[103] S. Kim, D. Zirkelbach, H.M. Künzel, J.-H. Lee, and J. Choi. Development of test reference year using iso 15927-4 and the influence of climatic parameters on building energy performance. *Build. Environ. 114, 374–386*, 2017.

[104] G. Pernigotto, A. Prada, F. Cappelletti, and A. Gasparella. Impact of reference years on the outcome of multi-objective optimization for building energy refurbishment. 2017.

[105] Antonio Capozza, Angelo Zarrella, and Michele De Carli. Analysis of vertical ground heat exchangers: The new carm tool. *Energy Procedia*, 81:288–297, 12 2015.

[106] National Climatic Data Center. Test reference year (try). *Tape Reference Man-ual TD-9706, National Climatic Data Center*, 1976.

[107] I.J. Hall, R.P. Richard, E.A. Herbert, and C.B. Eldon. Generation of typical meteorological years for 26 solmet stations. *Sandia Laboratories energy report*, 1978.

[108] Filkenstein JM and Schafer RE. Improved goodness to fit tests. *J Biometrica; 58*, 1971.

[109] Festa R and Ratto CF. Proposal of a numerical procedure to select reference years. *J Solar Energy;50*, 1993.

[110] Dogniaux R and Sneyers R. Méthodologie d'analyse statistique des données météorologique en vue de la constitution de périodes-types pour l'application à des problèmes spécifiques. *Rapport des Journeés Internationales d'Etude sur chauffage solaire dans le bâtiment. Liège: AIM; eptember 12e14*, 1977.

[111] Crow LW. Weather year for energy calculations. *ASHRAE J*, 1984.

[112] D.K. Pissimanis, G.S. Karras, V.A. Notaridou, and K. Gavra. The generation of a 'typical meteorological year' for the city of athens. *Sol. Energy, 40, 405–411*, 1988.

[113] Marion W and Urban K. User's manual for tmy2's typical meteorological years. *Golden, CO: National Renewable Energy Laboratory*, 1995.

[114] Gazela M and Mathioulakis E. A new method for typical weather data selection to evaluate long-term performance of solar energy systems. *Solar Energy*, 2001.

[115] Miguel A and Bilbao J. Test reference year generation from meteorological and simulated solar radiation data. *Solar Energy*, 2005.

[116] S.M. Wilcox and W. Marion. Users manual for tmy3 data sets. *National Renewable Energy Laboratory: Golden, CO, USA*, 2008.

[117] G. Pernigotto, A. Prada, A. Gasparella, and J.L.M. Hensen. Analysis and improvement of the representativeness of en iso 15927-4 reference years for building energy simulation. *J. Build. Perform. Simul. 7, 391–410*, 2014.

[118] Kwanho Lee, Hochun Yoo, and Geoff J. Levermore. Generation of typical weather data using the iso test reference year (try) method for major cities of south korea. 2010.

[119] Ricardo Aguiar, Susana Camelo, and Helder Gonçalves. Assessing the value of typical meteorological years built from observed and from synthetic data for building thermal simulation. *In Proceedings of the 6th international IBPSA Conference, Kyoto, Japan, 13–15 September*, 1999.

[120] Luo QX Van Paassen AHC. Weather data generator to study climate change on buildings. *Building Services Engineering Research and Technology 23:251–8*, 2002.

[121] C.O. Pedersen, Refrigerating Atlanta: American Society of Heating, and Inc. Air-Conditioning Engineers. *Aerographer's Mate, Module 05–Basic Meteorology.* 2004.

[122] L. Guan, J. Yang, and J.M. Bell. Cross-correlations between weather variables in australia. *Build. Environ. 42, 1054–1070*, 2007.

[123] Hosseini M., F. Tardy, and B. Lee. Cooling and variety of roof designs; the effects of future weather data in a cold climate. *Journal of Building Engineering, Volume 17, 107-114, 2352-7102*, 2018.

[124] Huws H., , and Jankovic L. Optimisation of zero carbon retrofit in the context of current and future climate. *2nd IBPSA-England Conference BSO, London, 23rd-24th June*, 2014.

[125] G. Ciulla, A. Galatioto, and R. Ricciu. Energy and economic analysis and feasibility of retrofit actions in italian residential historical buildings. *Energy and Buildings, Volume 128, 649-659*, 2016.

[126] Eames M., Kershaw T., and Coley D. The appropriate spatial resolution of future weather files for building simulation. *Journal of Building Performance Simulation*, 5:6:347–358, 2012.

[127] Pulido-Arcas J. A. Rubio-Bellido C., Pérez-Fargallo A. Optimization of annual energy demand in office buildings under the influence of climate change in chile. *Energy, Volume 114, Pages 569-585, ISSN 0360-5442*, 2016.

[128] EN ISO 13790:2008. Energy performance of buildings – calculation of energy use for space heating and cooling. 2008.

[129] Chiesa G. and Grosso M. The influence of different hourly typical meteorological years on dynamic simulation of buildings. *Energy Procedia, Volume 78, Pages 2560-2565, ISSN 1876-6102*, 2015.

[130] Murano G., Corrado V., and Dirutigliano D. The new italian climatic data and their effect in the calculation of the energy performance of buildings. *Energy Procedia, Volume 101, Pages 153-160, ISSN 1876-6102*, 2016.

[131] Pierangioli L., Carletti C., Cellai G., and Sciurpi F. Energy refurbishment of social housing stock in italy: Analysis of some scenarios from the impact of climate change to occupant behaviour. *Proceedings of Building Simulation Applications BSA, 8-10 February, Bolzano, Italy*, 2017.

[132] Tabula project. `http://episcope.eu/iee-project/tabula/`.

[133] Designbuilder, version 5.0.3. DesignBuilder Software Limited.

[134] Eppy documentation. `https://pythonhosted.org/eppy/index.html`.

[135] Tabula web tool. `http://webtool.building-typology.eu/`.

[136] Energyplus, version 8.6. U.S. Department of Energy.

[137] Gianni de giorgio try, energyplus source. `https://energyplus.net/weather-region/europe_wmo_region_6/ITA%20%20`.

[138] Cti try documentation. `https://try.cti2000.it/`.

[139] Lupato G., Manzan M., and A. Pezzi. The effect of climatic data on building performance optimization. *Building Simulation and Optimization, Cambridge, UK, 11-12 September*, 2018.

[140] Mazzarella L. Dati climatici g. de giorgio. *Proceedings of giornata di studio Giovanni De Giorgio. Milano: Politecnico di Milano*, 1997. `https://energyplus.net/sites/all/modules/custom/weather/weather_files/italia_dati_climatici_g_de_giorgio.pdf`.

[141] D.G. Erbs, S.A. Klein, and J.A. Duffie. Estimation of the diffuse radiation fraction for hourly, daily and monthly-average global radiation. *Solar Energy*, 28:293–302, 12 1982.

[142] Manuel Collares-Pereira and Ari Rabl. The average distribution of solar radiation-correlations between diffuse and hemispherical and between daily and hourly insolation values. *Solar Energy*, 22:155–164, 12 1979.

[143] Robert G. L. Briggs R. S., Taylor Z. T. Climate classification for building energy codes and standards: Part 2-zone definitions, maps and comparisons. *Energy Procedia, Volume 78, 2560-2565, 1876-6102*, 2003.

[144] Energyplus official documentation. `https://energyplus.net/weather/simulation`.

[145] UNI-EN-ISO 15927-6:2008. Hygrothermal performance of buildings – calculation and presentation of climatic data accumulated temperature differences (degree-days). 2008.

[146] modeFRONTIER. Version 2014. `http://www.esteco.com`.

[147] Pierangioli L. and Cellai G. The impact of climate change on energy-efficient refurbishment of social housing stock in italy. *3rd IBPSA-England Conference BSO, Newcastle, 12th-14th September*, 2016.

[148] Prezzario Regionale dei Lavori Pubblici. Regione autonoma friuli venezia giulia. `http://www.regione.fvg.it`.

[149] Manzan M. and Clarich A. Fast energy and daylight optimization of an office with fixed and movable shading devices. *Building and Environment, 113, 175-184*, 2017.

[150] Arlan Burdick. Strategy guideline: Hvac equipment sizing. 2012.

[151] Bill Smith. Hvac peak load calculation methods – history and comparisons. `https://www.elitesoft.com/web/newsroom/loadcalcs.html`.

[152] Chunliu Mao. *Analysis of building peak cooling load calculation methods for commercial buildings in the united states*. PhD thesis, Texas A&M University, 400 Bizzell St, College Station, TX 77843, USA, 5 2016.

[153] G.P. Mitalas. Transfer function method of calculating cooling loads, heat extraction and space temperature. 1972.

[154] W. Rudoy and F. Duran. Ashrae rp-138 development of an improved cooling load calculation method. 1974.

[155] E. F. Sowell. Classification of 200,640 parametric zones for cooling load calculations. 1988.

[156] J.D. Spitler, F.C. McQuiston, and K. Lindsey. The cltd/scl/clf cooling load calculation method. 1993.

[157] C.O. Pedersen, D.E. Fisher, and R.J. Liesen. Development of a heat balance procedure for calculating cooling loads. 1997.

[158] C.S. Barnaby, J.D. Spilter, and D. Xiao. Updating the ashrae/acca residential heating and cooling load calculation procedures and data. 2004.

[159] B.A. Nigusse. *Improvements to the Radiant Time Series Method Cooling Load Calculation Procedure*. PhD thesis, Department of Mechanical Engineering. Oklahoma State University., Stillwater, Oklahoma, USA, 2007.

[160] EnergyPlus. Loop, equipment sizing and other design data. `https://www.energyplus.net/sites/default/files/docs/site_v8.3.0/EngineeringReference/10-Sizing/index.html`.

[161] Ashrae. Ashrae climatic design conditions 2017. `http://ashrae-meteo.info/`.

[162] J.L. Threlkeld and R.C. Jordan. Direct radiation available on clear days. *ASHRAE Trans.; (United States)*, 64, 01 1958.

[163] Refrigerating American Society of Heating and Inc. Air-Conditioning Engineers. *2007 ASHRAE handbook: Fundamentals*. 2007.

[164] Toshiyuki Watanabe, Yoshimi Urano, and H. Hayashu. Procedures for separating direct and diffuse insolation on a horizontal surface and prediction of insolation on tilted surface. *Trans Architectural Inst Jpn*, 330:96–108, 08 1983.

[165] Qingyuan Zhang and Joe Huang. Development of typical year weather data for chinese locations. *ASHRAE Transactions*, 108, 01 2002.

[166] R. Hedrick. Generation of hourly design-day weather data. *Ashrae Research Project, Final Report*, 2009.

[167] D. Thevenard. Updating the ashrae climatic data for design and standards. *Ashrae Research Project, Final Report*, 2009.

[168] Refrigerating American Society of Heating and Inc. Air-Conditioning Engineers. *ANSI/ASHRAE/IES Standard 90.1-2016 – Energy Standard for Buildings Except Low-Rise Residential Buildings*. 2016.